



Emilia Strandback M.Sc.

Biochemical and biophysical characterization of cancer-associated variants of human NAD(P)H:quinone oxidoreductase 1

DOCTORAL THESIS

to achieve the university degree of
Doktorin der technischen Wissenschaften

submitted to

Graz University of Technology

Supervisor

Univ.-Prof. Mag. rer. nat. Dr. rer. nat. Peter Macheroux

Institute of Biochemistry

Graz University of Technology

Graz, October 2018

AFFIDAVIT

I declare that I have authored this thesis independently, that I have not used other than declared sources/resources, and that I have explicitly indicated all material which has been quoted either literally or by content from the sources used. The text document uploaded to TUGRAZonline is identical to the present doctoral thesis.

Date

Signature

“I need to write down my observations. Even the tiniest ones; they're the most important.”

Tove Jansson

Acknowledgements

First of all, I would like to thank my supervisor Prof. Peter Macheroux for giving me the outstanding opportunity to work in his group on a very fascinating project. I'm especially thankful for the diversity of the NQO1 project; it made things more challenging but also more intriguing. I also appreciate the chance to work on several related projects during my PhD; it gave me an excellent chance to broaden my research perspective and understanding.

Furthermore, I would also like to thank the PhD program "DK Molecular Enzymology" for giving me the opportunity to pursue my PhD and for providing excellent chances for collaborations and exchange of ideas.

I would also like to thank all my thesis committee members: Prof. Karl Gruber, Prof. Klaus Zangger and Prof. Rolf Breinbauer for their advice on the project and for successful collaborations. Several additional collaborators provided important scientific contributions to the projects, including Prof. Tobias Madl, Prof. Andreas Winkler, Prof. Beate Rinner, Prof. Ellen Heitzer, Dr. Altijana Hromic-Jahjefendic, Gesa Richter, Dr. Benjamin Bourgeois and Luka Brvar. Thanks for all the time and effort you spent!

Additional thanks to all the students I had the opportunity to supervise during the last five years: Gernot Kutlesa, Christoph Köberl, Andrea Lepir, Anja Högler, Daniel Waltenstorfer and Florian Weissensteiner. It was always enjoyable working with you. Thank you also for valuable contributions to the different projects and good luck in your future endeavors!

The time in the lab would not have been the same without any of the current or past AGM members. Thank you Venugopal Gudipati (who is responsible for making me select the NQO1 project in the first place, thanks for your advice!), Peter Augustin, Barbara Konrad, Bastian Daniel, Domen Zafred, Thomas Bergner, Johannes Niederhauser, Eveline Brodl, Stefan Ettl, Geoffrey Gourinchas, Samiullah Khan, Julia Messenlehner, Gustav Oberdorfer and Grazia Davidović for providing a friendly lab atmosphere – it would not have been so hard to leave if it wasn't for all of you! A special thank you to those of you who also contributed to the project in one way or another! And to all board game enthusiasts – thanks for enjoyable game evenings

together in the lab as well as elsewhere (thanks especially to Alexandra Binter and Marina Toplak for all lovely invitations)! Thanks also to all bachelor, master and visiting students who contributed to several great moments inside and outside the lab. Further thanks to all technicians; Rosemarie Trenker-El-Toukhy, Eva Frießer, Elfriede Zenzmaier and Alma Makic for valuable help over the years and to Annemarie Lehsl, Tinkara Kristovic and Kristina Schild for helping me with (sometimes annoying) administrative work.

And to the colleagues who became friends – thank you for your support during the last five years! Thanks to Silvia Wallner for always taking the time to visit the lab and for the traditional Christmas cookie baking sessions (this is one of my favorite occasions of the year!) Thanks to Majd Lahham for the late evening ice cream and coffee parties the last year! Thanks to Chanakan Tongsook for all great experiences over the years, many times including food and travelling to unexpected places (and yes, Istanbul is definitely on the way from Graz to Boston), and for taking the time to visit us last year! Thanks to Wolf-Dieter Lienhart for a great time working together on the NQO1 project, for enjoyable times in fitinn and for always making Fridays (or any other day) a time to laugh! Thanks to Chaitanya Tabib for being one of my first friends in Graz, for introducing me to your wonderful wife Savitri Tabib and for starting our travel and board game traditions (and for all combinations thereof). Thank you Shalinee Jha and Karin Koch for all enjoyable times working together and for all wonderful shared moments over the years, and for sometimes making me realize new things about myself and life in general! Finally thanks to all of you for many great times in the lab as well as far away - on our many scientific and unscientific adventures around the world. I'm always looking forward to the next time we meet!

And to all the friends and family that I left behind in the north, thanks for understanding my decision to pursue a PhD not too close to home.

And to Mikael – thank you and at the same time sorry, after too much time too far apart I'm now looking forward to a future together <3

Abstract

NAD(P)H:quinone oxidoreductase 1 (NQO1; EC 1.6.99.2) is a human FAD-dependent enzyme that catalyzes the two-electron reduction of quinones to hydroquinones. NQO1 plays a crucial role in the antioxidant defense system, where it lowers quinone levels and thereby prevents the formation of reactive oxygen species (ROS). The level of NQO1 is also increased in several tumors making it an important target for quinone based anti-cancer prodrugs.

There are two commonly occurring single nucleotide polymorphisms in the *nqo1* gene, *NQO1*2* and *NQO1*3*, that result in protein variants with single amino acid replacements, P187S and R139W, respectively. The distribution of the homozygous *NQO1*2* among the population varies between 2 and 20%, whereas *NQO1*3* is less frequent with a distribution of 0 to 5%. The amino acid exchange P187S has been shown to severely compromise the activity and stability of the enzyme *in vitro* and the *NQO1*2* genotype has been linked to a higher risk for several types of cancer. Additionally, this mutation is associated with poor prognosis after anthracycline-based chemo-therapy. On the other hand, involvement of *NQO1*3* in disease development is not well characterized.

In the first part of this thesis the behavior of the R139W variant was investigated. It could be established that the variant protein displays similar biochemical and structural properties as the wild-type enzyme. Consequently, the diminished enzyme activity reported in cancer cells homozygous to *NQO1*3* could be attributed to an erroneous splicing event. The second part of this thesis explores the possibility of restoring the activity and stability of the NQO1 P187S variant by using small-molecular chaperones. A combination of methods was employed to first identify potential ligands by virtual screening and to characterize the properties of the most promising hit, N-(2-bromophenyl)pyrrolidine-1-sulfonamide (BPPSA), on the stability and activity of the protein in solution. Several biophysical and biochemical measurements indicated that binding of BPPSA to the P187S variant repopulated the native wild-type conformation. As a consequence of the stabilizing effect, the activity of the variant protein is also strongly improved. These results demonstrate that development of molecular chaperones is a promising concept for the stabilization of

unstable protein variants, where the designed molecules can be exploited as a treatment alternative in human diseases caused by protein instability.

Kurzfassung

NAD(P)H:Chinon Oxidoreduktase 1 (NQO1; EC 1.6.99.2) ist ein menschliches FAD-abhängiges Enzym, das die Zwei-Elektronen-Reduktion von Chinonen zu Hydrochinonen katalysiert. Es spielt eine wichtige Rolle im antioxidativen Abwehrsystem, wo es die Anzahl an Chinonen reduziert und so die Bildung von Reaktiven Sauerstoffspezies (ROS) verhindert. Das Level von NQO1 ist auch in mehrere Tumorarten erhöht, was dieses Protein zu einem wichtigen Ziel für die Entwicklung neuer Krebstherapien macht.

Es gibt zwei häufig aufgetretene Einzelnukleotid-Polymorphismen (SNPs) in der Gensequenz von *nqo1*, *NQO1*2* und *NQO1*3*, welche zu den Aminosäure-Austauschen P187S und R139W in den Proteinsequenzen führen. Die Verbreitung von homozygotem *NQO1*2* unter der Bevölkerung variiert zwischen 2 und 20%, während *NQO1*3* mit 0 bis 5% weniger häufig ist. Die Proteinvariante P187S weist verglichen mit dem Wildtyp *in vitro* eine niedrigere enzymatische Aktivität und Stabilität auf. Der *NQO1*2* Genotyp wird mit einem erhöhten Krebsrisiko in Zusammenhang gebracht, außerdem wird diese Mutation mit einer schlechten Prognose bei Anthrazyklin-basierter Chemotherapie assoziiert. Die Beteiligung von *NQO1*3* an der Entstehung von Krankheiten ist hingegen nur unzureichend erforscht.

Im ersten Teil dieser Dissertation werden Eigenschaften der R139W Proteinvariante untersucht. Es konnte gezeigt werden, dass diese Variante ähnliche biochemische und strukturelle Eigenschaften wie das Wildtyp-Enzym aufweist. Die verringerte Enzymaktivität in Krebszellen könnte folglich auf ein fehlerhaftes Splicing zurückgeführt werden

Im zweiten Teil der Arbeit wurde die Möglichkeit untersucht die Aktivität und Stabilität der NQO1 P187S Variante mithilfe kleiner molekularer Chaperone wiederherzustellen. Mithilfe einer Kombination verschiedener Methoden wurden zunächst mögliche Liganden durch virtuelles Screening identifiziert, danach wurde der Einfluss der vielversprechendsten Komponente, N-(2-Bromphenyl)Pyrrolidine-1-Sulfonamid (BPPSA), auf Proteinstabilität und Aktivität untersucht. Mehrere biophysikalische und biochemische Experimente zeigten, dass die Bindung von

BPPSA an die P187S Variante deren Konformation als auch die Aktivität beeinflusst. Diese Ergebnisse zeigen, dass die Entwicklung molekularer Chaperone ein erfolgversprechendes Konzept für die Stabilisierung von instabilen Proteinvarianten darstellt, wobei die entwickelten Liganden als alternative Behandlungsmethode für durch Proteininstabilität verursachte menschliche Krankheiten verwendet werden können.

Part of this thesis has been published in:

1. K. Koch, **E. Strandback**, S. Jha, G. Richter, B. Bourgeois, T. Madl, P. Macheroux, Oxidative stress induced structural changes in the microtubule-associated flavoenzyme Irc15p from *Saccharomyces cerevisiae*. Protein Sci. (2018) doi: 10.1002/pro.3517.
2. K. Koch, A. Hromic, M. Sorokina, **E. Strandback**, M. Reisinger, K. Gruber, P. Macheroux, Structure, biochemical and kinetic properties of recombinant Pst2p from *Saccharomyces cerevisiae*, a FMN-dependent NAD(P)H:quinone oxidoreductase. Biochim Biophys Acta. 1865 (2017) 1046-1056.
3. W.-D. Lienhart[‡], **E. Strandback**[‡], V. Gudipati, K. Koch, A. Binter, M. K. Uhl, D. M. Rantasa, B. Bourgeois, T. Madl, K. Zangger, K. Gruber, P. Macheroux, Catalytic competence, structure and stability of the cancer associated R139W variant of the human NAD(P)H:quinone oxidoreductase 1 (NQO1). FEBS J. 2017, 284(8):1233-1245.

[‡] The first two authors have contributed equally to this work.

Table of Contents

Acknowledgements	IV
Abstract	VI
Kurzfassung.....	VIII
Introduction to flavoproteins and NAD(P)H:quinone oxidoreductase 1	13
Flavoproteins	3
Redox properties of flavins	4
Biological processes	5
Flavoproteins in disease	6
NAD(P)H:quinone oxidoreductase 1.....	7
Structure of NQO1	7
Enzymatic mechanism of NQO1.....	10
Single nucleotide polymorphisms in the <i>nqo1</i> gene	11
Biological roles of NQO1	13
References	17
Characterization of the naturally occurring R139W variant of NAD(P)H:quinone oxidoreductase 1	22
Abstract.....	24
Introduction	26
Results.....	28
Discussion.....	38
Experimental Procedures	41
References.....	46
Rescuing the stability and activity of the P187S variant of NAD(P)H:quinone oxidoreductase 1	51
Abstract.....	53
Introduction	55
Results.....	57

Discussion.....	68
Experimental Procedures	70
References.....	80
Flavoproteins from the yeast <i>Saccharomyces cerevisiae</i>	85
Structure, biochemical and kinetic properties of recombinant Pst2p from <i>Saccharomyces cerevisiae</i>	86
Abstract.....	87
Introduction.....	89
Results	91
Discussion	105
Materials & Methods	107
References	116
Oxidative stress induced structural changes in the microtubule-associated flavoenzyme Irc15p from <i>Saccharomyces cerevisiae</i>	122
Abstract.....	123
Introduction.....	125
Results	128
Discussion	139
Materials & Methods	142
References	150
Curriculum vitae	156
Publication list	158
Presentations at international conferences	159
Other presentations.....	160

CHAPTER 1

Introduction to flavoproteins and NAD(P)H:quinone
oxidoreductase 1

Abbreviations

FMN, flavin mononucleotide; FAD, flavin adenine dinucleotide; AMP, adenosine monophosphate; AIF, apoptosis inducing factor; MICAL, molecule interacting with CasL; LSD1, lysine-specific demethylase 1; NQO1, NAD(P)H:quinone oxidoreductase 1; NAD(P)⁺/NAD(P)H, nicotinamide adenine dinucleotide (phosphate) (oxidized and reduced); ARE, antioxidant response element; Nrf2, nuclear factor erythroid 2-related factor 2; Keap1, Kelch like ECH-associated protein 1; SOD, superoxide dismutase; PARP, poly ADP ribose polymerase; A1AT, alpha 1 antitrypsin

Flavoproteins

Riboflavin, or vitamin B₂, is the precursor of flavin mononucleotide (FMN) and flavin adenine dinucleotide (FAD), the yellow colored cofactors of flavoproteins. As there is no biosynthesis of riboflavin in humans or animals, this makes it an essential part of a healthy diet. Riboflavin (which consists of an isoalloxazine ring system covalently linked to a ribityl chain at the N-10 position) has no role by itself in any human enzyme. Therefore, it has to be modified by riboflavin kinase (EC 2.7.1.26), which phosphorylates the ribityl side chain forming FMN and, when required, further modified by FAD synthetase (EC 2.7.7.2.), which attaches the adenosine monophosphate (AMP) moiety to yield the FAD form. [1-3]

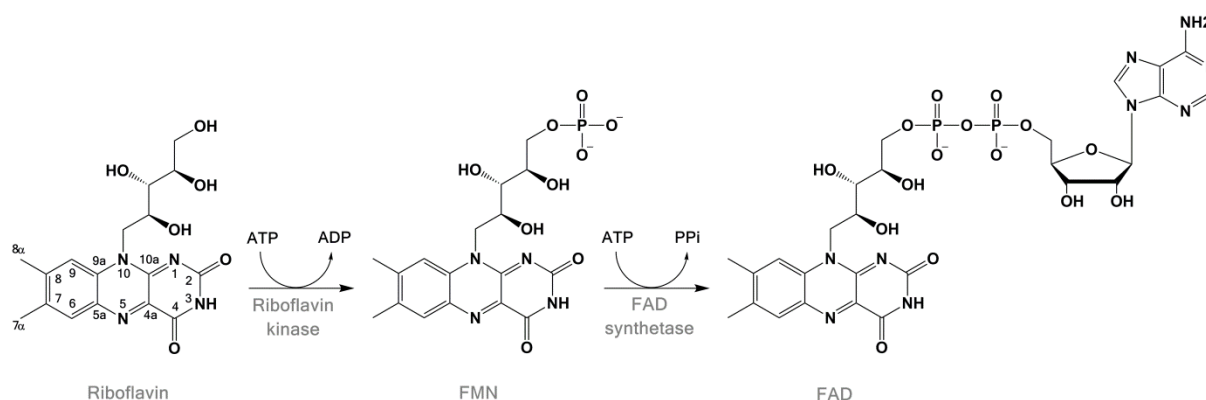


Figure 1. Synthesis of FMN and FAD from riboflavin. [1-3]

Around 1-3% of bacterial and eukaryotic genomes encode for flavin dependent proteins, including 90 genes in the human genome. [1, 3] A majority of flavoproteins, around 75% over all, use FAD as cofactor, whereas 25% use FMN. This ratio is even further shifted in the human flavoproteome, where 84% uses FAD and 16% FMN. Interestingly, there are also five enzymes in humans that require both cofactors. [1, 4] The cofactors are most of the time (90%) bound non-covalently to the protein with a dissociation constant in nanomolar or even lower range. [3, 4] There are, however, also cases where the flavin is covalently attached to the protein. This can happen either at the 8- α or the 6-position of the isoalloxazine ring or occasionally at both sides, and the covalent linkage take place either through one of the nitrogen atoms in the histidine, the thiol group in cysteine, the hydroxyl in tyrosine or the carboxyl group of aspartate. [3, 4] The covalent linkage naturally avoids the dissociation of the

cofactor, increases the protein stability as well as the resistance against proteolysis and increases the oxidative power of the enzyme. [5]

Due to the fact that the flavin cofactor is redox active, which will be discussed in more detail later on, most of the flavoenzymes (around 91%) belong to the oxidoreductases. [4] There are several ways in which flavoproteins can be further classified, including which type of reaction they catalyse, their reactivity towards different substrates, physicochemical properties, sequence and fold. The so called "simple" flavoenzymes can be classified as oxidases, disulphide oxidoreductases, monooxygenases and reductases. The reductases also include dehydrogenases and electron transferases. [6]

Redox properties of flavins

It is the isoalloxazine ring system component of FMN and FAD that constitutes the redox-active part of the cofactors. The side chain of the cofactors, including the AMP moiety and the ribityl phosphate, does not take part in the reaction but is instead important for positioning of the cofactor in the active site of the enzyme. [3, 6, 7] Flavin cofactors can take part in both one- and two-electron transfer reactions as well as in activation of molecular oxygen. The cofactor can consequently exist in three oxidation states; oxidized, one-electron reduced (semi-quinone) and two-electron reduced (hydroquinone) state. The semiquinone can be in a neutral blue form, with an absorbance maximum around 500-600 nm, or in a red anionic form, with an absorbance maximum around 370-400 nm. The semi-quinone form, which is unstable with only around 5% formed in a solution of equimolar amount of oxidized and reduced flavin at pH 7.0, can be either largely stabilized or destabilized based on the interactions with the protein. The large spectral changes observed between the different oxidation states make it possible to follow the changes in the redox state of the flavin during the reaction. [1, 3, 5, 8]

Redox potentials predict how easily the flavin accepts electrons and consequently gives information about the reactivity with different redox substrates as well as provide an estimate of the electrophilicity and nucleophilicity of the isoalloxazine ring. [3] The redox potentials for the two-electron reduction of the free FAD and FMN cofactors at pH 7.0 are -219 mV and -205 mV, respectively, and can be modulated in a range of 600 mV depending on the protein environment. [5, 7] The redox potentials

are highly dependent on the protein environment and are influenced by several factors including charges close to the isoalloxazine ring, hydrogen bonds, pi-stacking, van der Waals interactions, flavin modifications and covalent linkages to the protein. [5, 7]

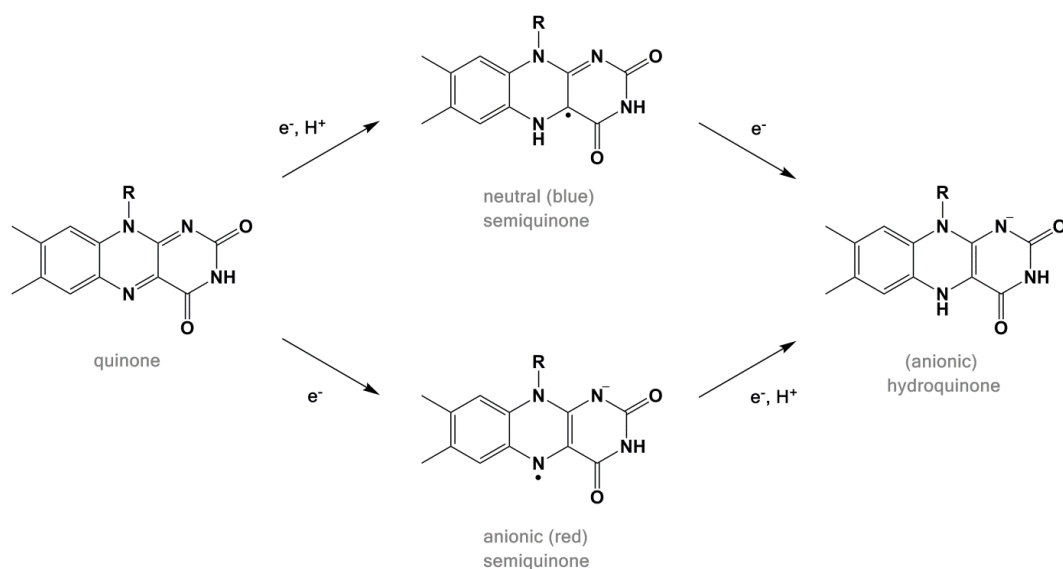


Figure 2. Overview of the redox states of flavin cofactors. The anionic hydroquinone state is usually stabilized in flavoenzymes. [9]

The catalytic cycle of flavoenzyme reactions can generally be divided into a reductive and an oxidative half-reaction, where the two half-reactions can be studied individually by rapid reaction techniques. [3, 6] In the reductive half-reaction the flavin is first reduced by the first substrate, whereafter the second substrate in the oxidative half-reaction will reoxidize the flavin cofactor, usually after dissociation of the first product from the reductive half-reaction. Due to the prevalent reactivity of the reduced cofactor with molecular oxygen, the reductive half-reaction is mostly studied under anaerobic conditions. [6] In most cases one of the half-reactions is the biologically significant one whereas the other mainly restores the original state. [3]

Biological processes

Due to the versatility of reactions that can be catalysed by flavoproteins, they play a central role in a variety of biological processes, which in eukaryotes are mostly localized to the mitochondria. Most flavoenzymes take part in redox reactions in primary metabolic pathways including for example the citric acid cycle, β -oxidation

and degradation of amino acids. Flavoproteins are also involved in the biosynthesis of other cofactors and hormones including for example coenzyme Q, heme, pyridoxal 5-phosphate and steroids. [1] Flavoproteins have furthermore been shown to be involved in induction of apoptosis (apoptosis inducing factor, AIF) [10], regulation of the biological clocks [11], detoxification of aromatic compounds [12], disulphide bond formation in oxidative protein folding [13], axonal growth signalling (molecule interacting with CasL, MICAL) [14], chromatin remodelling (lysine-specific demethylase 1, LSD1) [15] and generation as well as scavenging of reactive oxygen and nitrogen species [16]. [17] Flavoproteins also play a role in several light dependent processes as for example photosynthesis [18], light dependent repair of DNA [19] as well as phototropism [20]. [6]

Flavoproteins in disease

A surprisingly large percentage, around 60%, of the human flavoproteins are linked to diseases caused by mutations in the relevant gene. Since many flavoproteins are localized to the mitochondria, many of the observed diseases are linked to mitochondrial processes. There are also examples where the mutation causes an amino acid exchange that influences the binding of the flavin cofactor to the protein, and in some of these cases it has been suggested that a supplementation of riboflavin could improve the concentration of flavin cofactor and consequently the amount of holo-protein in the cell. In many cases it is unclear how exactly the mutation results in the decreased cofactor binding, making protein substitution one of the best treatment options. [1] NAD(P)H:quinone oxidoreductase 1 (NQO1) is one of these enzymes where a mutation causes a decreased cofactor affinity. This will be discussed in more detail later on (Chapter 2 and 3).

NAD(P)H:quinone oxidoreductase 1

NAD(P)H:quinone oxidoreductase 1 or NQO1 is a human FAD-dependent enzyme that catalyses the two-electron reduction of quinones to hydroquinones by utilizing NADH or NADPH as hydride donor. NQO1 is present as a homodimer with one FAD cofactor per protomer and the enzyme is primarily localized to the cytosol. [21]

Structure of NQO1

NQO1 is a homodimeric protein, where each protomer consists of two domains: the catalytic domain (consisting of 220 residues) that resembles the α/β fold of flavodoxins, and the C-terminal domain (made up of 54 residues), where the adenosine portion of NAD binds. The dimers have a high stability due to the large number of contacts between the protomers. [22-24]

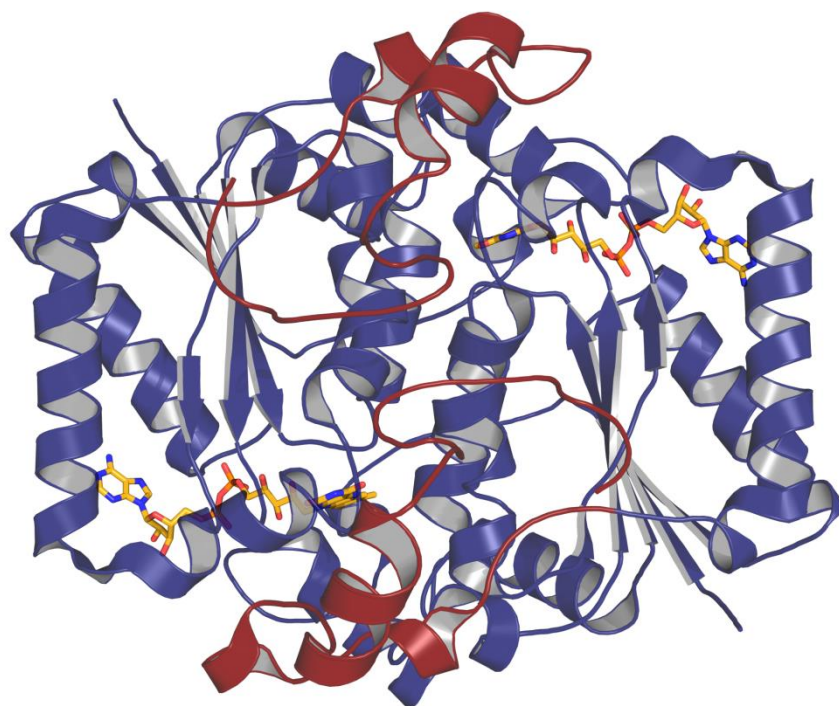


Figure 3. Structure of wild-type NQO1 (PDB code: 1d4a), with the catalytic domain coloured in blue, the C-terminal in red and the FAD cofactor in yellow. The figure was prepared with PyMOL. [25]

The catalytic domain consists of five parallel β -sheets (β 1- β 5) alternating with 5 α -helices (α 1- α 5), with an insertion of two α -helices (α 6 and α 7) and two antiparallel β -sheets (β 6 and β 7) between the second β -sheet and second α -helix. The residues in the insertion are important for stabilization and protect the flavin from interactions

with other proteins. The secondary structure elements are then connected with loops (L1-L8). [22-24]

The C-terminal domain on the other hand consists of two β -sheets ($\beta 8$ and $\beta 9$), an α -helix ($\alpha 8$), two loops (L9-10) and a part of one loop from the catalytic domain (L8). The two catalytic sites are situated on the interface between the two dimers, and are made up of the FAD binding site, a region that binds the adenosine part of NAD(P)H, as well as a substrate binding site, where either the hydride acceptor (quinone substrate) or hydride donor (nicotinamide part of NAD(P)H) binds. The two identical active sites function independently of each other. [22-24]

The isoalloxazine ring of the flavin is situated over loop L4, with which it has many interactions, including the main-chain atoms of residues 105-107 and the side chains of Leu-104 and Gln-105. It also has contact with loop L6, and four groups of the isoalloxazine ring system form hydrogen bonds with groups of the protein. The ribitol, diphosphate and adenosine parts of the flavin molecule are located in the cleft between the N-terminal parts of helices $\alpha 1$ and $\alpha 5$. [22-24]

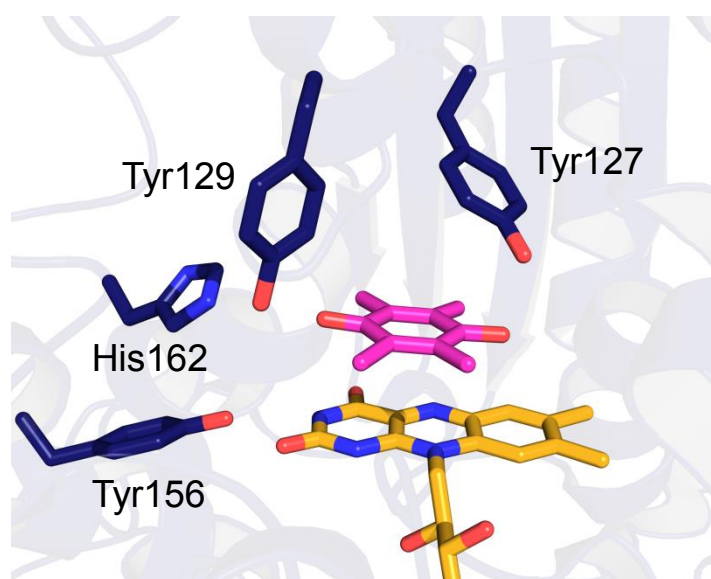


Figure 4. Overview of the active site of NQO1 WT (PDB code: 1d4a) with duroquinone bound as substrate. Duroquinone is situated in a good position for hydride transfer from FADH₂ (here FAD is shown). Tyr-127 and Tyr-129 form hydrogen bonds to the quinone, while His-162 and Tyr-156 are involved in the catalytic mechanism. Adapted from reference [23] with PyMOL. [25]

The substrate binding pocket is made up of the isoalloxazine ring system that creates the floor of the pocket, while Tyr-127' and Tyr-129' from loop 5 form the roof of the pocket. Tyr-127' and Tyr-129' also interact with the substrates. The internal walls are formed by Phe-107, Trp-106 and His-162 of one protomer and Gly-175' and Phe-179' of the other protomer, together with two water molecules. His-162 gives rise to polar interactions that are of mechanistic importance. Substrate binding leads to substantial changes of some residues, including Phe-107, His-162, Phe-233' and Tyr-129'. Additionally, Tyr-129' plays an important role in protecting the C4a-C10a bond of the isoalloxazine ring from attacks by molecular oxygen. [22-24]

Structural information is available for human, rat and mouse NQO1 and shows important differences in the enzymes, resulting in substantial changes in reactivity. The sequence identity is 86% between rat and human, 93% between mouse and rat and 86% between human and mouse, respectively. Interestingly, NQO1 from rat reduces natural substrates, as for example menadione, two to four times faster than the human NQO1. Also, chemotherapeutic prodrugs, including mitomycin C, EO9 and CB1954, are reduced at a faster rate in rat NQO1 as compared to mouse and human NQO1. One of the most significant differences between human and rat NQO1 is the exchange from Tyr-105 in rat to Gln in the human enzyme. The smaller side chain of Gln results in a larger FAD binding pocket in the human and mouse enzymes. Upon reduction of the flavin cofactor, bending of the isoalloxazine ring will therefore take place easier in the human and mouse enzymes, resulting in a more positive redox potential for these enzymes compared to rat NQO1. This is most probably the reason for the faster hydride transfer in the rat enzyme. One further difference occurs at the NAD(P) binding site, where Thr-131 in rat NQO1 is exchanged with Ala in human and mouse NQO1. This exchange results in a larger binding cleft in the case of the human and mouse enzyme, resulting in a lower affinity for NADH in the human and mouse enzymes. Mutagenesis studies of the residues in the two positions 105 and 130 of human and rat NQO1 have confirmed the importance of these residues for the reaction rate. [22, 24, 26]

	β 1	L1	α 1	β 2	α 6	L2	
NQO1_human	MVGRRALIVLAH	SERTS	FNYAMKEAAAAA	LKKKGW	EVVESD	LYAMN	FNPI 50
NQO1_mouse	-AA-----	-K-----	-VE-----	-R-----	-L-----		50
NQO1_rat	-AV-----	-A-----	-VE-----			-L-----	50
	β 6	L3	α 7	β 7	α 2	β 3	
NQO1_human	ISRK	DITGK	LKDPAN	FQYPAES	VLAYKE	GHLS	PDIVAEQKKLEAADLVIF 100
NQO1_mouse	---N---	G---S	K-----	S--S-----	R-----		100
NQO1_rat	---N---	GE--S	E-----	V--S-----	R-----		100
	L4	α 3	L5	β 4			
NQO1_human	QFPLQ	WFGVPA	ILKGW	FERVF	FIGEFAY	TYA	AMYDKGPF
NQO1_mouse	---Q---				LVAG-----		N---QN--T----- 150
NQO1_rat	---Y---				LVAG-----		T-----QN--TL----- 150
	L6	α 4	β 5	L7			
NQO1_human	GSGSMYS	LQGIH	GDMNV	ILWPIQ	SGILH	FCGFQ	VLEPQLTYSIGHTPADA 200
NQO1_mouse	-----	V-----			R-----		V-----P-- 200
NQO1_rat	-----	V-----			R-----		V-----P-- 200
	α 5	L8	β 8	L9	β 9	α 8	
NQO1_human	RIQILE	GWKKR	LENIW	DETP	LYFAP	SSLFD	LNFQAGFLMKKEVQDEEKNK 250
NQO1_mouse	-M-----	TV-E-----					-----E-Q-KN 250
NQO1_rat	-V-V-----	TV-E-S-----					-----L-----E-Q-KN 250
NQO1_human	KFGLSVGHHLGKSIPTDNQIKARK						
NQO1_mouse	-----A-----						
NQO1_rat	-----A-----						

Figure 5. Sequence alignment of human, mouse and rat NQO1 with the secondary structure elements labelled. The alignment is adapted from [22, 24].

Enzymatic mechanism of NQO1

NQO1 has, due to the highly plastic active site, a broad substrate specificity and catalyses the reduction of a wide range of quinones, quinone-imines, dichlorophenolindophenol, methylene blue and azo and nitro compounds. [21, 27] Ortho as well as para quinones can be substrates for NQO1. Due to the obligatory two electron reduction of quinones catalysed by NQO1, formation of reactive oxygen species by one electron reductases can be prevented and therefore NQO1 plays an important role as a detoxifying enzyme. [24] Apart from two-electron reductions, also four-electron reductions of for example azo-dyes and nitro compounds can be catalysed by NQO1. Interestingly, it could be shown that the two protomers of NQO1 function independently in the conversion of two-electron substrates but dependently in the case of four-electron substrates. [28]

Since both the nicotinamide part of NAD(P)H and the quinone bind to the same site, the mechanism has to occur through a ping-pong mechanism. During this process two hydride steps take place: the first one from the NAD(P)H to the FAD and the second from the reduced FADH₂ to the quinone substrate. Residues His-162 and Tyr-156 have been shown to play crucial roles in the mechanism. After the first hydride transfer, a negative charge is formed in the flavin. This charge has to be stabilized, which under normal conditions would happen by moving the negative charge to the N1 position of the isoalloxazine ring. However, since N1 in NQO1 forms a hydrogen bond to Gly-150, the charge has to be stabilized in a different way, most likely through tautomerisation to the enolic form, which positions the negative charge on the O2 in the isoalloxazine ring. Since the OH group of residue Tyr-156 forms a hydrogen bond to O2, a proton can be transferred from Tyr-156. Tyr-156 is then stabilized by the positive charge of His-162.

After NAD(P)⁺ leaves, the quinone substrate binds in such a way that it can easily accept a hydride from FADH₂; consequently the quinone is reduced to its hydroquinolate form at the same time as the flavin is reoxidized. The proton at the O2 position of the isoalloxazine ring is transferred back to Tyr-156 and His-162 is reprotonated again, whereafter it can either transfer a proton to the hydroquinolate or stabilize its negative charge. [23, 24]

Single nucleotide polymorphisms in the *nqo1* gene

There are two commonly occurring single nucleotide polymorphisms in the *nqo1* gene, *NQO1*2* and *NQO1*3*, that result in protein variants with single amino acid replacements, P187S and R139W, respectively. The distribution of the homozygous *NQO1*2* among the population varies between 2 and 20% depending on the ethnic background and has the highest prevalence in the Asian population. [29] *NQO1*3* on the other hand is less frequent with a distribution of 0 to 5%. [30]

The *NQO1*2* genotype is associated with an increased toxicity of benzene and higher risk for several types of cancers including lung, colon, breast and leukemia. Additionally, an adverse breast cancer outcome has been reported after anthracycline-based chemo-therapy, with a survival rate of 17% for patients with the *NQO1*2* genotype compared to 75% for other genotypes [31, 32].

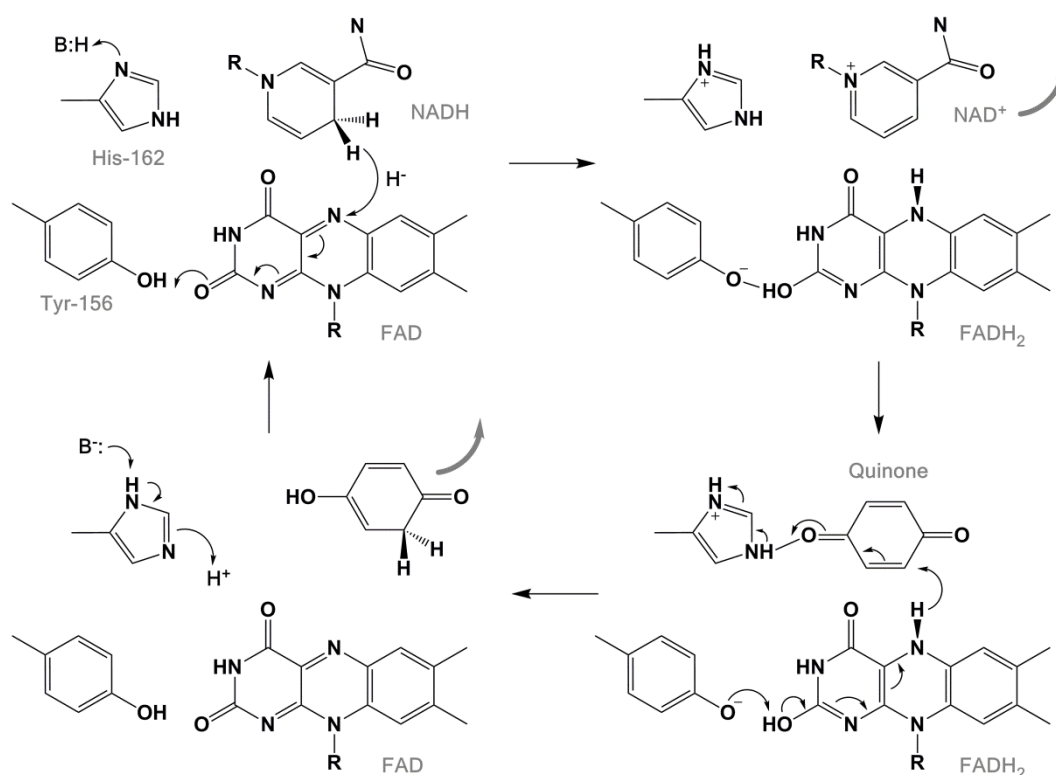


Figure 6. Mechanism of the two-electron reduction of quinones by NQO1. The thick grey arrows indicate that the compound is released from the protein. Adapted from [23, 24].

A recent study investigated the structural characteristics of the NQO1 P187S variant and concluded that the single amino acid exchange destabilizes interactions between the core and C-terminal domain of the variant protein in solution. It has also been shown that the cofactor affinity and consequently also the activity are negatively affected in the variant protein as a consequence of the structural instability [33].

On the other hand, involvement of *NQO1*3* in disease development is not well characterized. It has been demonstrated that the nucleotide transition changes the splicing of pre-mRNA, leading to exon-4-deleted mRNA, thus explaining the decreased amount of correctly spliced protein in HCT-116R30A cells. [34] A biochemical and structural study of the NQO1 R39W variant is the main topic of Chapter 2.

Biological roles of NQO1

NQO1 has been shown to be highly inducible under oxidative stress conditions as a mechanism of the cellular protection system. [35] The Keap1/Nrf2/ARE pathway mediates the induction of the *nqo1* gene; this pathway is involved in controlling the expression of over 100 cytoprotective genes. The pathway involves three main components: the antioxidant response element (ARE, which are sequences in the regulatory part of the genes), the nuclear factor erythroid 2–related factor 2 (Nrf2, which is a leucine zipper transcription factor that together with a small Maf protein binds to the ARE), and Kelch like ECH-associated protein 1 (Keap1). The latter is a repressor protein that binds Nrf2 and promotes the ubiquitination and proteasomal degradation of the transcription factor by working as an adapter to Cul3-based E3 ligase. Under stress conditions reactive cysteine residues of Keap1 are modified by inducers that react with sulfhydryl groups of the protein. Because of these modifications, Keap1 undergoes a conformational change and can no longer target Nrf2 for degradation. The stabilized transcription factor then translocates to the nucleus where it binds to ARE, thereby triggering expression of NQO1, see Figure 7. [36, 37]

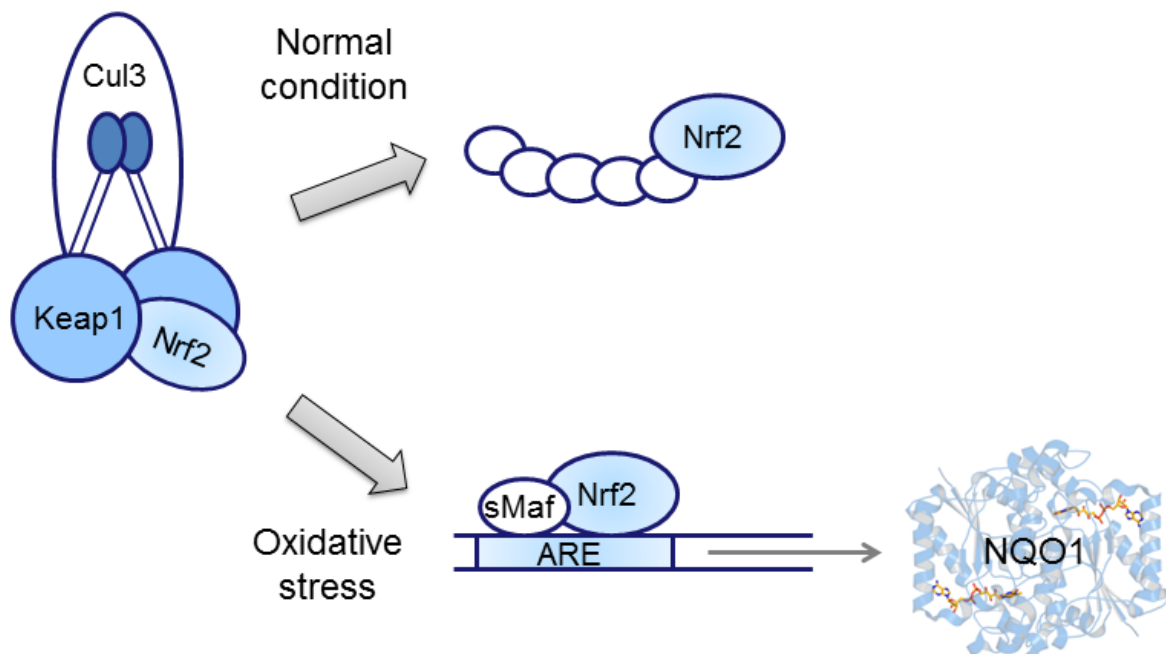


Figure 7. Overview of the Keap1/Nrf2/ARE pathway and how it leads to the expression of NQO1. Adapted from reference [36].

The reduction of quinones to hydroquinones is highly efficiently catalysed by NQO1. As already mentioned, the two-electron reduction prevents formation of semiquinones and consequently prevents the formation of reactive oxygen species. The hydroquinone formed can, depending on the properties of the compound, either result in detoxification or toxicity. [35] NQO1 can for example reduce the endogenous substrates coenzyme Q9 and coenzyme Q10 and α -tocopherol quinone, thereby forming the antioxidant version of these compounds. These compounds are crucial for the redox system of the plasma membrane and hence help in the protection against oxidative stress and lipid peroxidation. [38] NQO1 has been shown to be overexpressed in many tumours, including breast, lung, colon and liver, making it an ideal target for anti-cancer therapy. Since the level of NQO1 is increased in many tumours compared to normal tissue, many anticancer prodrugs that can be bioactivated by NQO1 have been developed. [27] Examples of compounds that can be activated by NQO1 include mitomycin C, E09, β -lapachone and CB1954. The chemical structures can be seen in Figure 8. [21, 24, 39]

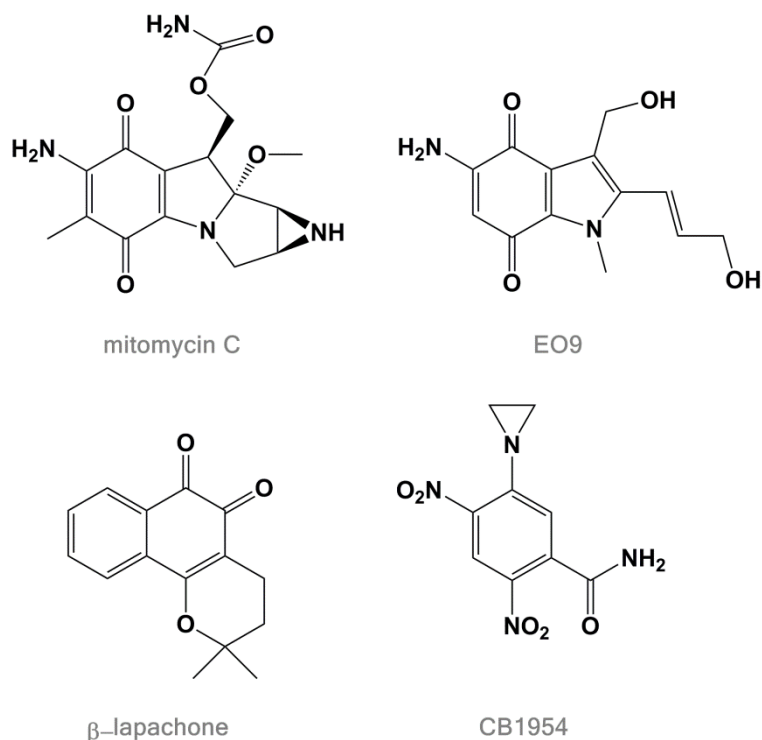


Figure 8. Chemical structure of mitomycin C, E09, β -lapachone and CB1954, all are prodrugs that can be activated by NQO1. [21, 24, 39]

NQO1 also shows a limited superoxide reductase activity because of the flavin cofactor that can reduce superoxide and form hydrogen peroxide. However, unless the level of NQO1 is very high in comparison to the level of superoxide dismutase (SOD), it is unlikely that this activity is of relevance to the cell. [35, 38]

The redox modulation of NAD(P)H/NAD(P)⁺ due to the conversion of different quinone substrates by NQO1 is also suggested to be of importance since higher levels of NAD⁺ can result in activation of poly ADP ribose polymerase (PARP) and sirtuins. [35] PARP is involved in DNA repair caused by oxidative stress, whereas sirtuins have been demonstrated to play a protective role against oxidative stress. [38]

Apart from the biological functions directly related to the enzymatic activity, NQO1 also demonstrates other important roles. These include for example the interaction of NQO1 with tumour suppressors like p53, p33 and p73, resulting in protection of these tumour suppressors from ubiquitin-independent degradation by the 20S proteasome. [40-42]

NQO1 has also been shown to be involved in the polymerization of microtubule, since inhibition of the enzyme turned out to be associated with microtubule depolymerisation. A possible explanation for the involvement of NQO1 could be that some quinone substrates need to be reduced by NQO1 in order to avoid depolymerisation. Another option could be that there is a direct interaction between NQO1 and microtubule, or alternatively that tubulin is a substrate of NQO1. [43]

NQO1 has also been identified as one of several FAD oxidoreductases that bind to mRNA. It could be demonstrated that NQO1 binds to mRNAs in human HepG2 cells, including the SERPINA1 mRNA, which encodes alpha 1 antitrypsin (A1AT), consequently leading to an elevated translation. It is therefore possible that NQO1 plays a role in controlling translation. [35, 38, 44]

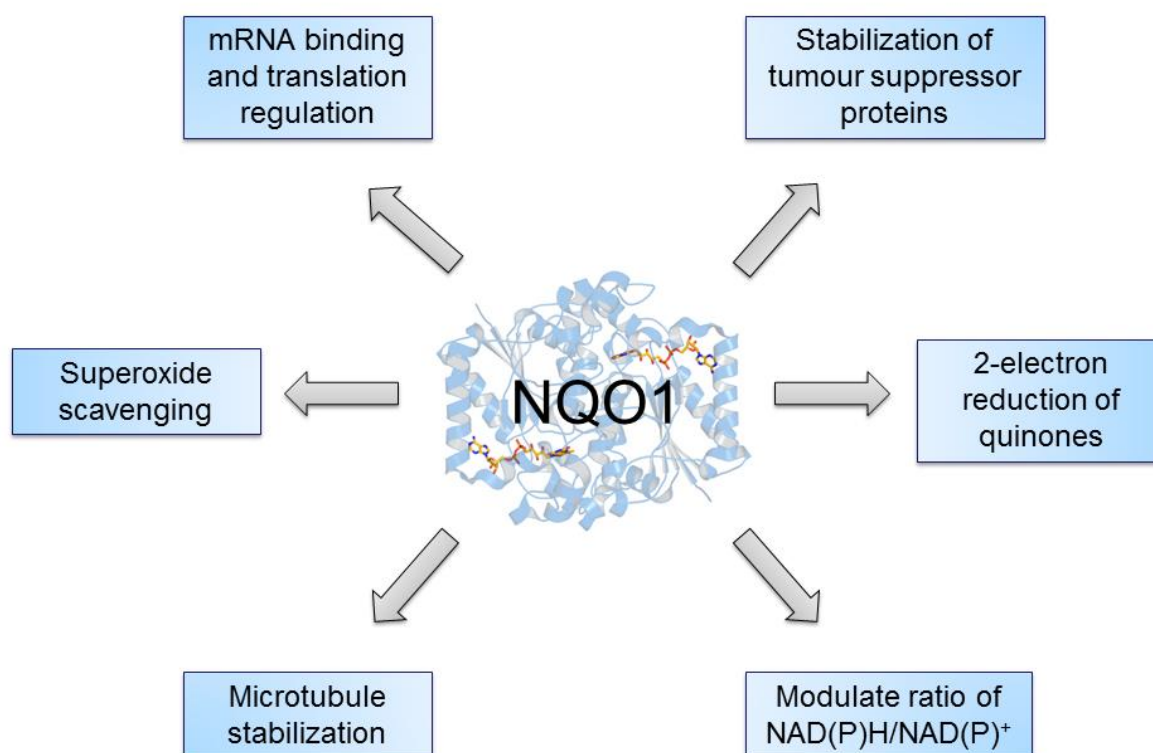


Figure 9. Summary of the different functions of NQO1, the scheme is adapted from [35, 36].

References

- [1] W. D. Lienhart, V. Gudipati, P. Macheroux, The human flavoproteome, *Arch. Biochem. Biophys.* 535 (2013) 150-162.
- [2] P. Macheroux, UV-visible spectroscopy as a tool to study flavoproteins, *Methods Mol. Biol.* 131 (1999) 1-7.
- [3] R. L. Fagan, B. A. Palfey, 7.03 - Flavin-Dependent Enzymes, *Comprehensive Natural Products II* (2010)37-113.
- [4] P. Macheroux, B. Kappes, S. E. Ealick, Flavogenomics--a genomic and structural view of flavin-dependent proteins, *Febs J.* 278 (2011) 2625-2634.
- [5] R. H. H. van den Heuvel, M. W. Fraaije, W. J. H. van Berkel, Redox properties of vanillyl-alcohol oxidase, *Meth. Enzymol.* 353 (2002) 177-186.
- [6] V. Massey, The chemical and biological versatility of riboflavin, *Biochem. Soc. Trans.* 28 (2000) 283-296.
- [7] S. Ghisla, V. Massey, Mechanisms of flavoprotein-catalyzed reactions, *Eur. J. Biochem.* 181 (1989) 1-17.
- [8] A. M. Edwards, Structure and general properties of flavins, *Methods Mol. Biol.* 1146 (2014) 3-13.
- [9] W. J. H. van Berkel, "Flavoenzymes, chemistry of," in *Wiley Encyclopedia of Chemical Biology*, T. P. Begley, Ed. 2008.
- [10] S. A. Susin, H. K. Lorenzo, N. Zamzami, I. Marzo, B. E. Snow, G. M. Brothers, J. Mangion, E. Jacotot, P. Costantini, M. Loeffler, N. Larochette, D. R. Goodlett, R. Aebersold, D. P. Siderovski, J. M. Penninger, G. Kroemer, Molecular characterization of mitochondrial apoptosis-inducing factor, *Nature* 397 (1999) 441-446.
- [11] S. M. Reppert, D. R. Weaver, Coordination of circadian timing in mammals, *Nature* 418 (2002) 935-941.

- [12] B. Entsch, B. Van, Structure and mechanism of para-hydroxybenzoate hydroxylase, *FASEB Journal* 9 (1995) 476-483.
- [13] E. Gross, D. B. Kastner, C. A. Kaiser, D. Fass, Structure of Ero1p, source of disulfide bonds for oxidative protein folding in the cell, *Cell* 117 (2004) 601-610.
- [14] J. R. Terman, T. Mao, R. J. Pasterkamp, H. Yu, A. L. Kolodkin, MICALs, a family of conserved flavoprotein oxidoreductases, function in plexin-mediated axonal repulsion, *Cell* 109 (2002) 887-900.
- [15] Y. Shi, F. Lan, C. Matson, P. Mulligan, J. R. Whetstine, P. A. Cole, R. A. Casero, Y. Shi, Histone demethylation mediated by the nuclear amine oxidase homolog LSD1, *Cell* 119 (2004) 941-953.
- [16] M. Fransen, M. Nordgren, B. Wang, O. Apanasets, Role of peroxisomes in ROS/RNS-metabolism: implications for human disease, *Biochim. Biophys. Acta*, 1822 (2012) 1363-1373.
- [17] M. Barile, T. A. Giancaspero, P. Leone, M. Galluccio, C. Indiveri, Riboflavin transport and metabolism in humans, *J. Inherit. Metab. Dis.* 39 (2016) 545-557.
- [18] M. Medina, Structural and mechanistic aspects of flavoproteins: photosynthetic electron transfer from photosystem I to NADP⁺, *FEBS J.* 276 (2009) 3942-3958.
- [19] M. S. Jorns, B. Wang, S. P. Jordan, DNA repair catalyzed by *Escherichia coli* DNA photolyase containing only reduced flavin: elimination of the enzyme's second chromophore by reduction with sodium borohydride, *Biochemistry* 26 (1987) 6810-6816.
- [20] J. M. Christie, P. Reymond, G. K. Powell, P. Bernasconi, A. A. Raibekas, E. Liscum, W. R. Briggs, Arabidopsis NPH1: A flavoprotein with the properties of a photoreceptor for phototropism, *Science* 282 (1998) 1698-1701.

- [21] D. Ross, J. K. Kepa, S. L. Winski, H. D. Beall, A. Anwar, D. Siegel, NAD(P)H:quinone oxidoreductase 1 (NQO1): chemoprotection, bioactivation, gene regulation and genetic polymorphisms, *Chem. Biol. Interact.* 129 (2000) 77-97.
- [22] M. Faig, M. A. Bianchet, P. Talalay, S. Chen, S. Winski, D. Ross, L. M. Amzel, Structures of recombinant human and mouse NAD(P)H:quinone oxidoreductases: species comparison and structural changes with substrate binding and release, *Proc. Natl. Acad. Sci. USA* 97 (2000) 3177-3182.
- [23] R. Li, M. A. Bianchet, P. Talalay, L. M. Amzel, The three-dimensional structure of NAD(P)H:quinone reductase, a flavoprotein involved in cancer chemoprotection and chemotherapy: mechanism of the two-electron reduction, *Proc. Natl. Acad. Sci. USA* 92 (1995) 8846-8850.
- [24] M. A. Bianchet, M. Faig, L. M. Amzel, Structure and mechanism of NAD[P]H:quinone acceptor oxidoreductases (NQO), *Meth. Enzymol.* 382 (2004) 144-174.
- [25] Schrödinger LLC, The PyMOL Molecular Graphics System Version 1.5.0.4.
- [26] S. Chen, R. Knox, K. Wu, P. S. Deng, D. Zhou, M. A. Bianchet, L. M. Amzel, Molecular basis of the catalytic differences among DT-diaphorase of human, rat, and mouse, *J. Biol. Chem.* 272 (1997) 1437-1439.
- [27] D. Ross, D. Siegel, NAD(P)H:quinone oxidoreductase 1 (NQO1, DT-diaphorase), functions and pharmacogenetics, *Meth. Enzymol.* 382 (2004) 115-144.
- [28] K. Cui, A. Y. Lu, C. S. Yang, Subunit functional studies of NAD(P)H:quinone oxidoreductase with a heterodimer approach, *Proc. Natl. Acad. Sci. USA* 92 (1995) 1043-1047.
- [29] K. T. Kelsey, D. Ross, R. D. Traver, D. C. Christiani, Z. F. Zuo, M. R. Spitz, M. Wang, X. Xu, B. K. Lee, B. S. Schwartz, J. K. Wiencke, Ethnic variation in the prevalence of a common NAD(P)H quinone oxidoreductase polymorphism and

- its implications for anti-cancer chemotherapy, *Br. J. Cancer* 76 (1997) 852-854.
- [30] A. Gaedigk, R. F. Tyndale, M. Jurima-Romet, E. M. Sellers, D. M. Grant, J. S. Leeder, NAD(P)H:quinone oxidoreductase: polymorphisms and allele frequencies in Caucasian, Chinese and Canadian Native Indian and Inuit populations, *Pharmacogenetics* 8 (1998) 305-313.
- [31] D. W. Nebert, A. L. Roe, S. E. Vandale, E. Bingham, G. G. Oakley, NAD(P)H:quinone oxidoreductase (NQO1) polymorphism, exposure to benzene, and predisposition to disease: a HuGE review, *Genetics in Medicine : Official Journal of the American College of Medical Genetics* 4 (2002) 62-70.
- [32] R. Fagerholm, B. Hofstetter, J. Tommiska, K. Aaltonen, R. Vrtel, K. Syrjakoski, A. Kallioniemi, O. Kilpivaara, A. Mannermaa, V. M. Kosma, M. Uusitupa, M. Eskelinen, V. Kataja, K. Aittomaki, K. von Smitten, P. Heikkila, J. Lukas, K. Holli, J. Bartkova, C. Blomqvist, J. Bartek, H. Nevanlinna, NAD(P)H:quinone oxidoreductase 1 NQO1*2 genotype (P187S) is a strong prognostic and predictive factor in breast cancer, *Nat. Genet.* 40 (2008) 844-853.
- [33] W. D. Lienhart, V. Gudipati, M. K. Uhl, A. Binter, S. A. Pulido, R. Saf, K. Zangger, K. Gruber, P. Macheroux, Collapse of the native structure caused by a single amino acid exchange in human NAD(P)H:quinone oxidoreductase 1, *The FEBS Journal* 281 (2014) 4691-4704.
- [34] S. S. Pan, Y. Han, P. Farabaugh, H. Xia, Implication of alternative splicing for expression of a variant NAD(P)H:quinone oxidoreductase-1 with a single nucleotide polymorphism at 465C>T, *Pharmacogenetics* 12 (2002) 479-488.
- [35] D. Ross, D. Siegel, Functions of NQO1 in Cellular Protection and CoQ10 Metabolism and its Potential Role as a Redox Sensitive Molecular Switch, *Front. Physiol.* 8 (2017) 595.
- [36] A. T. Dinkova-Kostova, P. Talalay, NAD(P)H:quinone acceptor oxidoreductase 1 (NQO1), a multifunctional antioxidant enzyme and exceptionally versatile cytoprotector, *Arch. Biochem. Biophys.* 501 (2010) 116-123.

- [37] B. E. Hast, D. Goldfarb, K. M. Mulvaney, M. A. Hast, P. F. Siesser, F. Yan, D. N. Hayes, M. B. Major, Proteomic analysis of ubiquitin ligase KEAP1 reveals associated proteins that inhibit NRF2 ubiquitination, *Cancer Res.* 73 (2013) 2199-2210.
- [38] D. Ross, D. Siegel, NQO1 in protection against oxidative stress, *Curr. Opin. Toxicol.* 7 (2018) 67-72.
- [39] D. Siegel, C. Yan, D. Ross, NAD(P)H:quinone oxidoreductase 1 (NQO1) in the sensitivity and resistance to antitumor quinones, *Biochem. Pharmacol.* 83 (2012) 1033-1040.
- [40] G. Asher, P. Tsvetkov, C. Kahana, Y. Shaul, A mechanism of ubiquitin-independent proteasomal degradation of the tumor suppressors p53 and p73, *Genes Dev.* 19 (2005) 316-321.
- [41] O. Moscovitz, P. Tsvetkov, N. Hazan, I. Michaelievski, H. Keisar, G. Ben-Nissan, Y. Shaul, M. Sharon, A mutually inhibitory feedback loop between the 20S proteasome and its regulator, NQO1, *Mol. Cell* 47 (2012) 76-86.
- [42] M. Garate, R. P. Wong, E. I. Campos, Y. Wang, G. Li, NAD(P)H quinone oxidoreductase 1 inhibits the proteasomal degradation of the tumour suppressor p33(ING1b), *EMBO Rep.* 9 (2008) 576-581.
- [43] S. M. Wignall, N. S. Gray, Y. Chang, L. Juarez, R. Jacob, A. Burlingame, P. G. Schultz, R. Heald, Identification of a novel protein regulating microtubule stability through a chemical approach, *Chem. Biol.* 11 (2004) 135-146.
- [44] A. Di Francesco, C. Di Germanio, A. C. Panda, P. Huynh, R. Peadar, I. Navas-Enamorado, P. Bastian, E. Lehrmann, A. Diaz-Ruiz, D. Ross, D. Siegel, J. L. Martindale, M. Bernier, M. Gorospe, K. Abdelmohsen, R. de Cabo, Novel RNA-binding activity of NQO1 promotes SERPINA1 mRNA translation, *Free Radic. Biol. Med.* 99 (2016) 225-233.

Chapter 2

Characterization of the naturally occurring R139W variant of
NAD(P)H:quinone oxidoreductase 1

Catalytic competence, structure and stability of the cancer associated R139W variant of the human NAD(P)H:quinone oxidoreductase 1 (NQO1)

Wolf-Dieter Lienhart^{1‡}, Emilia Strandback^{1‡}, Venugopal Gudipati¹, Karin Koch¹, Alexandra Binter¹, Michael K. Uhl², David M. Rantasa¹, Benjamin Bourgeois³, Tobias Madl³, Klaus Zangger⁴, Karl Gruber² and Peter Macheroux¹

¹Institute of Biochemistry, Graz University of Technology, Austria

²Institute of Molecular Biosciences, University of Graz, Austria

³Institute of Molecular Biology and Biochemistry, Austria

⁴Institute of Chemistry, University of Graz, Austria

Author contributions

‡ The first two authors have contributed equally to this work.

K.G. and P.M. initiated the project; W.-D.L., E.S., V.G., M.K.U., K.Z., K.G. and P.M. designed the experiments and analysed the data; W.-D.L., E.S. and V.G. expressed and purified NQO1; M.K.U. and K.G. crystallized NQO1 and determined the crystal structure; W.-D.L., E.S., V.G., K.K., A.B. and D.M.R. performed analytical and biochemical experiments, and determined dissociation constants as well as kinetic parameters; K.Z. performed NMR-experiments; B.B. and T.M. performed and interpreted SAXS measurements; W.-D.L., E.S., V.G., M.K.U., K.Z., K.G. and P.M. wrote the manuscript.

Abstract

The human NAD(P)H:quinone oxidoreductase 1 (NQO1; EC 1.6.99.2) is an essential enzyme in the antioxidant defence system. Furthermore, NQO1 protects tumour suppressors like p53, p33^{ING1b} and p73 from proteasomal degradation. The activity of NQO1 is also exploited in chemotherapy for the activation of quinone-based treatments. Various single nucleotide polymorphisms are known, such as *NQO1*2* and *NQO1*3* yielding protein variants of NQO1 with single amino acid replacements, *i.e.* P187S and R139W, respectively. While the former NQO1 variant is linked to a higher risk for specific kinds of cancer, the role, if any, of the arginine 139 to tryptophan exchange in disease development remains obscure. On the other hand, mitomycin C resistant human colon cancer cells were shown to harbour the *NQO1*3* variant resulting in substantially reduced enzymatic activity. However, the molecular cause for this decrease remains unclear. In order to resolve this issue, recombinant NQO1 R139W has been characterized biochemically and structurally. In this report we show by X-ray crystallography and 2D-NMR spectroscopy that this variant adopts the same structure both in the crystal as well as in solution. Furthermore, the kinetic parameters obtained for the variant are similar to those reported for the wild-type protein. Similarly, thermostability of the variant was only slightly affected by the amino acid replacement. Therefore, we conclude that the previously reported effects in human cancer cells cannot be attributed to protein stability or enzyme activity. Instead it appears that loss of exon 4 during maturation of a large fraction of pre-mRNA is the major reason of the observed lack of enzyme activity and hence reduced activation of quinone-based chemotherapeutics.

Abbreviations

ITC, isothermal titration microcalorimetry; NQO1; NAD(P)H:quinone oxidoreductase 1; PDB, Protein Data Bank; SAXS, small-angle X-ray scattering; SNP, single-nucleotide polymorphism; WT, wild-type

Keywords

cancer, crystal structure, enzyme kinetics, microcalorimetry, NMR-spectroscopy, single nucleotide polymorphism.

Introduction

NAD(P)H:quinone oxidoreductase 1 (NQO1; EC 1.6.99.2) [1] is an important enzyme in the human antioxidant defence system. Among other functions, the dimeric flavoprotein is catalysing the conversion of quinones to hydroquinones preventing the formation of semiquinone radicals [2]. Yet another important role is the regulation and stabilisation of various tumour suppressors like p33^{ING1b}, p53 and p73. This effect appears to be related to the interaction of NQO1 with the 20S proteasome in a NADH dependent manner [3,4]. Single nucleotide polymorphisms result in the expression of different protein variants of NQO1. The two most prevalent variants in the human population are *NQO1*2* (*NQO1* 609C>T; NQO1 P187S; allelic frequency: 0.22-0.47) and *NQO1*3* (*NQO1* 465C>T; NQO1 R139W; allelic frequency: 0.00-0.05), which are connected to a higher risk for specific cancers [5-11]. Several studies have focused on *NQO1*2* and have shown a reduction or even a loss of the enzymatic activity of NQO1 P187S [12-14]. Furthermore, this single nucleotide polymorphism (SNP) gives rise to reduced stability of the protein and to a loss of the FAD cofactor. On the other hand, the involvement of *NQO1*3* in the development of cancer is currently unclear. Initial observations indicated that splicing of the transcript of *NQO1*3* yields mature mRNA lacking exon 4, which consequently leads to the loss of the FAD binding domain [15]. In the mitomycin C resistant tumour cell lines HCT 116-R30A solely the mRNA of *NQO1*3* could be detected while in the mitomycin C sensitive HCT 116 cell line mRNAs of *NQO1*1* and *NQO1*3* were detectable [16]. These findings led to the assumption that the higher cancer risk for the *NQO1*3* polymorphism might be caused by erroneous splicing of the pre-mRNA derived from *NQO1*3*. As a matter of fact, the nucleotide transition found in *NQO1*3* disrupts the consensus sequence of the 5' splicing site required for the correct splicing by the spliceosome and thus rationalizes the observations mentioned above [11]. Since the full length mRNA of *NQO1*3* is still representing one to two thirds of the whole mRNA [11], it is unclear if the higher risk for specific cancers can be explained solely by erroneous splicing. Thus far enzyme activities were determined only in cell extracts [11] or with the unspecific redox dye DCPIP [17] but not with a quinone substrate. Moreover, information concerning the potential impact of the R139W exchange on structural properties of the enzyme is currently not available.

A loss of enzymatic activity is increasing the toxicity of benzene as well as aggravating the cancer treatment of patients [18]. The broad substrate specificity of NQO1 allows the activation of chemotherapeutic prodrugs, like mitomycin C or β -lapachone. Since various tumours are upregulating the NQO1 levels, these chemotherapeutics are acting more specific on cancer than healthy cells [19-21]. The success of the prevalent cancer treatment with cisplatin is also affected by the NQO1 activity. One limitation for the use of cisplatin is the induced nephrotoxicity. Activation of NQO1 can improve the negative effects of the treatment to the kidneys while a loss of enzyme activity can cause an accelerated damage of the renal system [22]. Taken together the status of NQO1 expression and activity is essential for the success of quinone-based chemotherapies and therefore detailed biochemical and structural studies are paramount to generate a sound basis for the development and design of cancer intervention strategies.

In order to remedy the current lack of sound biochemical information on the NQO1 R139W variant, we have undertaken a biochemical, enzymatic and structural investigation to fully comprehend the effect of this widely occurring variant of the human enzyme.

Results

Expression and basic biochemical characterisation of the R139W variant

Heterologous expression of the NQO1 R139W variant in *E. coli* BL21 yielded similar amounts of soluble protein as was previously reported for wild-type NQO1 [14]. Preparations of the R139W variant showed the typical yellow colour indicating that the protein tightly binds the FAD cofactor in stark contrast to the P187S variant that was isolated largely as an apo-protein [14]. Further analysis showed that wild-type NQO1 and the R139W variant have nearly identical absorption spectra with maxima at 375 and 450 nm (Figure 1). In addition, titration of apo-proteins with FAD gave rise to a similar difference absorption spectrum indicating that the FAD binding pockets provided by wild-type NQO1 and the R139W variant are comparable (Figure 1).

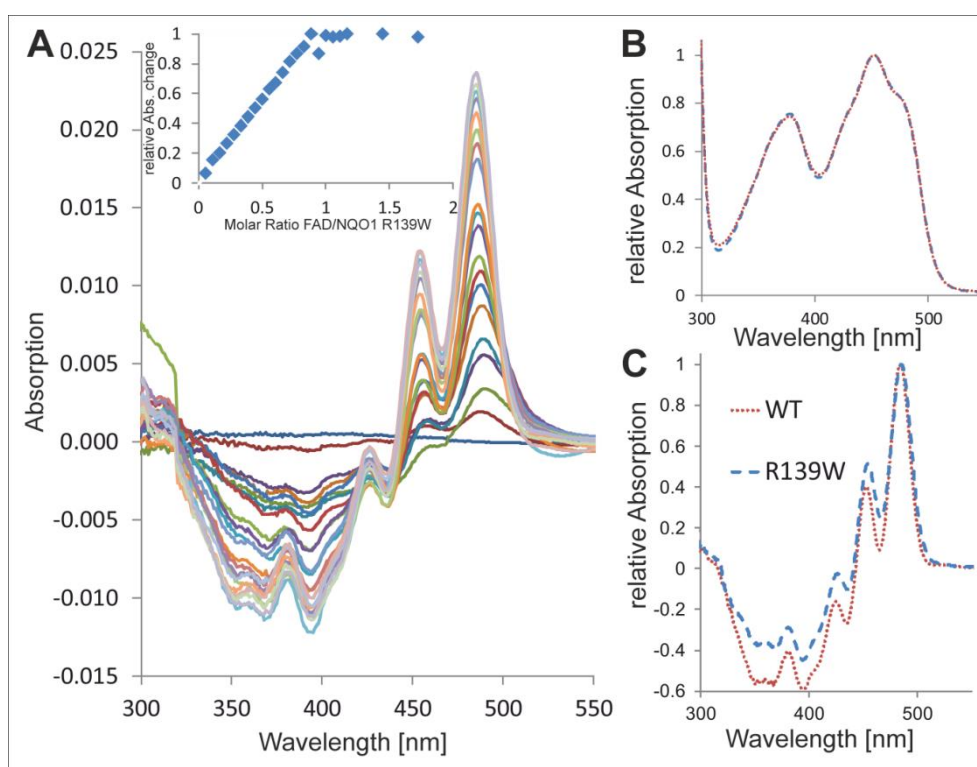


Figure 1. UV-visible and difference titration absorption spectra of wild-type NQO1 and NQO1 R139W. A: Difference titration spectra of 800 μ l NQO1 R139W (45 μ M) with 0-42 μ l in 2 μ l intervals FAD (1 mM). The insert shows the change of the absolute absorption values at 436 nm and 455nm against the FAD/protein molar ratio with two additional points (with additional 10 μ l FAD each) compared to the main figure. B: Absorption spectra of wild-type NQO1 and NQO1 R139W normalised to the maximum at 450 nm. C: Difference titration spectra of wild-type NQO1 and NQO1 R139W with protein/FAD ratio of 1 normalised to the maximum at 480 nm.

The melting points of the NQO1 WT and NQO1 R139W variant were determined in different buffers and showed a decrease of 2 °C for the R139W variant. Measurements with SYPRO® Orange of the holo- and apo-form of the proteins showed a decrease of the melting points for the apoprotein. The small differences of the melting points observed between FAD and SYPRO® Orange may indicate that the latter has an adverse effect of thermal stability by promoting the unfolding of the protein (Table 1).

Table 1. Thermostability measurements. Melting points were determined with a CFX Connect™ Real-Time PCR Detection System under different buffer and salt conditions of NQO1 and NQO1 R139W with FAD or SYPRO® Orange as fluorescent reporter. Melting points are given in °C (values given are the average of two independent measurements).

Buffer	NQO1	NQO1 R139W
50 mM potassium phosphate, pH 7	54.0	52.0
50 mM sodium phosphate, pH 7	54.0	52.0
50 mM Tris/Cl, pH 7	54.5	52.5
50 mM HEPES, pH 7	56.0	54.0
Holoprotein in 50 mM HEPES, pH 7 +SYPRO® Orange	52.8	51.2
Apoprotein in 50 mM HEPES, pH 7 +SYPRO® Orange	50.8	48.5

Isothermal titration calorimetry and small-angle X-ray scattering

To obtain quantitative information on the binding affinity of the FAD cofactor to the R139W variant isothermal titration calorimetry experiments were conducted. As reported recently, reproducible measurements are obtained by titration of a fixed concentration of FAD with apo-protein [14]. The raw data could be nicely fitted to a one binding site model [14] (Figure 2). The average of three measurements was used to determine the K_D values for the NQO1 R139W variant as 155 ± 27 nM, which is 2.5-fold higher than the K_D for wild-type enzyme [14]. Thus it can be concluded that the arginine to tryptophan replacement has only a marginal effect on the binding affinity of the FAD cofactor.

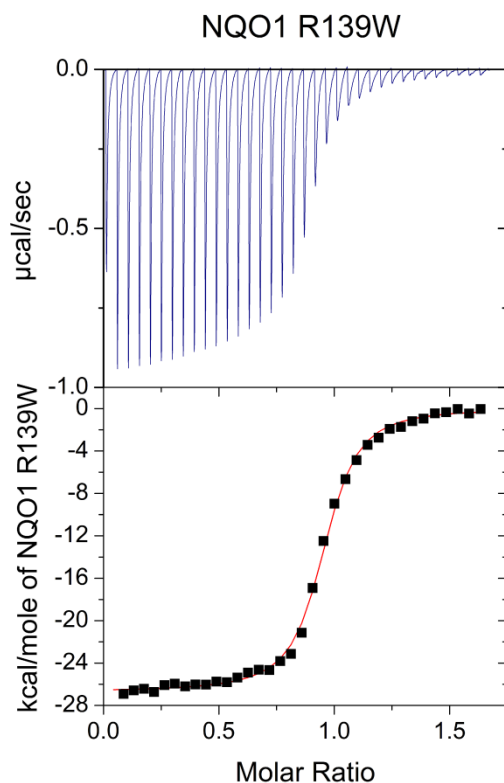


Figure 2. ITC measurement of NQO1 R139W. NQO1 R139W: 35 injections with 6 μl of 298 μM NQO1 R139W apoprotein solution in 29 μM FAD solution and 300 seconds spacing (top) at 25 $^{\circ}\text{C}$. From three independent measurements under the same conditions the dissociation constant was calculated to $K_D = 155 \pm 27$ nM. Data was fitted using the one binding site model.

In this context it is important to note, that the experimental set-up of the ITC experiment is critical to obtain reliable data both in terms of stoichiometry and the dissociation constant. In principal, reversal of the order of titration should not influence the outcome of the experiment in terms of the model used to fit the raw data. However, when apo-proteins (wild-type as well as the R139W variant) were titrated with FAD the raw data could not be satisfactorily fitted with a one binding site model. Instead, the raw data were best fitted to a two binding site model, a result that is difficult to reconcile with the structural identity of the two FAD binding pockets in the homodimeric protein (Figure 3; data with wild-type).

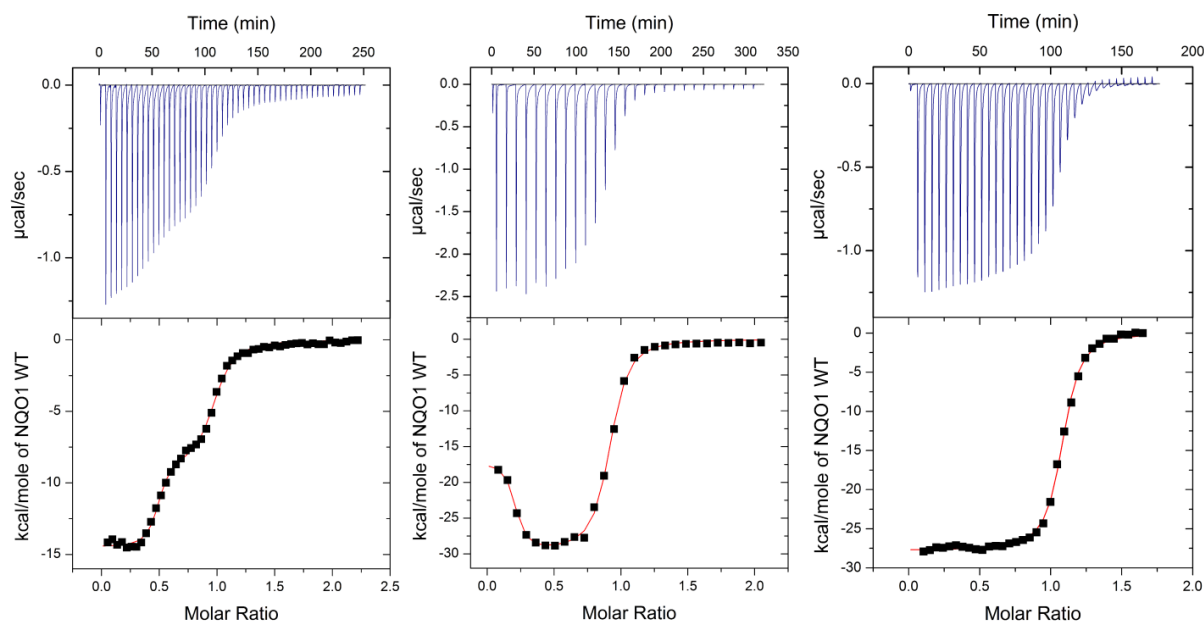


Fig. 3. ITC measurements of NQO1 wild-type in HEPES buffer. The left and the middle measurements were conducted with apo-NQO1 in the sample cell of the microcalorimeter and FAD in the injection syringe. Data was fitted using the two binding site model. Left: First injection with 2 μl and 49 injections with 6 μl of 477 μM FAD solution in 49.4 μM NQO1 apo-protein solution and 300 seconds spacing at 25 $^{\circ}\text{C}$. The determined K_D and N values are: $K_{D1} = 9,2$ nM; $K_{D2} = 780$ nM; $N1 = 0,47$; $N2 = 0,5$. Middle: First injection with 2 μl and 27 injections with 10 μl of 457 μM FAD solution in 46.8 μM NQO1 apo-protein solution and 600 seconds spacing at 25 $^{\circ}\text{C}$. The determined K_D and N values are: $K_{D1} = 4$ nM; $K_{D2} = 295$ nM; $N1 = 0,18$; $N2 = 0,71$

The right measurement was conducted with FAD in the sample cell of the microcalorimeter and apo-NQO1 in the injection syringe. Data was fitted using the one binding site model. First injection with 2 μl and 34 injections with 6 μl of 284 μM NQO1 apoprotein solution in 29 μM FAD solution and 300 seconds spacing at 25 $^{\circ}\text{C}$. From three independent measurements under the same conditions the dissociation constant was calculated to $K_D = 64 \pm 23$ nM.

Interestingly, we observed that variable amounts of protein had apparently precipitated during the experiment. Thus, a possible source for the irreproducibility observed with this particular experimental set-up appears to be the instability of apo-proteins in the microcalorimeter cell where constant stirring is required over the entire time course of the experiment. Similarly, when wild-type NQO1 was constantly stirred in an optical cuvette, we observed a gradual increase at 600 nm indicating

denaturation and finally precipitation of protein. After removal of the precipitated protein by centrifugation the residual protein appeared to be intact as it behaved similar to unstirred protein in size exclusion chromatography. Attempts to stabilize the apo-proteins by lowering the temperature (e.g. 4 °C) or testing different buffers influenced the overall shape of the obtained raw data but failed to improve the reproducibility of the experiment. Importantly, SAXS measurements of wild-type NQO1 showed that the protein forms a dimer in solution both in the holo- and the apo-form, with the holo-protein being more compact compared to the more extended apo-protein (radius of gyration 2.5 and 2.94 nm, Figure 4). Thus, the dimeric apo-protein seems to be partially open or unfolded as a consequence of FAD depletion.

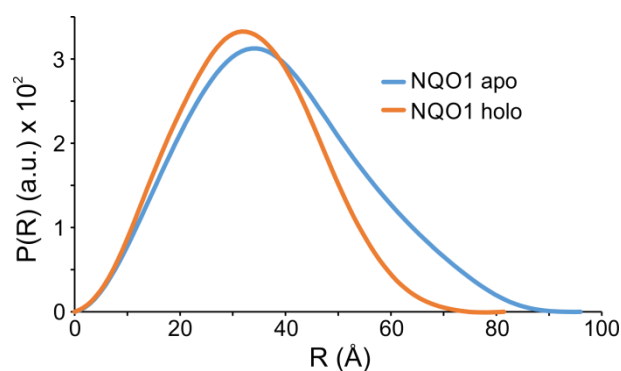


Fig.4. SAXS measurement of NQO1. SAXS data showing a comparison of the experimental radial density distribution ($P(r)$) of apo- and holo-NQO1 in cyan and orange, respectively.

Kinetic measurements

The reductive rates for the NQO1 R139W variant, with NADH and NADPH as reducing co-substrates, were determined. As shown in Table 2, the limiting values for reduction are comparable to those determined earlier for wild-type NQO1 [14]. Interestingly the observed transients showed a biphasic behaviour with a second slower substrate-independent rate, which might have been caused by product release. The oxidative half reaction of the NQO1 R139W variant was completed within the dead time of the stopped flow device as was reported previously for the wild-type and the NQO1 P187S variant [14]. In addition, we have determined steady-state kinetic parameters for WT enzyme and the R139W variant using NADH and menadione as reducing and oxidising substrate, respectively.

Table 2. Reductive half reaction. Bimolecular rate constants (with standard deviations) of NQO1 WT and NQO1 R139W with NADH or NADPH as reducing agent.

Protein	NADH k_{red} ($\text{M}^{-1}\text{s}^{-1}$)	NADPH k_{red} ($\text{M}^{-1}\text{s}^{-1}$)
NQO1 WT	$3.9 \times 10^6 \pm 0.4 \times 10^6$	$7.3 \times 10^6 \pm 1.4 \times 10^6$
NQO1 R139W	$4.6 \times 10^6 \pm 0.2 \times 10^6$	$8.2 \times 10^6 \pm 0.2 \times 10^6$

As summarised in Table 3 and seen in Figure 5, the values for k_{cat} and K_{M} are virtually identical for WT enzyme and the R139W variant for both NADH and menadione again indicating that the single amino acid replacement does not affect the kinetic properties.

Table 3. Steady state kinetic parameters for NQO1 and NQO1 R139W. Kinetic parameters with standard deviations determined for NQO1 and NQO1 R139W, using NADH as electron donor and menadione as electron acceptor.

	NADH			Menadione		
	$k_{\text{cat,app}}$ (s^{-1})	$K_{\text{M,app}}$ (mM)	$k_{\text{cat,app}}/K_{\text{M,app}}$ ($\text{mM}^{-1}\text{s}^{-1}$)	k_{cat} (s^{-1})	K_{M} (μM)	$k_{\text{cat}}/K_{\text{M}}$ ($\mu\text{M}^{-1}\text{s}^{-1}$)
NQO1 WT	1590 ± 52	3.22 ± 0.27	494 ± 44	1830 ± 82	11.6 ± 2.2	158 ± 31
NQO1 R139W	1580 ± 73	3.31 ± 0.38	478 ± 60	1730 ± 100	10.6 ± 2.8	162 ± 44

Structural studies: X-ray crystallography, NMR-spectroscopy and partial proteolysis

To gain further insight into the structural properties of the R139W variant the crystal structure of this protein was solved (see Materials & Methods and Table 4). The structure was determined to 2.1 Å and contains four protein chains in the asymmetric unit. These crystallographically independent molecules are very similar to each other, indicated by an average root-mean-square-deviation (rmsd) of 0.14 Å for a superposition of (on average) 224 out of 271 C α -atoms. The subunit structure of the R139W variant is also virtually identical to the wild-type structure with the exception

of the amino acid replacement at position 139 (Figure 6). The respective average rmsd in this case is 0.18 Å for a superposition of 230 out of 271 C α -atoms.

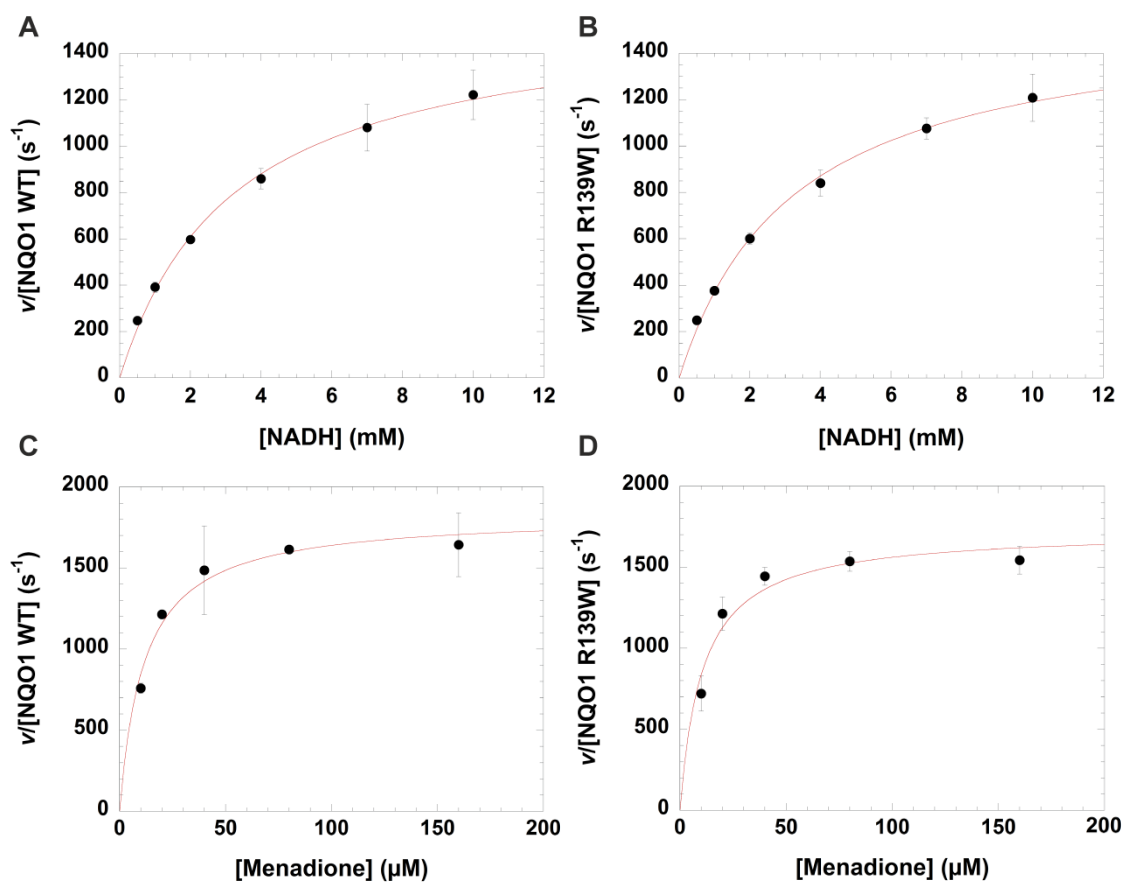


Figure 5. Steady state kinetics of NQO1 WT and NQO1 R139W. In the case of variation of NADH, the velocity v over the enzyme concentration is plotted against NADH concentration for NQO1 WT (A) and NQO1 R139W (B). For the variation of menadione, the velocity v over the enzyme concentration is plotted against menadione concentration for NQO1 WT (C) and NQO1 R139W (D). Standard deviations are shown with error bars.

Recently, it was shown for the NQO1 P187S variant that despite adopting the same structure in the crystal it behaved very differently in solution as evidenced by 2D HSQC NMR-spectroscopy [14] (Figure 7, insert). Thus the R139W variant was also analysed using this technique. As shown in Figure 7, the 2D HSQC spectra of NQO1 (red) and NQO1 R139W (black) are again nearly identical with the exception of an additional signal found in the region typical for a nitrogen of the indole ring in tryptophan side chains (marked by an arrow in Figure 7). Minor shifts observed for a few signals are typical for a single amino acid exchange. Identical line-widths also indicate that the flexibilities of the two proteins are essentially unchanged.

Table 4. Data collection and refinement statistics.

	NQO1 R139W
Data collection	
X-ray source	SLS-X06DA
Wavelength (Å)	1.0
Temperature	100 K
Space group	<i>P</i> 1
Cell dimensions	
<i>a</i> , <i>b</i> , <i>c</i> (Å)	54.61, 59.93, 99.83
α , β , γ (°)	100.37, 92.85, 90.22
Resolution (Å)*	49.03-2.09 (2.17-2.09)
Total reflections	194450 (16603)
Unique reflections	67587 (5937)
Multiplicity*	2.9 (2.8)
Completeness (%)*	97.1 (86.89)
R_{meas}	0.093 (0.339)
R_{merge}	0.076 (0.296)
$\langle I/\sigma_I \rangle^*$	12.27 (4.1)
CC _{1/2} *	0.995 (0.906)
CC*	0.999 (0.975)
Refinement	
Resolution (Å)	49.03-2.09
$R_{\text{work}} / R_{\text{free}}$	0.1693 / 0.2013
No. of atoms	
Protein	8659
Cofactor/ligands	240
Water	1052
Mean B-factors (Å ²)	
Protein	23.40
Cofactor/ligands	26.60
Water	32.30
All atoms	24.40
R.m.s. deviations	
Bond lengths (Å)	0.004
Bond angles (°)	0.95
Ramachandran outliers (%)	0
PDB-entry	5A4K

*Values in parentheses are for highest-resolution shell.

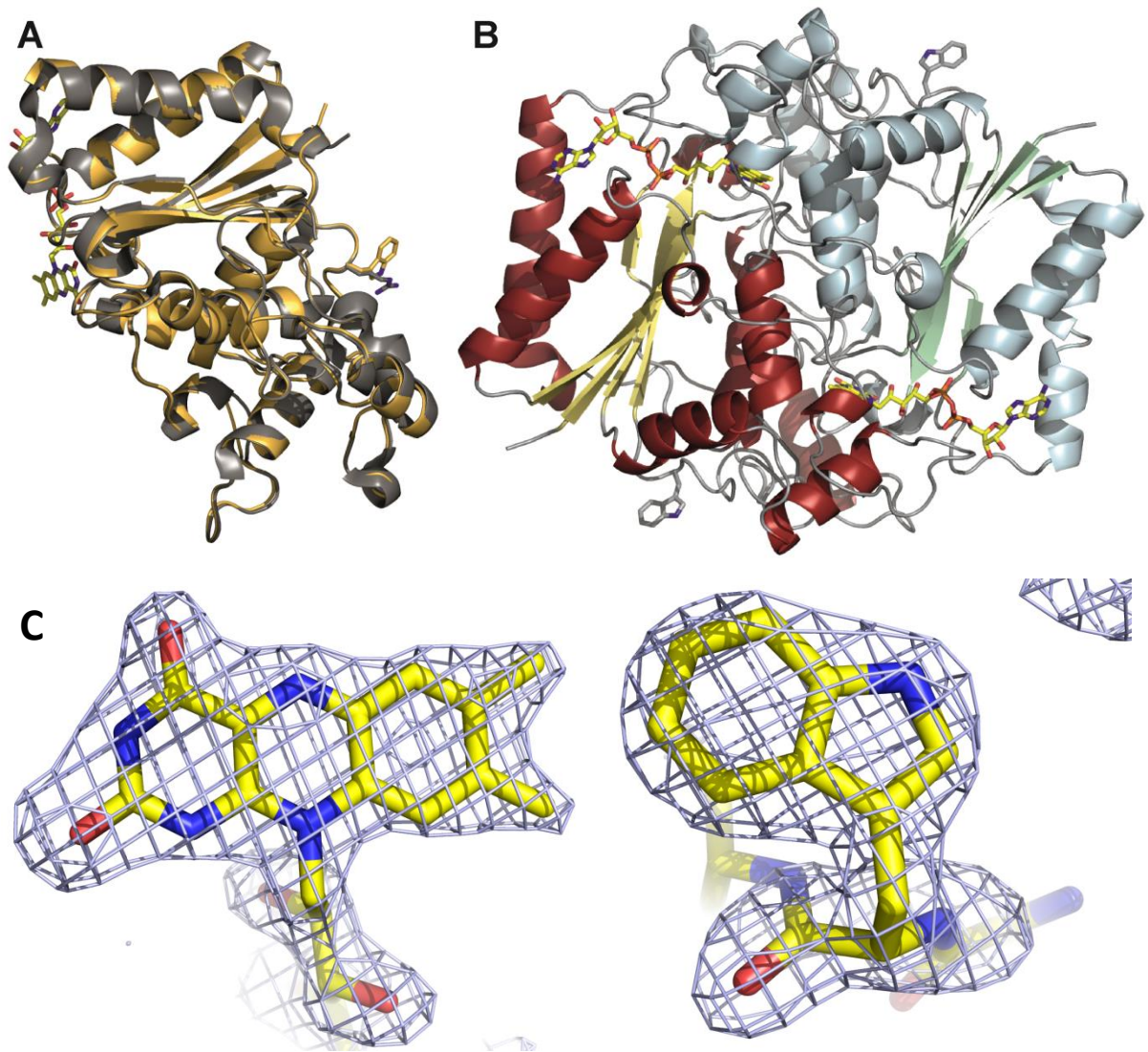


Figure 6. Crystal structure of NQO1 R139W. Panel A: Cartoon model of the superposition of NQO1 and NQO1 R139W with the arginine and tryptophan residue (right) and the FAD (left) shown as a stick model. Panel B: Cartoon model of the NQO1 R139W homodimer with the tryptophan residue and the FAD shown as a stick model. Panel C: $F_o - F_c$ omit electron density contoured at 3σ for the isoalloxazine moiety of FAD bound to one of the subunits (left) and for tryptophan 139 (right).

Recently, we also demonstrated that limited tryptic digestion can be used to monitor the structural flexibility of NQO1 variants, i.e. the unstable and partially unfolded P189S variant. In the case of the R139W variant no difference in the digestion pattern compared to WT was detectable in agreement with the NMR-spectroscopic results (Figure 8).

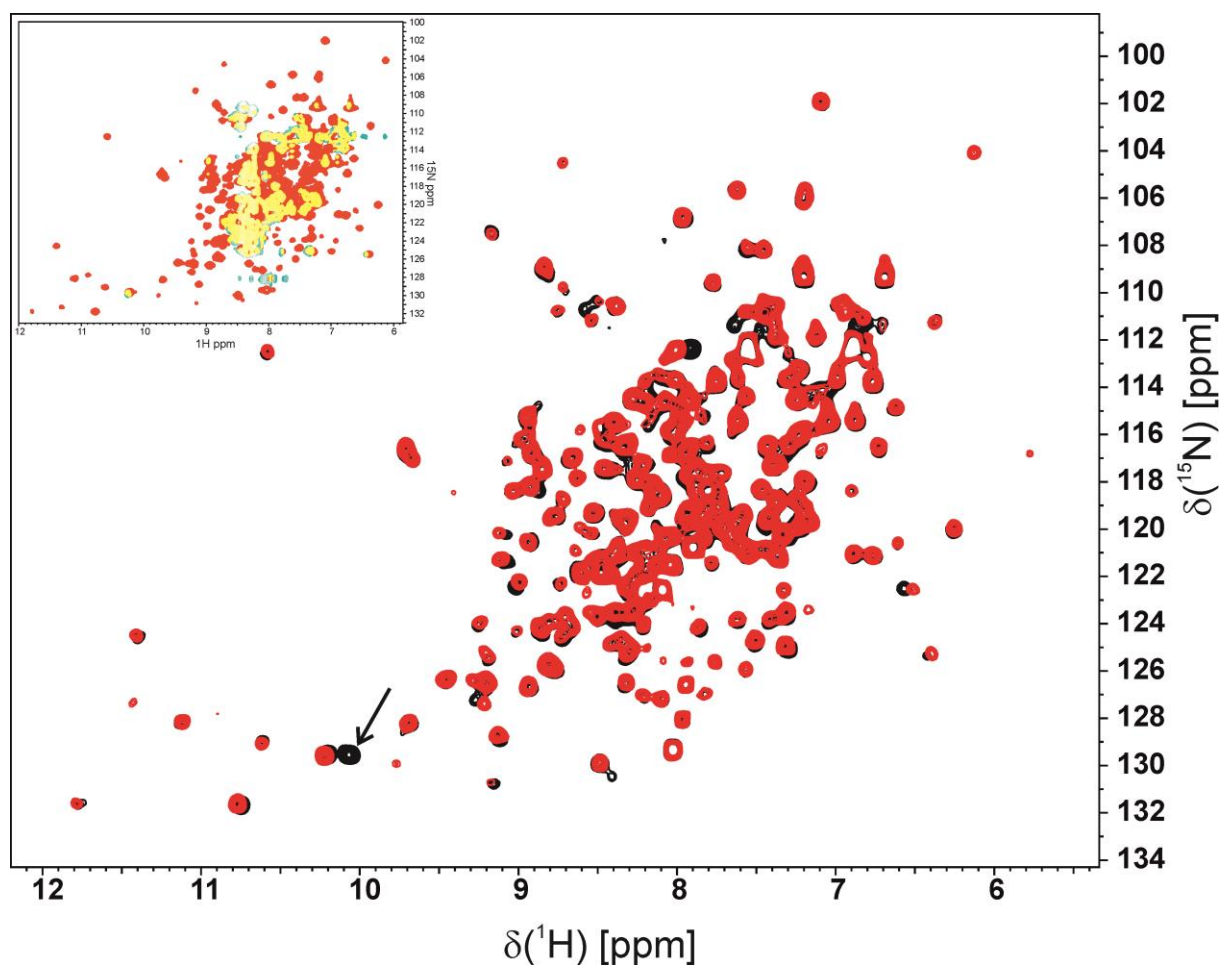


Figure 7. 2D ^1H - ^{15}N HSQC spectra. Overlay of the 2D ^1H - ^{15}N HSQC spectrum of NQO1 R139W (black) and wild-type (red). An additional tryptophan side chain NH signal is visible in the R139W variant and indicated by an arrow. All other signals are almost identical in the HSQC spectrum of the R139W variant and wild-type, respectively, indicative of a very similar structure. A few minor shift differences result from residues close to residue 139. The insert in the upper left corner shows an overlay of the NMR spectra of NQO1 WT (red) and NQO1 P187S (green) where overlapping areas are marked yellow.

Discussion

NQO1 constitutes an important enzyme of the cellular defence system and plays a central role in the activation of quinone-based chemotherapeutics. The occurrence of genetic variants in the human population necessitates the proper evaluation of the biochemical properties of the resulting protein variants. Previous studies on the P187S protein variant (encoded by *NQO1*2*) demonstrated that this single amino acid exchange causes strong destabilization of the tertiary structure leading to a substantial loss of function [14,17]. Astonishingly, it could be demonstrated that the variant adopts a very similar crystal structure, while in solution the protein is present largely in an unfolded state [14]. This very unusual and unexpected behaviour of the P187S variant prompted us to initiate a parallel study on the R139W variant caused by a single nucleotide transition in the *nqo1* gene (*NQO1*3*).

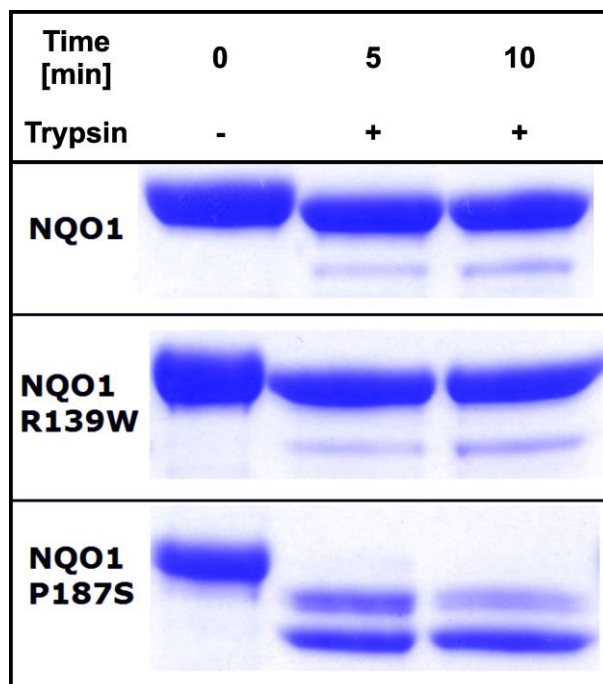


Figure 8. Trypsin digestion of different NQO1 variants. Comparison of Trypsin digestion of three NQO1 variants without addition of Trypsin (0 minutes) and two measurements after addition of Trypsin (5 and 10 minutes).

Initial analysis of the recombinant R139W variant by UV-visible absorption spectroscopy indicated that the affinity of the FAD cofactor as well as the nature of the cofactor binding site were not or only marginally affected by the arginine to tryptophan replacement (Figure 1). Further studies by ITC intended to obtain

dissociation constants for FAD binding revealed that the apo-proteins of both wild-type and the R139W variant precipitated during the experiment, probably due to the damaging effect of shearing forces exerted by constant mixing in the sample cell. As a consequence, this particular experimental set-up resulted in non-reproducible and erroneous results leading to artefacts for the stoichiometry as well as binding affinities. SAXS measurements showed that the apo-protein is not as compact as the holoprotein but still forms a dimer (Figure 4). This may result in a lowered stability against shearing forces as well as in a lowered melting point (Table 1). Similar experiments were recently reported for wild-type NQO1 as well as the P187S and R139W variants and a sequential two site binding model was assumed to fit the data despite the fact that there is neither biochemical nor structural evidence that the two observed binding sites in the homodimeric protein are interdependent or different [17,23]. Depending on the experimental set-up the ratio of the two assumed binding sites was variable rendering the sequential binding site mode unlikely. Importantly, our ITC studies clearly demonstrate that these experimental artefacts can be avoided by simply reversing the order of the titration leading to reproducible data that is in accordance to the biochemical and structural background. We believe that this observation may also have implications for other biochemical systems investigated by ITC where one binding partner (in most cases this will be the macromolecule rather than the small ligand) is unstable under the experimental conditions. In the case of flavoproteins it is well-known that apo-proteins are much less stable than the holoproteins in part due to the damaging effects required to prepare the apo-protein as well as the intrinsic destabilisation of the overall protein structure due to depletion of the flavin prosthetic group (mostly FMN or FAD). [24]

The detailed biochemical and structural analysis of the R139W variant revealed only minor differences in comparison to wild-type NQO1. Similarly, pre-steady state measurements yielded almost identical bimolecular rate constants for both enzyme variants (Table 2). The reductive half reaction was extremely fast making it impossible to determine a reliable dissociation constant of NAD(P)H in our experimental setup. This indicates a low affinity of the pyridine nucleotides resulting in high K_D values as was already shown for the rat liver NQO1 [25]. Also, steady state measurements with the two enzyme variants produced comparable results. Interestingly, our measurements demonstrated that turnover hyperbolically increased

with higher concentrations of NADH of up to 10 mM (!) suggesting that a canonical Michaelis-complex is not formed. This is in stark contrast to previous studies that reported K_M values in the order of about 50 to 300 μ M. However, these studies have only covered a very low concentration range of NADH and thus failed to recognize the non-classical behaviour of the enzyme [17, 26]. These findings from pre-steady state and the steady state kinetic measurements indicate that NADH rapidly reduces the FAD cofactor of NQO1 without prior formation of a Michaelis-complex.

While the crystal structure of the previously studied variant NQO1 P187S was similar to the wildtype structure the NMR measurements revealed considerable movements of the residues [14]. In the case of the NQO1 R139W variant we found that the crystal structure as well as the solution structure, as evidenced by NMR-spectroscopy, is virtually identical to the wildtype protein (Figure 7). Self-association of the R139W variant caused by the higher hydrophobicity could not be observed in size exclusion chromatography. Nevertheless, we cannot exclude that under cellular conditions self-association may take place or the surface changes result in altered interaction with other proteins like the tumour suppressor p53. Tryptic digestion shows a comparable stability of NQO1 WT and NQO1 R139W in contrast to the faster degradation of NQO1 P187S as was already shown and confirmed in previous studies [14,17]. The NQO1 R139W variant only slightly differentiates from the NQO1 WT concerning FAD affinity (ca. 2.5 times weaker binding) and thermostability, by ca. 2 °C. Thus it can be safely concluded that the expression of this variant in humans has no adverse effect on the level of NQO1 activity. Therefore, the observed effects are most probably primarily caused by erroneous splicing of the premature mRNA, leading to the loss of exon 4 and thus reducing the amount of correctly spliced NQO1 in the cell [11].

Experimental Procedures

Reagents

All chemicals and reagents were of the highest purity commercially available from Sigma-Aldrich (St. Louis, MO, USA) and Merck (Darmstadt, Germany). Ni-NTA-agarose columns were obtained from GE Healthcare (Little Chalfont, UK).

*Molecular cloning of *nqo1*, protein expression and purification*

The cloning of NQO1 and the generation of the NQO1 R139W variant as well as the expression and purification was carried out according to the already described procedure from Lienhart and Gudipati *et al.* [14]. The wild type gene of NQO1 in a pET28a vector was modified with the Quick Change II XL Site-Directed Mutagenesis Kit (Agilent, Santa Clara, CA, USA) according the provided manual with gene specific primers from Eurofins (Luxembourg).

Apoprotein preparation and UV/Vis absorption difference titration

Apoprotein preparation and difference titration spectra were conducted as described by Lienhart and Gudipati *et al.* [14]. The measurements were made with a Specord 200 plus spectrophotometer (Analytik Jena, Jena, Germany) at 25 °C in Tandem cuvettes (Hellma Analytic, Müllheim, Germany). 800 µl of NQO1 R139W (45 µM) in the sample cell was titrated with 0-42 µl (in 2 µl intervals) and 52 µl and 62 µl in (10 µl intervals) of a FAD stock solution (1 mM). At the same time the same volume of FAD as in the sample cell was added to the buffer chamber in the reference cell and the same amount of buffer was also added to the protein chamber in the reference cell to adjust the volumes of cells. For analysis, the sum of the absolute values at 436 nm and 455 nm were plotted against the FAD/protein molar ratio.

Small-angle X-ray scattering.

SAXS data for solutions of the FAD-free and bound forms of wild type NQO1 were recorded with an in-house SAXS instrument (SAXSspace, Anton Paar, Graz, Austria) equipped with a Kratky camera, a sealed X-ray tube source and a one-dimensional Mythen2 R 1k hybrid photon coupling detector (Dectris, Baden-Daettwil, Switzerland). The scattering patterns were measured with a 60-min exposure time (20 frames, each 3 min) with a solute concentration of 300 µM. Radiation damage was excluded on the basis of a comparison of individual frames of the 60-min exposures, wherein no changes were detected. A range of momentum transfer of

$0.010 < s < 0.63 \text{ \AA}^{-1}$ was covered ($s = 4\pi \sin(\theta)/\lambda$, where 2θ is the scattering angle, and λ is the X-ray wavelength, in this case 1.5 \AA).

All SAXS data were analyzed with the ATSAS package (version 2.8, Hamburg, Germany). The data were processed with SAXSQuant (version 3.9) and desmeared with GNOM [27]. The forward scattering ($I(0)$), the radius of gyration, (R_g), the maximum dimension (D_{\max}) and the interatomic distance distribution function ($P(r)$) were computed with GNOM [27]. The masses of the solutes were evaluated based on their Porod volume.

Isothermal titration microcalorimetry (ITC)

A VP-ITC system (MicroCal, GE Healthcare, Little Chalfont, UK) was used for calorimetric determination of the dissociation constants for FAD. The experiments were performed at $10 \text{ }^\circ\text{C}$ or $25 \text{ }^\circ\text{C}$ in 50 mM HEPES, $\text{pH } 7.0$ buffer or 50 mM sodium phosphate buffer with 150 mM NaCl, $\text{pH } 7.0$. The solutions were degassed before measurements. The titration experiments were performed with either apo-protein solution or FAD solution in the syringe and in each case the other solution in the sample cell. The concentrations of FAD and the apo-protein (concentration of NQO1 protomers) were determined spectrophotometrically. The first measurement point is rejected while the remaining data points were analysed assuming a single site or a two site binding model with Origin version 7.0 (MicroCal) for ITC data analysis [14]. To remove aggregated protein solutions were centrifuged at 21.130 g for 20 minutes at $22 \text{ }^\circ\text{C}$.

Steady state kinetics

Steady state parameters for NQO1 WT and NQO1 R139W were determined using a Specord 200 plus spectrophotometer (Analytik Jena, Jena, Germany) at $25 \text{ }^\circ\text{C}$. NADH was used as electron donor and menadione as electron acceptor for the assays. The concentrations of all components were determined spectrophotometrically. For the assay with variation of NADH the reaction mixture contained 2.5 nM WT NQO1 or the R139W variant, $200 \text{ }\mu\text{M}$ menadione ($\epsilon_{333\text{nm}} = 2,450 \text{ M}^{-1}\text{cm}^{-1}$, dissolved in ethanol, final concentration in the cuvette $1\% \text{ v/v}$) and $1\text{--}10 \text{ mM}$ NADH ($\epsilon_{340\text{nm}} = 6,220 \text{ M}^{-1}\text{cm}^{-1}$) in 50 mM HEPES containing 150 mM NaCl, $\text{pH } 7.0$ and for the variation of menadione 2 nM NQO1 WT or NQO1 R139W, 10 mM NADH, $10\text{--}160 \text{ }\mu\text{M}$ menadione (dissolved in ethanol, final concentration in the

cuvette 1% v/v) in 50 mM HEPES containing 150 mM NaCl, pH 7.0. The reaction mixtures were incubated for 3 minutes at 25 °C and then the reaction was initiated by addition of the enzyme and the decrease in absorption of NADH was measured at 400 nm due to the high concentrations of NADH that were needed. In the case of measurements as a function of NADH concentration the slope corresponding to the first 60 s was used for the analysis whereas in the case of menadione variation only 10 s was used for analysis due to the fast reaction. The kinetic parameters were determined using the KALEIDAGRAPH software (Synergy Software, Reading, PA, USA).

Transient kinetics

The rates of the reductive half reactions were determined using a Hi-Tech (SF-61DX2) stopped-flow device (TgK Scientific Limited, Bradford-on-Avon, UK), placed in a glovebox from Belle Technology (Weymouth, UK), at 4 °C. Buffer were first flushed with nitrogen and thereafter incubated in the glove box. In the same way enzyme and substrate solutions were deoxygenated in the glove box and diluted to the desired concentration. During the experiments, enzyme was rapidly mixed with substrate and reduction of the FAD cofactor was measured by monitoring changes at 455 nm with a photomultiplier detector (PM-61s, TgK Scientific Limited, Bradford-on-Avon, UK). For these measurements 40 µM protein was mixed with 50-2500 µM NADH or NADPH in 50 mM HEPES buffer containing 50 mM NaCl at pH 7.0. Initial rates were analysed with a hyperbolic function using the KINETIC STUDIO software (TgK Scientific).

Crystallization and structure determination of NQO1 R139W

NQO1 R139W at 6.1 mg/ml in 50 mM HEPES (pH 7.5) was crystallized by the microbatch method in a precipitating solution containing 200 mM Li₂SO₄, 100 mM BisTris (pH 6.5), 25% w/v PEG 3350 (Hampton Research Index Screen, condition 75), and incubated at 289 K. The total drop volume was 1 µL, with equal amounts of protein and precipitant solution. Yellow crystals grew to full size (~ 100 µm) within 2 months. Crystals were harvested from their mother liquor with CryoLoops™ (Hampton Research), and flash-cooled in liquid nitrogen.

A complete diffraction dataset was collected up to 2.09 Å resolution from a single triclinic crystal (space group *P*1) at the Swiss Light Source (SLS) of the Paul Scherrer

Institute in Villigen, Switzerland (beamline X06DA). The data were processed using the program XDS [28]. The calculated Matthews coefficient [29] indicated the presence of four molecules per asymmetric unit. The structure was determined by molecular replacement using the program PHASER [30] and the wild type structure of NQO1 (PDB code: 1QBG) as search template.

R_{free} values were computed from 5% randomly chosen reflections which were not used during refinement [31]. Structure refinement and model rebuilding were carried out with the programs PHENIX [32] and COOT [33,34] by alternating real-space fitting against σ_A -weighted $2F_o - F_c$ and $F_o - F_c$ electron density maps and least square optimizations. Validation of the structure was carried out with the program MOLPROBITY [35] yielding a Ramachandran plot with 97.0% of the residues in favoured regions, 3.0% in allowed and none in disallowed regions. Prediction of the biologically active form of NQO1 R137W was done using the PISA server [36]. Figures were created using the program PyMOL (<http://www.pymol.org>).

The final model was refined to $R = 16.9\%$ and $R_{\text{free}} = 20.1\%$. Details of the data reduction and structure refinement are listed in Table 4.

Limited proteolysis

NQO1 and NQO1 R139W (30 μM in 50 mM HEPES and 150 mM NaCl buffer at pH 7.5) were partially digested with trypsin (Promega, Madison, WI, USA) with a final concentration of 2 $\mu\text{g/ml}$ at 37 °C. The reaction was stopped after 5 and 10 minutes by addition of SDS sample buffer to aliquots of the reaction mixture and immediately boiled at 95 °C for 10 min. The samples were analysed by SDS-PAGE with precast gradient gels (Thermo Scientific, Waltham, MA, USA) (Figure 8) [14,17,23,37].

¹⁵N-Labeling of NQO1 and NQO1 R139W

Minimal medium containing 6.8 g/l Na_2HPO_4 , 3 g/l KH_2PO_4 , 0.5 g/l NaCl, 1 g/l $^{15}\text{NH}_4\text{Cl}$, 3 g/l glucose, 1 $\mu\text{g/l}$ biotin, 1 $\mu\text{g/l}$ thiamin, 50 $\mu\text{g/ml}$ kanamycin and 1 ml 1000x microsals [150 mM CaCl_2 , 20 mM, FeCl_3 , 50 mM H_3BO_3 , 150 μM CoCl_2 , 800 μM CuCl_2 , 1.5 mM ZnCl_2 , 15 μM $(\text{NH}_4)_6\text{Mo}_7\text{O}_{24}\cdot 4\text{H}_2\text{O}$] was used for protein expression as described in Lienhart and Gudipati *et al.* [14].

NMR spectroscopy

All NMR experiments were carried out with a Bruker Avance III 700 MHz spectrometer using a cryogenically cooled 5 mm TXI probe with z-axis gradients at 298 K. Samples containing between 20-40 mg/ml NQO1 or NQO1 R139W in 50 mM HEPES, pH 6.5 in 90% H₂O and 10% D₂O were used. For the ¹H-¹⁵N HSQC spectra, data matrices of 2048 x 160 points were acquired and zero filled to 4k x 256 points prior to Fourier transformation. Sixty degree phase shifted squared sine bell window functions were applied in both dimensions [14].

Thermal stability

The melting points were determined with a CFX Connect™ Real-Time PCR Detection System (Bio-Rad Laboratories, Inc.; Hercules; California; USA) by detecting the fluorescence change of SYPRO® Orange Protein Gel Stain (1:5000) or the fluorescence change caused by the release of the FAD cofactor during heating [38]. The tested proteins (100 μM for FAD and 10 μM for SYPRO® Orange, measured in duplicates) have been dialysed in water over night and mixed with concentrated buffer and salt solutions to obtain all tested conditions.

Acknowledgements

This work was supported by the Austrian Fonds zur Förderung der wissenschaftlichen Forschung (FWF) through project P22361 to PM and KG and project P28854) to TM. Additional funding was received by the PhD programs “Molecular Enzymology” (W901) and “Molecular Basis of Cardiovascular Disease” (W1226) to KZ, KG, PM and to TM, respectively. We also thank the interuniversity program in natural sciences, NAWI Graz, for financial support.

References

- [1] W.D. Lienhart, V. Gudipati, P. Macheroux, The human flavoproteome. *Arch. Biochem. Biophys.* 535 (2013) 150-162.
- [2] D. Ross, D. Siegel, NAD(P)H:quinone oxidoreductase 1 (NQO1, DT-diaphorase), functions and pharmacogenetics, *Methods Enzymol.* 382 (2004) 115-144.
- [3] M. Garate, R.P. Wong, E.I. Campos, Y. Wang, G. Li, NAD(P)H quinone oxidoreductase 1 inhibits the proteasomal degradation of the tumour suppressor p33(ING1b), *EMBO Rep.* 9 (2008) 576-581.
- [4] G. Asher, P. Tsvetkov, C. Kahana, Y. Shaul, A mechanism of ubiquitin-independent proteasomal degradation of the tumor suppressors p53 and p73, *Genes Dev.* 19 (2005) 316-321.
- [5] K.T. Kelsey, D. Ross, R.D. Traver, D.C. Christiani, Z.F. Zuo, M.R. Spitz, M. Wang, X. Xu, B.K. Lee, B.S. Schwartz, J.K. Wiencke, Ethnic variation in the prevalence of a common NAD(P)H quinone oxidoreductase polymorphism and its implications for anti-cancer chemotherapy, *Br. J. Cancer* 76 (1997) 852-854.
- [6] A. Gaedigk, R.F. Tyndale, M. Jurima-Romet, E.M. Sellers, D.M. Grant, J.S. Leeder, NAD(P)H:quinone oxidoreductase: polymorphisms and allele frequencies in Caucasian, Chinese and Canadian Native Indian and Inuit populations, *Pharmacogenetics* 8 (1998) 305-313.
- [7] M. Eguchi-Ishimae, M. Eguchi, E. Ishii, D. Knight, Y. Sadakane, K. Isoyama, H. Yabe, S. Mizutani, M. Greaves, The association of a distinctive allele of NAD(P)H:quinone oxidoreductase with pediatric acute lymphoblastic leukemias with MLL fusion genes in Japan, *Haematologica* 90 (2005) 1511-1515.
- [8] M. Krajcinovic, H. Sinnett, C. Richer, D. Labuda, D. Sinnett, Role of NQO1, MPO and CYP2E1 genetic polymorphisms in the susceptibility to childhood acute lymphoblastic leukemia, *International Journal of Cancer* 97 (2002) 230-236.

- [9] R.K. Mandal, K. Nissar, R.D. Mittal, Genetic variants in metabolizing genes NQO1, NQO2, MTHFR and risk of prostate cancer: a study from North India, *Mol. Biol. Rep.* 39 (2012) 11145-11152.
- [10] J.J. Freriksen, J. Salomon, H.M. Roelofs, R.H. Te Morsche, J.W. van der Stappen, P. Dura, B.J. Witteman, M. Lacko, W.H. Peters, Genetic polymorphism 609C>T in NAD(P)H:quinone oxidoreductase 1 enhances the risk of proximal colon cancer, *J. Hum. Genet.* 59 (2014) 381-386.
- [11] S.S. Pan, Y. Han, P. Farabaugh, H. Xia, Implication of alternative splicing for expression of a variant NAD(P)H:quinone oxidoreductase-1 with a single nucleotide polymorphism at 465C>T, *Pharmacogenetics* 12 (2002) 479-488.
- [12] R.D. Traver, D. Siegel, H.D. Beall, R.M. Phillips, N.W. Gibson, W.A. Franklin, D. Ross, Characterization of a polymorphism in NAD(P)H: Quinone oxidoreductase (DT-diaphorase), *Br. J. Cancer* 75 (1997) 69-75.
- [13] D. Siegel, A. Anwar, S. Winski, J. Kepa, K. Zolman, D. Ross, Rapid polyubiquitination and proteasomal degradation of a mutant form of NAD(P)H:Quinone oxidoreductase 1, *Mol. Pharmacol.* 59 (2001) 263-268.
- [14] W.D. Lienhart, V. Gudipati, M.K. Uhl, A. Binter, S.A. Pulido, R. Saf, K. Zangger, K. Gruber, P. Macheroux, Collapse of the native structure caused by a single amino acid exchange in human NAD(P)H:quinone oxidoreductase 1, *FEBS Journal* 281 (2014) 4691-4704.
- [15] P.Y. Gasdaska, H. Fisher, G. Powis, An alternatively spliced form of NQO1 (DT-diaphorase) messenger RNA lacking the putative quinone substrate binding site is present in human normal and tumor tissues, *Cancer Res.* 55 (1995) 2542-2547.
- [16] L.T. Hu, J. Stamberg, S. Pan, The NAD(P)H:quinone oxidoreductase locus in human colon carcinoma HCT 116 cells resistant to mitomycin C, *Cancer Res.* 56 (1996) 5253-5259.
- [17] A.L. Pey, C.F. Megarity, D.J. Timson, FAD binding overcomes defects in activity and stability displayed by cancer-associated variants of human NQO1, *Biochim. Biophys. Acta* 1842 (2014) 2163-2173.

- [18] D.W. Nebert, A.L. Roe, S.E. Vandale, E. Bingham, G.G. Oakley, NAD(P)H:quinone oxidoreductase (NQO1) polymorphism, exposure to benzene, and predisposition to disease: a HuGE review, *Genet. Med.* 4 (2002) 62-70.
- [19] A. Begleiter, N. El-Gabalawy, L. Lange, M.K. Leith, L.J. Guziec, F.S. Guziec Jr., A Model for NAD(P)H:Quinoneoxidoreductase 1 (NQO1) Targeted Individualized Cancer Chemotherapy, *Drug Target Insights* 4 (2009) 1-8.
- [20] D. Siegel, C. Yan, D. Ross, NAD(P)H:quinone oxidoreductase 1 (NQO1) in the sensitivity and resistance to antitumor quinones, *Biochem. Pharmacol.* 83 (2012) 1033-1040.
- [21] Z. Dai, A.C. Papp, D. Wang, H. Hampel, W. Sadee, Genotyping panel for assessing response to cancer chemotherapy. *BMC Med Genomics* 1 (2008) 24-8794-1-24.
- [22] G.T. Gang, Y.H. Kim, J.R. Noh, K.S. Kim, J.Y. Jung, M. Shong, J.H. Hwang, C.H. Lee, Protective role of NAD(P)H:quinone oxidoreductase 1 (NQO1) in cisplatin-induced nephrotoxicity, *Toxicol. Lett.* 221 (2013) 165-175.
- [23] D. Svergun, Determination of the regularization parameter in indirect-transform methods using perceptual criteria, *Journal of applied crystallography* 25 (1992) 495-503.
- [24] W. Kabsch, XDS. *Acta Crystallogr.* 66,(2010) 125-132.
- [25] Collaborative Computational Project N4, The CCP4 suite: programs for protein crystallography, *Act. Crystallogr.* 50 (1994) 760-763.
- [26] A.J. McCoy, R.W. Grosse-Kunstleve, P.D. Adams, M.D. Winn, L.C. Storoni, R.J. Read Phaser crystallographic software, *J. Appl. Crystallogr.* 40 (2007) 658-674.
- [27] G.J. Kleywegt, A.T. Brunger, Checking your imagination: applications of the free R value, *Structure* 4 (1996) 897-904.
- [28] P.D. Adams, P.V. Afonine, G. Bunkoczi, V.B. Chen, I.W. Davis, N. Echols, J.J. Headd, L.W. Hung, G.J. Kapral, R.W. Grosse-Kunstleve, A.J. McCoy, N.W.

- Moriarty, R. Oeffner, R.J. Read, D.C. Richardson, J.S. Richardson, T.C. Terwilliger, P.H. Zwart, PHENIX: a comprehensive Python-based system for macromolecular structure solution, *Acta Crystallogr.* 66 (2010) 213-221.
- [29] P. Emsley, K. Cowtan, Coot: model-building tools for molecular graphics, *Acta Crystallogr.* 60 (2004) 2126-2132.
- [30] P. Emsley, B. Lohkamp, W.G. Scott, K. Cowtan, Features and development of Coot, *Acta Crystallogr.* 66 (2010) 486-501.
- [31] V.B. Chen, W.B. Arendall 3rd, J.J. Headd, D.A. Keedy, R.M. Immormino, G.J. Kapral, L.W. Murray, J.S. Richardson, D.C. Richardson, MolProbity: all-atom structure validation for macromolecular crystallography, *Acta Crystallogr.* 66 (2010) 12-21.
- [32] E. Krissinel, K. Henrick, Inference of macromolecular assemblies from crystalline state, *J. Mol. Biol.* 372 (2007) 774-797.
- [33] M.C. Encarnacion, R.J. Palomino-Morales, J.E. Fuchs, P.G. Esperanza, M.T. Noel, E. Salido, D.J. Timson, A.L. Pey, Conformational dynamics is key to understanding loss-of-function of NQO1 cancer-associated polymorphisms and its correction by pharmacological ligands, *Sci. Rep.* 6 (2016) 20331.
- [34] S. Chen, P.S. Deng, J.M. Bailey, K.M. Swiderek, A two-domain structure for the two subunits of NAD(P)H:quinone acceptor oxidoreductase, *Protein Sci.* 3 (1994) 51-57.
- [35] F. Forneris, R. Orru, D. Bonivento, L.R. Chiarelli, A. Mattevi, ThermoFAD, a Thermofluor-adapted flavin ad hoc detection system for protein folding and ligand binding, *FEBS J.* 276 (2009) 2833-2840
- [36] M.H. Hefti, J. Vervoort, W.J. van Berkel, Deflavination and reconstitution of flavoproteins, *Eur. J. Biochem.* 270 (2003) 4227-4242.
- [37] G. Tedeschi, S. Chen, V. Massey, DT-diaphorase. Redox potential, steady-state, and rapid reaction studies, *J. Biol. Chem.* 270 (1995) 1198-1204.

- [38] S. Pan, G.L. Forrest, S.A. Akman, L. Hu, NAD(P)H:Quinone oxidoreductase expression and Mitomycin C resistance developed by human colon cancer HCT 116 cells, *Cancer Research* 55 (1995) 330-335.

Chapter 3

Rescuing the stability and activity of the P187S variant of
NAD(P)H:quinone oxidoreductase 1

Rescuing the stability and activity of a cancer associated variant of human NAD(P)H:quinone oxidoreductase 1 (NQO1) by small-molecular chaperones

Emilia Strandback^{1‡}, Wolf-Dieter Lienhart^{1‡}, Altijana Hromic-Jahjefendic², Luka Brvar³, Benjamin Bourgeois⁴, Anja Högler¹, Daniel Waltenstorfer¹, Andreas Winkler¹, Klaus Zangger⁵, Ellen Heitzer⁶, Beate Rinner³, Tobias Madl⁴, Karl Gruber², Peter Macheroux^{1*}

¹ Institute of Biochemistry, Graz University of Technology, Austria

² Institute of Molecular Biosciences, University of Graz, Austria

³ Core Facility Alternative Biomodels und Preclinical Imaging, Medical University of Graz, Austria

⁴ Institute of Molecular Biology and Biochemistry, Medical University of Graz, Austria

⁵ Institute of Chemistry, University of Graz, Austria

⁶ Institute of Human Genetics, Medical University of Graz, Austria

Author contributions

‡ The first two authors have contributed equally to this work.

W.-D.L. and P.M. initiated the project; E.S., W.-D.L., A.H.-J., L.B., B.R., K.Z., K.G. and P.M. designed the experiments and analysed the data; E.S. and W.-D.L. expressed and purified NQO1; A.H.-J. and K.G. crystallized NQO1 and determined the crystal structure; E.S., W.-D.L., A.H. and D.W. performed analytical and biochemical experiments, determined dissociation constants and kinetic parameters; L.B., E.H. and B.R. performed cell culture experiments and sequenced cell lines, A. W. performed and interpreted HDX-MS measurements, K.Z. performed NMR-experiments; B.B. and T.M. performed and interpreted SAXS measurements; E.S., W.-D.L., B.B., A. W., K.Z., K.G. and P.M. wrote the manuscript.

Manuscript in preparation

Abstract

NAD(P)H:quinone oxidoreductase 1 (NQO1) is a human FAD-dependent enzyme that plays a crucial role in the antioxidant defense system. The level of NQO1 is also increased in several tumors making it an important target for quinone based anti-cancer prodrugs. A naturally occurring single nucleotide polymorphism (*NQO1*2*) in the NQO1 gene leads to an amino acid exchange (P187S), which severely compromises the activity and stability of the enzyme. The *NQO1*2* genotype has been linked to a higher risk for several types of cancer and poor survival rate after anthracycline-based chemo-therapy. This study investigates the possibility to restore the activity and stability of the NQO1 P187S variant by using small-molecular chaperones. By employing a combination of methods to characterize the effect of the best hit, N-(2-bromophenyl)pyrrolidine-1-sulfonamide, on the stability of the protein in solution, it could be demonstrated that the variant protein repopulates the native wild-type conformation at the same time as the C-terminal is stabilized. As a consequence of the stabilizing effect the enzymatic activity of the variant protein *in vitro* is also strongly improved in the presence of the ligand. Therefore, our study demonstrates that development of molecular chaperones is a promising concept for the stabilization of unstable protein variants, where the designed molecules can be exploited as a treatment alternative in human diseases caused by protein instability.

Abbreviations

BPPSA, N-(2-bromophenyl)pyrrolidine-1-sulfonamide; HDX-MS, hydrogen-deuterium exchange coupled to mass spectrometry; HSQC, heteronuclear single quantum coherence; NQO1, NAD(P)H:quinone oxidoreductase 1; PDB, protein data bank; SAXS, small-angle X-ray scattering; SNP, single-nucleotide polymorphism; WT, wild-type.

Keywords

NQO1, cancer, single-nucleotide polymorphism, chemical chaperone, quinone, chemotherapeutics

Introduction

NAD(P)H:quinone oxidoreductase 1 (NQO1; EC 1.6.99.2) is a human FAD-dependent enzyme catalyzing the two-electron reduction of quinones to hydroquinones. NQO1, for instance, plays an important role in the antioxidant defense system where it lowers the quinone levels and thereby prevents the formation of reactive oxygen species (ROS). Furthermore, it binds to the 20S proteasome, thus rescuing several tumor suppressors like p33^{ING1b}, p53 and p73 from proteasomal degradation [1, 2]. Due to the broad substrate specificity, NQO1 can activate chemotherapeutic prodrugs, as for example mitomycin C and β -lapachone, and since the level of NQO1 is increased in several tumors, the quinone-based chemotherapeutic will also act specifically on the tumor cells [3-5].

A naturally occurring single nucleotide polymorphism (*NQO1**2) in the NQO1 gene (C609T, on chromosome 16q22.1) results in the replacement of proline 187 to serine (P187S) in the protein sequence [6]. The distribution of the homozygous *NQO1**2 among the population varies between 2 and 20% depending on the ethnic background and is most common in Asian populations [7]. The *NQO1**2 genotype is associated with an increased toxicity of benzene and higher risk for several types of cancers including lung, colon, breast and leukemia. Additionally, an adverse breast cancer outcome has been reported after anthracycline-based chemo-therapy, with a survival rate of 17% for patients with the *NQO1**2 genotype compared to 75% for other genotypes [8, 9].

A previous study gave insights into the structural characteristics of the NQO1 P187S variant, and concluded that the single amino acid exchange destabilizes interactions between the core and C-terminal domain of the variant protein in solution. It could also be shown that the cofactor affinity and thereby also the activity are affected in the variant protein as a consequence of the structural instability [10]. This led to the idea that binding of small molecules to NQO1 may affect the conformational dynamics of the protein such that the native structure is stabilized thereby rescuing the activity of the variant protein.

Here we report on the effect of a ligand that binds to and stabilizes the NQO1 P187S variant and consequently rendering the conformation of the variant more similar to that of the wild-type protein. Moreover, it could be demonstrated that, as a result of

the stabilizing effect, the ligand improves the enzymatic activity of the NQO1 P187S variant *in vitro* and *in vivo*.

Results

Virtual and initial in vitro screening of possible stabilizing ligands

Initially, the goal of the virtual screening was to identify a small molecule that binds to the variant protein and may exert a stabilizing effect. The docked molecules from the ZINC database were ranked according to the binding free energy. A subset of the best hits were selected for an initial *in vitro* screening using the ThermoFAD method, where N-(2-bromophenyl)pyrrolidine-1-sulfonamide (BPPSA) stood out as the ligand leading to the largest stabilizing effect, with an increase in melting temperature of 1 °C for the wild-type and 2.5 °C for the NQO1 P187S variant. Because of the promising stabilizing effects of BPPSA, further experiments were performed investigating the effects of this compound on the stability and activity of NQO1 P187S as well as NQO1 WT.

Binding and stabilizing effect of N-(2-bromophenyl)pyrrolidine-1-sulfonamide

To further investigate how the ligand BPPSA influences the stability of NQO1, limited proteolysis experiments were performed in the presence and absence of BPPSA. In Figure S1 the resulting SDS-PAGE analyses are displayed. Apparently, both the wild-type and variant protein is partly stabilized in the presence of BPPSA. However, the stabilizing effect is different for the two proteins and correlates with the loss of peptides at the C-terminus (Figure 1).

The binding of BPPSA to the wild-type and the P187S variant could also be monitored using difference UV-Vis absorption spectroscopy. As shown in Figure 2, titration of BPPSA to wild-type protein produces a sharp endpoint whereas the equivalent experiment with the variant leads to a biphasic binding behavior. In both cases, however, the absorption changes are similar and clearly indicate that binding of BPPSA affects the absorption properties of the FAD cofactor.

The binding of the ligand was further investigated by isothermal titration calorimetry (ITC). The dissociation constants for the binding of BPPSA to NQO1 WT and NQO1 P187S could be determined to be $8.1 \pm 0.2 \mu\text{M}$ and $20.0 \pm 0.2 \mu\text{M}$ respectively, see Figure 3.

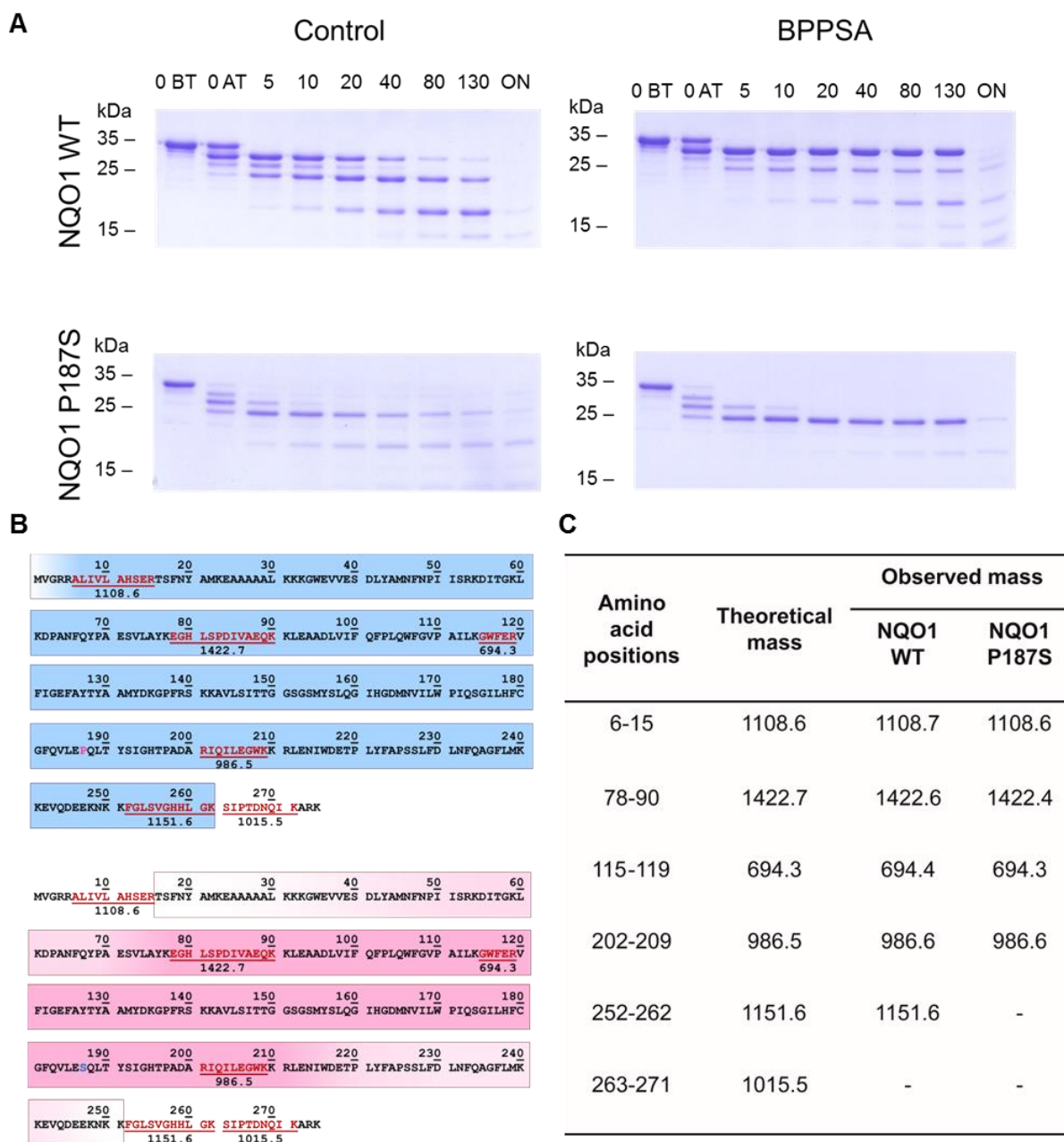


Figure 1. Limited trypsin proteolysis and MALDI-TOF analysis of NQO1 WT and NQO1 P187S in presence and absence of BPPSA. The compound stabilizes both the wild-type and the variant protein. (A) SDS-PAGE displaying the digestion over time for NQO1 WT and NQO1 P187S in presence and absence of BPPSA. Lane 1 and 2 show protein without trypsin (O BT) and protein taken out directly after addition of trypsin (O AT), lane 3-8 show the digestion after 5-130 minutes and the last lane show the digestion overnight. (B) Theoretical fragments after trypsin digestion (displayed in red) were used to determine which part of NQO1 WT (blue) and NQO1 P187S (pink) that was stabilized by the compound over time, areas illustrated with a gradient could not be assigned due to too less information. (C) Peptides observed after MALDI-TOF analysis of the stabilized SDS gel bands.

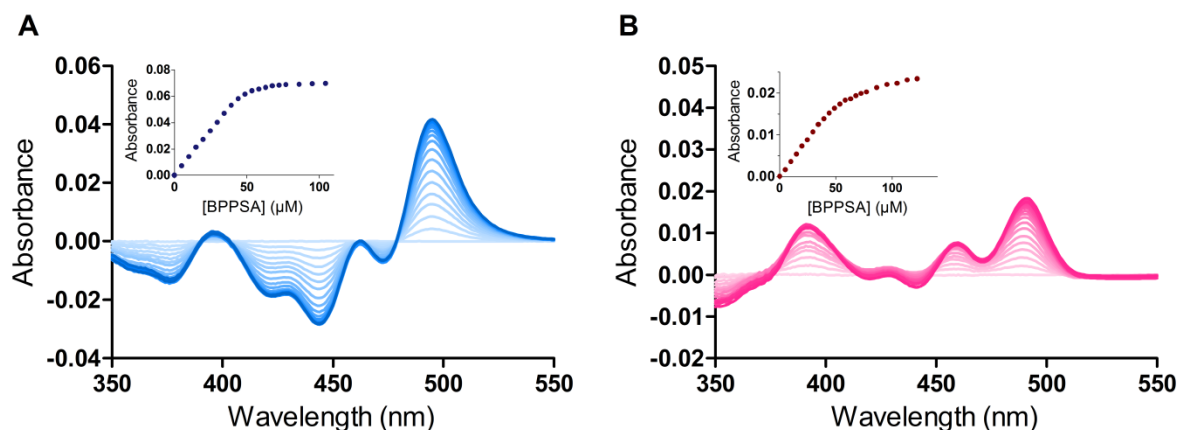


Figure 2. Difference absorption spectra of the ligand BPPSA to NQO1 WT and NQO1 P187S. UV-visible difference absorption spectra of (A) 40 μM NQO1 WT titrated with BPPSA (0-104 μM), the absorption spectra in the range from 350 nm to 550 nm are displayed in different shades of blue. The inset shows a plot of the change in the absolute absorption values at 444 nm and 496 nm against the concentration of BPPSA. (B) UV-visible difference absorption spectra of 40 μM NQO1 P187S titrated with BPPSA (0-122 μM), the absorption spectra in the range from 350 nm to 550 nm are displayed in different shades of red. The inset shows a plot of the change in the absolute absorption values at 440 nm and 491 nm against the concentration of BPPSA.

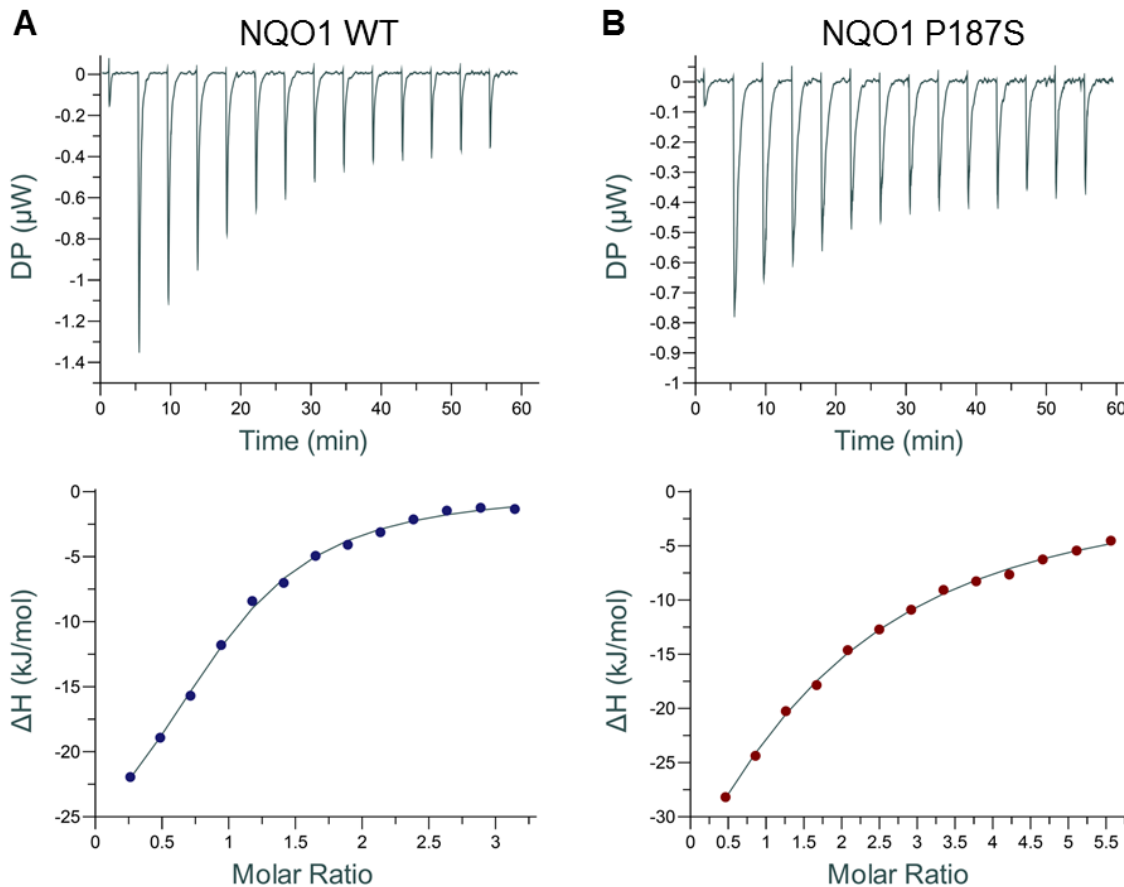


Figure 3. Isothermal titration calorimetry measurements of BPPSA titrated with NQO1 WT or NQO1 P187S. The dissociation constants for the binding of BPPSA to NQO1 WT and NQO1 P187S could be determined to be $8.1 \pm 0.2 \mu\text{M}$ and $20.0 \pm 0.2 \mu\text{M}$ respectively.

NMR spectroscopy, SAXS and HDX-MS measurements

Several different methods were used to assess the stability of wild-type and the P187S variant in the presence and absence of BPPSA in solution. It was earlier demonstrated that the ^1H - ^{15}N -HSQC spectra of wild-type NQO1 and the P187S variant exhibit dramatic differences. [10] While the HSQC of the wild-type enzyme is indicative of a relatively rigid and well-structured protein, the P187S variant mainly shows signals in the random coil region, which likely results from increased flexibility of this variant (Figure 4A). The addition of BPPSA to NQO1 P187S significantly improves the quality of the HSQC (Figure 4B), which is indicative for reduced mobility of amino acid residues in the protein structure. In fact, the spectrum of the P187S variant in the presence of BPPSA is similar to wild-type NQO1 and almost identical to wild-type with bound ligand (Figure 4C and 4D). This also confirms that the ligand binds in the same way to the wild-type and variant protein.

SAXS measurements revealed that both wild-type and the variant protein occur as dimers in solution. However, the P187S variant featured an increase in both radius of gyration (R_g) and maximum distance (D_{max}) compared to the wild type protein (R_g of 2.60 and 3.04 nm, D_{max} of 8 and 11 nm for wild-type and the variant protein, respectively). This indicates a more extended conformation of the P187S dimer compared to the wild type protein. The addition of BPPSA led to a decrease in both R_g and D_{max} for the P187S variant, whereas no significant changes were observed for the wild-type protein (R_g of 3.04 and 2.69 nm and D_{max} of 11 and 9 nm, for the P187S variant in the absence and presence of BPPSA, respectively). This indicates that the NQO1 P187S variant undergoes a compaction towards the native conformation upon binding of BPPSA (Figure 5A).

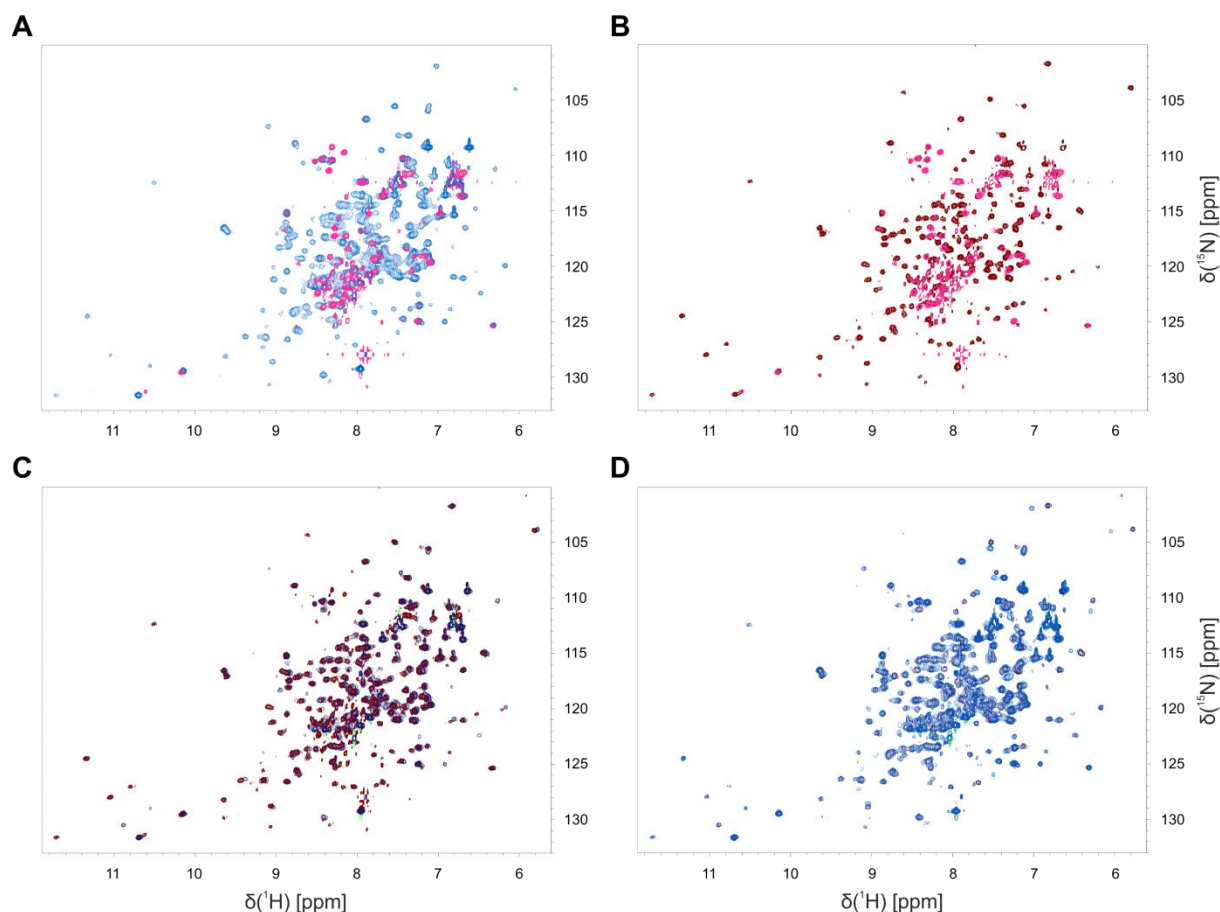


Figure 4. ^1H - ^{15}N HSQC spectra of NQO1 WT and P187S in presence and absence of BPPSA. Overlay of ^1H - ^{15}N HSQC spectra of a) NQO1 P187S (pink) and NQO1 WT (light blue), b) NQO1 P187S (pink) and NQO1 P187S with BPPSA (maroon), c) NQO1 P187S with BPPSA (maroon) and NQO1 WT with BPPSA (dark blue), d) NQO1 WT (light blue) and NQO1 WT with BPPSA (dark blue).

The conformational dynamics of the P187S variant was also investigated by hydrogen-deuterium exchange coupled to mass spectrometry (HDX-MS). This method gives information about the changes in conformation dynamics of the protein under different conditions, in our case in the presence and absence of BPPSA. As can be seen in Figure 5B, BPPSA stabilized the flexible C-terminal part of the variant protein leading to slower incorporation of deuterium.

Crystal structure and docking

The strong stabilizing effect of BPPSA observed with the solution methods, prompted us to elucidate the exact binding site using x-ray crystallography (see Figure 5B-C and Table 1). Therefore, wild-type NQO1 was co-crystallized with BPPSA and the structure was determined to a resolution of 2.7 Å. As shown in Figure 5C, the overall structure of the protein is identical to previously described structures of wild-type NQO1 and the P187S variant. [10] Although, we obtained rather weak electron density for BPPSA in the active site of the protein near the isoalloxazine ring of the FAD cofactor, docking calculations were used to interpret the electron density and suggested that the ligand can bind in two possible ways with either the bromophenyl- or the sulfonyl group fitting in the electron density (Figure 5D).

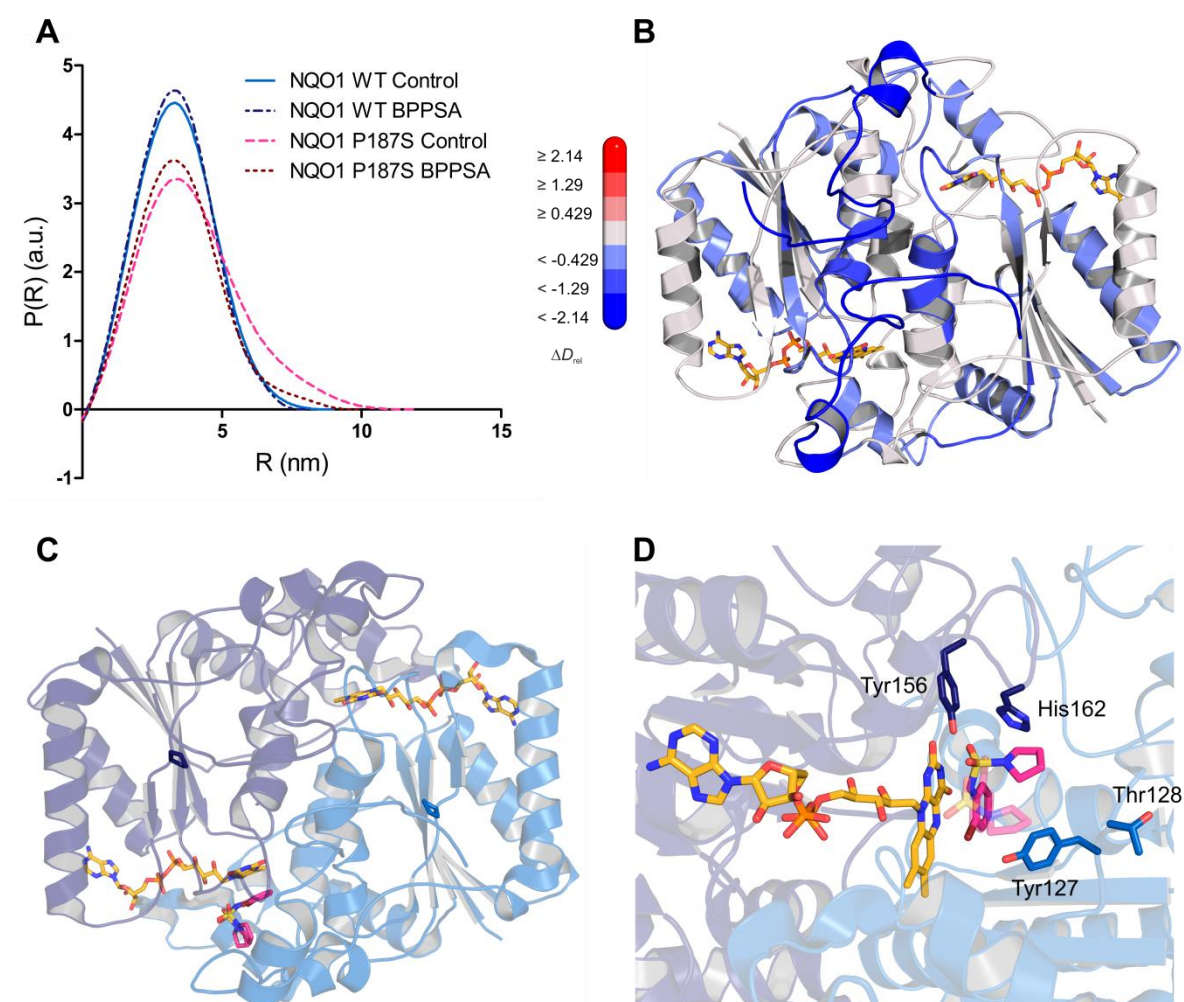


Figure 5. SAXS radial density distribution, conformational dynamics observed by HDX-MS and crystal structure of NQO1 WT with docked ligand. A. Small-angle scattering measurement of NQO1 WT and P187S in presence and absence of BPPSA. The SAXS data displays a comparison of the experimental radial density

distribution (P (R)) of NQO1 WT control (dark blue), NQO1 WT with BPPSA (light blue), NQO1 P187S control (maroon) and NQO1 P187S with BPPSA (pink). B. Structure of NQO1 P187S with colors corresponding to the relative incorporation of deuterium, ΔD_{rel} , between NQO1 P187S in presence of BPPSA relative to NQO1 P187S without BPPSA after 6 min of deuteration. The scale bar indicates the changes in ΔD_{rel} where blue corresponds to less incorporation of deuterium and red to higher incorporation. C and D. Structure of NQO1 WT with BPPSA. C. Overall structure of NQO1 WT with the 2 protomers colored in different shades of blue. The amino acid position P187 that is exchanged to serine in the variant protein is highlighted. FAD is colored yellow and the ligand is colored pink. D. Binding of the ligand to the active site illustrated in pink with an overlay of the two possible orientations with different transparency. The possible interacting residues Tyr-127 and Thr-128 are displayed with light blue stick representation and the catalytic residues Tyr-156 and His-162 are shown in dark blue.

Inhibition and activation assays

Since the crystal structure together with the HDX-MS measurements indicated that BPPSA binds to the active site, it was of interest to find out whether it acts as an inhibitor. From inhibition assays without co-incubation of ligand and NQO1, IC_{50} -value were calculated to be $8.6 \pm 1.1 \mu\text{M}$ for NQO1 WT and $26.2 \pm 1.2 \mu\text{M}$ for NQO1 P187S respectively from the inhibition curves displayed in Figure 3A. However, if the protein is co-incubated with the ligand, an activation effect can be observed, with an increase in activity especially for the variant protein as can be seen in Figure 3B. The largest activating effect, leading to an 80% increase in activity for the variant protein, could be observed at a final concentration of 400 nM ligand.

Steady state kinetics

Based on the activation assay, the concentration of ligand that exhibited the largest increase in activity was selected, and steady state kinetic parameters were determined for NQO1 P187S and WT in the presence and absence of BPPSA. As can be seen in Figure 6C-F and Table 2, presence of the ligand results in an increase in k_{cat}/K_M for both NADH and the quinone substrate menadione in the case of the variant protein. Under the same conditions no substantial change in activity can be observed for NQO1 WT.

Table 1. Data collection and refinement statistics for the crystal structure of NQO1 WT with BPPSA.

	NQO1 WT complex with BPPSA
Wavelength (Å)	1.009
Resolution range	52.75-2.76 (2.86-2.76)
Space group	$P3_112$
Unit cell (Å, °)	a=b=121.37, c=158.25 $\alpha=\beta=90, \gamma=120$
Total reflections	641366 (81424)
Unique reflections	34531 (4561)
Multiplicity	18.6 (17.9)
Completeness (%)	100 (100)
$\langle I/\sigma(I) \rangle$	15.1 (5.3)
Wilson B-factor (Å ²)	49.0
R_{merge}	0.158 (0.587)
R_{meas}	0.162 (0.604)
R_{pim}	0.038 (0.142)
$CC_{1/2}$	0.996 (0.950)
Reflections used in refinement	34483 (3393)
Reflections used for R_{free}	1717 (139)
R_{work}	0.2180 (0.3038)
R_{free}	0.2903 (0.3797)
CC_{work}	0.825 (0.810)
CC_{free}	0.836 (0.745)
Number of non-H atoms	8860
Macromolecules	8616
Ligands	244
Average B-factor (Å ²)	43.6
Macromolecules	43.8
Ligands	38.1
RMSD bonds (Å)	0.009
RMSD angles (°)	1.2
Ramachandran plot favoured/allowed/outliers (%)	96.6/3.4/0.0
Rotamer outliers (%)	1.3
Clashscore	8.5

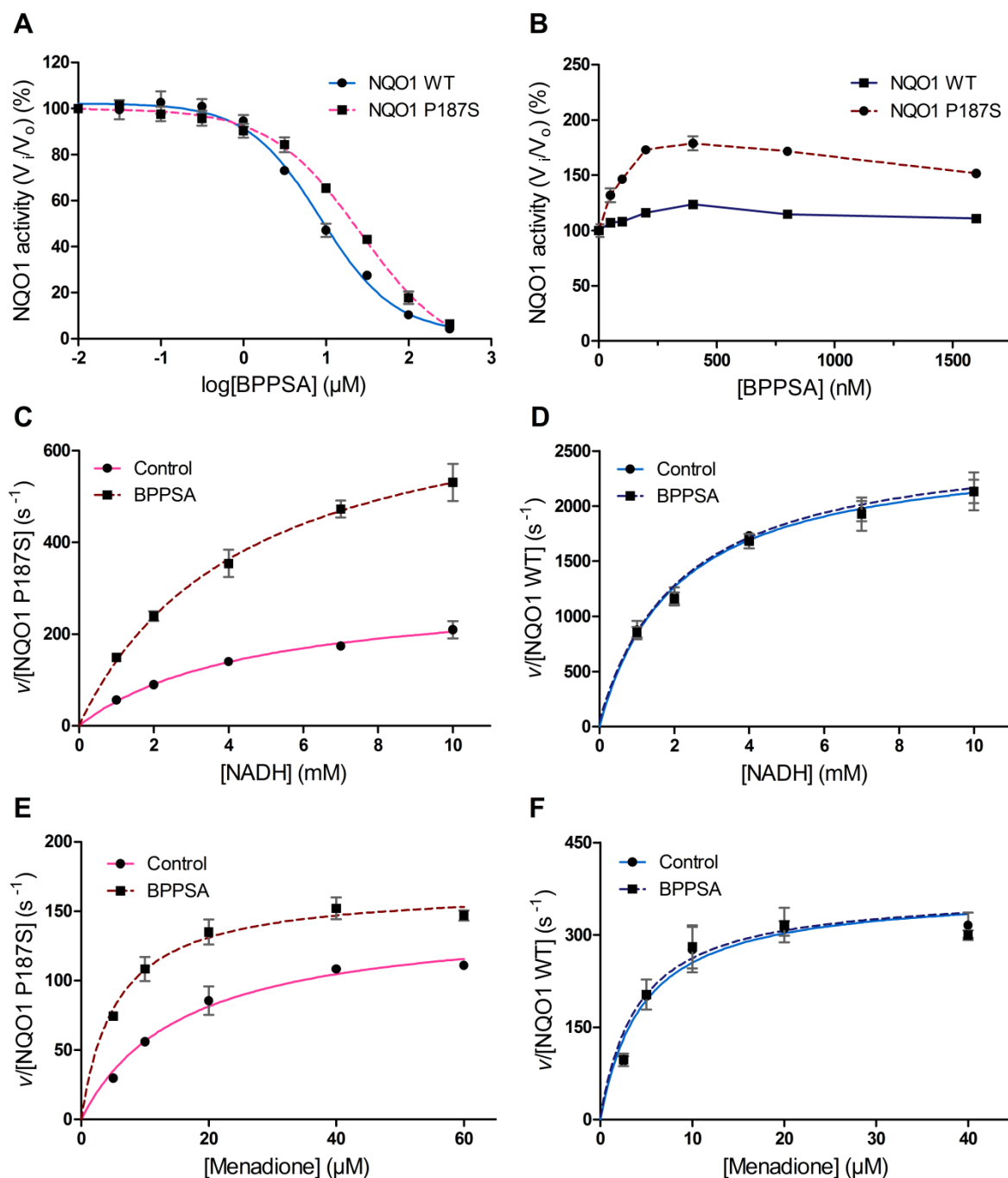


Figure 3. Inhibition, activation and steady state kinetic assays for NQO1 WT and P187S in presence and absence of BPPSA. Inhibition by BPPSA is in (A) shown for NQO1 WT (in blue) and NQO1 P187S (in pink) and the corresponding IC_{50} values were calculated to be $8.55 \mu\text{M}$ for NQO1 WT and $25.9 \mu\text{M}$ for NQO1 P187S. (B) Activation of NQO1 WT (dark blue) and NQO1 P187S (maroon) in presence of BPPSA. The velocity v over the enzyme concentration is plotted against the concentration of NADH for (C) NQO1 P187S and (D) NQO1 WT and against the concentration of menadione for (E) NQO1 P187S and (F) NQO1 WT.

Table 2. Steady state kinetic parameters determined for NQO1 WT and NQO1 P187S with and without BPPSA. Kinetic parameters with standard errors were determined for NQO1 WT and NQO1 P187S, using NADH as electron donor and menadione as electron acceptor and in the presence and absence of BPPSA.

		NADH			Menadione		
		$k_{cat,app}$ (s^{-1})	$K_{M,app}$ (mM)	$k_{cat,app}/K_{M,app}$ ($mM^{-1}s^{-1}$)	k_{cat} (s^{-1})	K_M (μM)	k_{cat}/K_M ($\mu M^{-1}s^{-1}$)
NQO1	Ctrl	300 ± 20	5 ± 1	70 ± 10	150 ± 7	16 ± 2	9 ± 1
P187S	BPPSA	770 ± 40	4 ± 0.5	170 ± 20	170 ± 4	6 ± 1	30 ± 4
NQO1	Ctrl	2550 ± 70	2 ± 0.2	1250 ± 110	370 ± 20	5 ± 1	80 ± 16
WT	BPPSA	2580 ± 90	2 ± 0.5	1180 ± 140	370 ± 23	4 ± 1	90 ± 20

Cell viability in combination with mitomycin C

MCF7 cells (NQO1*1/NQO1*2 homozygote for the SNP) and MCF-12A cells (NQO1*1/NQO1*1 homozygote WT) were treated with BPPSA concentration range of 0-640 μM and depending on the IC_{50} concentration of mitomycin C, MCF7 with 0-8 μM and MCF-12A with 0-2 μM . By treating MCF7 and MCF-12A with 160 μM BPPSA a synergy effect was achieved in MCF12A with a very low mitomycin C concentration compared to MCF7, where the used concentration was ten times higher (Figure 7), which might attribute to the different genetic profile of the tested cell lines.

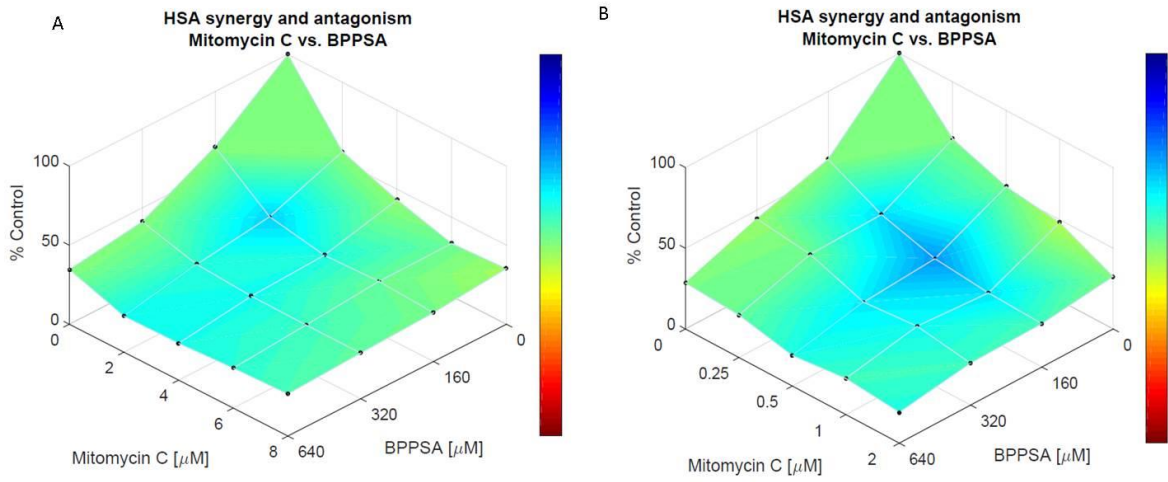


Figure 7. HSA synergy and antagonism of MCF7 (A) and MCF-12A (B) treated with mitomycin C and BPPSA. Blue indicates synergy, red indicates antagonism.

Discussion

In the present study, we performed virtual screening as a starting point for the search of possible stabilizing ligands, followed by initial *in vitro* screening experiments including thermal stability assays, absorption difference titrations, limited proteolysis and ITC). These experiments confirmed that the selected ligand BPPSA clearly binds to both the wild-type and variant protein, leading to a significant stabilization of the protein structures. Interestingly, both the wild-type and variant structures were stabilized, however to a different degree, as was observed in limited proteolysis experiments, indicating that a larger portion of the C-terminal domain was stabilized in the wild-type as compared to the variant (Figure 1).

Due to the interesting effect on the protein stability, further analyses of the stabilizing effect of BPPSA were performed using more advanced techniques, such as HSQC-NMR, HDX-MS and SAXS. Based on our HSQC-NMR data, it was observed that the variant protein in the presence of the ligand, displayed a clearly improved HSQC-spectrum most probably due to a reduced flexibility of residues in the variant protein. The variant protein also occupied a more compact conformation, more similar to that of the wild-type, in presence of the ligand as shown by SAXS measurements. Finally, HDX-MS experiments revealed in detail that the flexible C-terminal domain of the protein was stabilized. Consequently, these experiments have illustrated that the variant in the presence of the ligand repopulates a conformation more similar to the wild-type, in particular with regard to the C-terminal domain. This is consistent with other data showing that the C-terminus is largely destabilized in the P187S variant, leading to the loss of the FAD cofactor and consequently of enzymatic activity. [10]

The determination of the crystal structure further demonstrated that the ligand binds to the active site, where it seems to interact with the residues Tyr-127 and Thr-128. Since binding of the ligand in or near the active site could potentially compromise the activity of the enzyme, the possible inhibitory effect as well as steady state kinetic parameters were determined, showing that co-incubation of the ligand with the enzyme (in the presence of excess flavin cofactor) leads to a substantial increase in catalytic efficiency of the variant protein. Hence, under ideal conditions it is possible that the ligand can be used to rescue the enzymatic activity *in vitro*. The most probable reason for the advantageous effect on the activity seems to be connected to a higher loading of FAD cofactor to the variant protein, consequently resulting in a

higher population of holoenzyme present during the reaction. This also explains the minor differences observed in the activity of the wild-type enzyme, since the cofactor binding is approximately 7 times tighter. [10]

Because of the promising effects of the ligand on the activity *in vitro*, some initial experiments were also carried out on cell lines homozygous (*NQO1*1/NQO1*1*) and heterozygous (*NQO1*1/NQO1*2*) to the SNP. Owing to the challenge of comparing two cell lines with different growth behavior, different doubling time and different types of media, a constant BPPSA concentration range was chosen for both cell lines, whereas the mitomycin C concentration was adjusted to the respective cell line. Interestingly, a synergistic effect of mitomycin C and BPPSA could be observed for both cell lines at a concentration of 160 μ M BPPSA. The difference in the required mitomycin C concentration also fits to earlier reports on the difference in bioactivation of mitomycin C depending on the genetic profile of the cell line [11]. These results indicate that there might be a beneficial effect of BPPSA on some types of cancer cell lines; however the effect seems not to be directly connected to the genotype and has to be studied in more detail in the future. Furthermore, it could be determined that BPPSA is nontoxic to the cells at low concentrations (in Figure 7 a larger concentration range is shown) making it promising for further tests as an activating ligand.

In conclusion the current study could prove that binding of a small ligand to the active site of the variant protein leads to an improved stability and consequently also an increased activity of the variant protein *in vitro*. The beneficial effect on cancer cell lines will be investigated further in the future. Therefore, our study has demonstrated that the development of small molecular chaperones is a promising option for rescuing the activity of unstable protein variants and consequently an interesting alternative for treatment of human diseases associated with protein instability.

Experimental Procedures

Reagents

All chemicals and reagents were of highest quality available either from Sigma-Aldrich (St. Louis, MO, USA), Carl Roth GmbH (Karlsruhe, Germany) or Thermo Fisher Scientific (Waltham, USA) unless otherwise mentioned. Purification columns were obtained from GE Healthcare (Little Chalfont, UK). Trypsin was from Promega (Madison, Wisconsin, United States). Labelled ammonium sulphate was from CortecNet (Voisins-Le-Bretonneux, France). The investigated ligand BPPSA was purchased from Enamine LLC (Monmouth Junction, New Jersey, USA).

*Molecular cloning of *nqo1**

The cloning of NQO1 as well as the generation of the NQO1 P187S variant have been described previously [10]. Briefly, the *NQO1* gene optimized for expression in *Escherichia coli* was obtained from GeneArt (Carlsbad, California, USA) and cloned into a pET28a vector from Merck (Darmstadt, Germany). NQO1 P187S was generated with the Quick Change II XL Site-Directed Mutagenesis Kit from Agilent (Santa Clara, California, USA) by the use of gene specific primers from Eurofins (Luxembourg).

Heterologous protein expression and purification

The protein expression and purification were performed according to the procedure described by Lienhart *et al.*[10]. In brief, the protein expression was carried out in lysogeny broth (bacto-tryptone 10 g/L, bacto yeast extract 5 g/L, NaCl 5 g/L) containing 50 µg/L kanamycin. The main culture was inoculated with 5% of an overnight culture and incubated at 37 °C at 140 rpm in shake flasks in a HT Multitron Standard shaking system (Infors AG, Basel, Switzerland) until an OD₆₀₀ of around 0.8 was reached, the cultures were then induced with 0.5 mM isopropyl-β-D-thiogalactoside and grown for 16 h at 25 °C. Cells were harvested by centrifugation at 4420 g at 4 °C for 10 min, resuspended in 1% saline solution and thereafter centrifuged again at 4570 g for 45 min. The cell pellets were then resuspended in 2 mL/g pellet of lysis buffer (HEPES 50 mM, NaCl 150 mM, imidazole 10 mM, pH 7.0) and 1 mg FAD, 10 µL protease inhibitor cocktail for histidine-tagged proteins (Sigma-Aldrich, Missouri, USA), 1 mM phenylmethylsulfonyl fluoride dissolved in dimethylsulfoxide and 20 µg/mL lysozyme were added to 25 mL of the cell

suspension. Next, the cells were disrupted by sonication in a Sonopuls glass rosette cell RZ (Bandelin, Berlin, Germany) on ice with a Labsonic L instrument from Braun Biotech. International (Berlin, Germany) with 120 W for 6 x 3 min and 3 min pause in between each cycle. The cell debris was removed by centrifugation at 38 470 g at 4 °C for 1 h. The supernatant was then loaded onto a 5 mL HisTrap FF column equilibrated with lysis buffer, whereafter the column was washed with wash buffer (HEPES 50 mM, NaCl 150 mM, imidazole 50 mM, pH 7.0). Proteins were finally eluted with elution buffer (HEPES 50 mM, NaCl 150 mM, imidazole 300 mM, pH 7.0). The protein containing fractions were combined and concentrated by using centrifugal filter units with 10 kDa cut-off from Pall Life Sciences (Michigan, USA). The concentrated protein was further purified by size-exclusion chromatography on a HiLoad 16/60 Superdex 200 prep grade column equilibrated with HEPES 50 mM, NaCl 150 mM, and pH 7.0 at 4 °C. The column was connected to an ÄKTA FPLC system (GE Healthcare, Little Chalfont, UK). The purity of the protein containing fractions were checked using SDS-PAGE, the pure fractions were then pooled and concentrated by using centrifugal filter units and finally rebuffered with a PD-10 desalting column to HEPES 50 mM, pH 7.0. The protein was then shock frozen and stored at -80 °C.

Virtual screening

Potentially stabilizing compounds were found by *in silico* docking using Dock blaster (<http://blaster.docking.org>, University of California, San Francisco), and refinement [12]. Dockings were performed using the available structure of the NQO1 P187S variant (PDB code 4CET). In order to search for possible lead compounds, the ZINC database (<http://zinc.docking.org>, University of California, San Francisco) with commercially available lead compounds was used.

Thermal shift assay

The melting point determinations were performed as described by Forneris *et al.* and Ericsson *et al.* [13, 14]. Briefly, 25 µL of 50 µM NQO1 WT or P187S with or without ligand at a concentration of 300 µM were mixed in a white 96-well RT-PCR plate (Bio-Rad Laboratories, Hercules, California, USA) sealed with optical-quality sealing tape (Bio-Rad Laboratories, Hercules, California, USA). The plate was heated from 20 to 95 °C, with 0.5 °C steps, in a CFX Connect™ Real-Time PCR Detection

System from Bio-Rad Laboratories (Hercules, California, USA) and the change in fluorescence due to the release of the FAD cofactor upon unfolding of the protein was detected. The thermal stability was analysed using the CFX Manager 3.0 software from Bio-Rad Laboratories (Hercules, California, USA).

UV/Vis absorption difference titration

The difference absorption spectra were recorded with a Specord 200 plus spectrophotometer from Analytik Jena (Jena, Germany) at 25 °C in tandem cuvettes from Hellma Analytic (Müllheim, Germany). For the measurement 800 µl of NQO1 WT or NQO1 P187S in HEPES 50 mM, pH 7.0, at a concentration of 40 µM in the measurement cell, was titrated with BPPSA (in 2 µL steps from a 2 mM stock, dissolved in 50 % v/v ethanol). The same volume of compound was added to the buffer chamber in the reference cuvette at the same time as the same volume of 50% ethanol in buffer was added to the protein chamber in the reference cuvette in order to always keep the dilution the same in all chambers. For the analysis the sum of the absorption values at 444 nm and 496 nm in the case of NQO1 WT and 440 nm and 491 nm in the case of NQO1 P187S were plotted against the concentration of BPPSA.

Isothermal titration calorimetry

ITC measurements were performed using a PEAQ-ITC (Malvern Panalytical Ltd, United Kingdom). 380 µM NQO1 WT or P187S and 23 µM BPPSA in the case of NQO1 WT and 13 µM BPPSA in the case of NQO1 P187S was used for the experiments. All samples were prepared in HEPES 50 mM at pH 7.0 with 1% DMSO in the final samples. The experiments were performed at 25 °C, with a stirring speed of 500 rpm. One experiment consisted of 13-14 injections with a volume of 2.8 µL (including a first injection with a volume of 0.4 µL) and the spacing used was 250 seconds.

Steady state kinetics

Measurements of the initial-velocity were performed for NQO1 WT and NQO1 P187S in presence and absence of the ligand by using a Specord 200 plus spectrophotometer (Analytik Jena, Jena, Germany) at 25 °C. The assays were performed in 50 mM HEPES containing 150 mM NaCl, pH 7.0, with NADH as electron donor and menadione as electron acceptor. For all components the

concentrations were determined spectrophotometrically. The reaction mixture for the assay performed with variation of the concentration of NADH contained 2.5 nM NQO1 WT or 20 nM NQO1 P187S, 200 μ M menadione ($\epsilon_{333\text{nm}} = 2,450 \text{ M}^{-1}\text{cm}^{-1}$, prepared in ethanol with a final concentration of 1% v/v), 1-10 mM NADH ($\epsilon_{340\text{nm}} = 6,220 \text{ M}^{-1}\text{cm}^{-1}$) and 10 times the K_D of FAD equal to 0.6 μ M for NQO1 WT and 4.2 μ M for NQO1 P187S respectively. For the assay with variation of the concentration of menadione the reaction mixture consisted of 1 nM NQO1 WT or 5 nM NQO1 P187S, 10 mM NADH, 45 μ M cytochrome C and 2.5-40 μ M menadione in the case of NQO1 WT and 5-60 μ M in the case of NQO1 P187S (dissolved in ethanol with a final concentration of 1% v/v) and 0.6 μ M and 4.2 μ M of FAD for wild-type and variant respectively. The reaction mixtures were incubated for 2 minutes at 25 °C and the reaction was initiated by addition of the enzyme and the decrease in absorption of NADH was measured at 400 nm (determined for these measurements) in the case of variation of NADH and the increase at 555 nm due to the reduction of cytochrome C in the case of variation of menadione. The slope corresponding to the first 20 s was used for the analysis for all conditions. The kinetic parameters were determined using the GraphPad Prism 5.01 software for Windows (La Jolla, California, USA).

Inhibition and activation assays

The inhibiting and activating effects of BPPSA on NQO1 WT and NQO1 P187S were investigated by using a Specord 200 plus spectrophotometer (Analytik Jena, Jena, Germany) at 25 °C. The concentrations for the used components were all determined spectrophotometrically. The final reaction mixture contained 500 μ M NADH ($\epsilon_{340\text{nm}} = 6,220 \text{ M}^{-1}\text{cm}^{-1}$), 200 μ M menadione ($\epsilon_{333\text{nm}} = 2,450 \text{ M}^{-1}\text{cm}^{-1}$, dissolved in ethanol), 10 nM NQO1 WT or 20 nM NQO1 P187S and 0-316 μ M BPPSA (dissolved in ethanol) for the inhibition assay and 0-1600 nM ligand for the activation assay respectively. In the case of NQO1 P187S a final concentration of 4.2 μ M FAD was included in the assay. The reaction mixtures were first incubated for 2 min at 25 °C whereafter the reaction was started by addition of enzyme. For the activation assay the ligand was co-incubated with the protein for at least 30 minutes before the reaction was started. The decrease in absorption caused by the breakdown of NADH was measured at 380 nm. For analysis the slope corresponding to the first 30 s of the reaction was used. The IC_{50} values were calculated using the GraphPad Prism 5.01 software for Windows (La Jolla, California, USA).

Limited proteolysis

NQO1 WT and NQO1 P187S at a concentration of 15 μ M in HEPES 50mM, NaCl 150 mM and pH 7.0 were digested with trypsin from Promega (Madison, WI, USA) at a final concentration of 2 μ g/mL at 37 °C. Samples were prepared with only protein (NQO1 WT or NQO1 P187S), with protein and 30 μ M FAD and with protein, 30 μ M FAD and 300 μ M BPPSA. Trypsin was preincubated at 37 °C for 15 min where, after the digestion was started, samples were taken out after specific time points (0, 5, 10, 20, 40, 80, 160 min and overnight, 18 h) and the reactions were stopped by addition of SDS sample buffer followed by boiling at 95 °C for 10 min. The samples were then analysed by SDS-PAGE. [10, 15]

MALDI-TOF MS

The protein bands from the SDS-PAGE were cut out, washed and destained. The protein samples were in gel reduced by 10 mM dithiothreitol and the cysteines were alkylated by 55 mM iodoacetamide. The proteins were then in gel digested with trypsin at 37 °C over night, whereafter peptides were extracted from the gel by using an buffer containing 50% acetonitrile and 5% formic acid. The extraction buffer was then evaporated in an ISS100 SpeedVac[®] system (Thermo Scientific, Waltham, MA, USA) for 2 hours. The peptide mixtures were dissolved in double distilled water and 0.1% TFA and desalted with ZipTip (Millipore Merck, Burlington, MA, USA). The purified samples were spotted on a MALDI plate together with the matrix *a*-cyano-4-hydroxycinnamic acid (10 mg/mL in a 1:1 v/v ratio). After a washing step with cold double distilled water and 0.1% TFA, spectra were then recorded on a Micromass ToFSpec 2E in reflectron mode with an accelerating voltage of +20 kV. A calibration of the instrument was done with a poly(ethylene glycol) mixture (Sigma-Aldrich, St Louis, MO, USA) and ProteoMass ACTH fragment 18 – 39 MALDI-MS Standard (Sigma-Aldrich, St Louis, MO, USA) was used as the calibration standard for peptides. The spectra were analyzed with MASSLYNX 4.1 (Micromass UK Limited, Wilmslow, United Kingdom) and compared to peptide fragments predicted by PeptideMass (Ref).

¹⁵N-Labeling of NQO1 and NQO1 P187S

For the expression of the ¹⁵N-labelled proteins a minimal medium containing 6.8 g/L Na₂HPO₄, 3 g/L KH₂PO₄, 0.5 g/L NaCl, 1 g/L ¹⁵NH₄Cl, 3 g/L glucose, 1 μ g/L biotin, 1 μ g/L thiamine, 50 μ g/mL kanamycin and 1 mL 1000x microsals (150 mM CaCl₂, 20

mM, FeCl₃, 50 mM H₃BO₃, 150 μM CoCl₂, 800 μM CuCl₂, 1.5 mM ZnCl₂, 15 μM (NH₄)₆Mo₇O₂₄·4H₂O) was used for the protein expression that apart from the different media was carried out as described under the section *Heterologous protein expression and purification*.

NMR spectroscopy

For NMR acquisitions, ¹⁵N-labelled NQO1 or NQO1 P187S were dialyzed into a HEPES buffer (50 mM, pH 6.5) to final concentrations of 300 μM (NQO1 WT) and 530 μM (NQO1 P187S). To each sample 10% ²H₂O was added for field-frequency locking. BPPSA was added to final concentrations of 440 μM in the case of NQO1 WT and 680 μM in the case of NQO1 P187S. All spectra were recorded at 300 K on a Bruker Avance III 700 MHz NMR spectrometer, equipped with a 5 mm cryogenically cooled TCI probe with z-axis gradients. Two-dimensional ¹H-¹⁵N-HSQC were acquired with data matrices of 2048 x 128 data points. Forty-eight scans were recorded for each increment and 60° phase shifted squared sine-bell window functions were applied in both dimensions prior to Fourier transformation using TopSpin 3.1.

Small-angle X-ray scattering

SAXS data for solutions of the ligand bound or free forms of NQO1 wild type and P187S variant in presence of the FAD cofactor were recorded on an in-house SAXS instrument (SAXSspace, Anton Paar, Graz, Austria) equipped with a Kratky camera, a sealed X-ray tube source and a Mythen2 R 1K Detector (Dectris). The scattering patterns were measured with a 60-min exposure time (60 frames, each 1 min) with a solute concentration of 200 μM. Radiation damage was excluded on the basis of a comparison of individual frames of the 60-min exposures, wherein no changes were detected. A range of momentum transfer of $0.010 < s < 0.63 \text{ \AA}^{-1}$ was covered ($s = 4\pi \sin(\theta)/\lambda$, where 2θ is the scattering angle, and λ is the X-ray wavelength, in this case 1.5 Å).

All SAXS data were analyzed and processed using the SAXS analysis package (Anton Paar, version 3.0). The data were desmeared using GIFT (PCG-Software). The forward scattering ($I(0)$), the radius of gyration, (R_g), the maximum dimension (D_{max}) and the interatomic distance distribution function ($P(r)$) were computed with GNOM [16]. The masses of the solutes were evaluated based on their Porod volume.

Hydrogen-deuterium exchange coupled to mass spectrometry

2 μL aliquots of 200 μM wild-type NQO1 as well as the P187S variant were diluted 1:20 with deuteration buffer (10 mM HEPES pD 7.0, 150 mM NaCl and 10 mM MgCl_2). Analogous dilutions were prepared with wild-type and variant samples preincubated with 750 μM BPPSA to achieve the same final protein concentrations. Ligand concentrations in the labelling reaction are still 4.6- and 1.9-fold above the K_D for the interaction of BPPSA with wild-type NQO1 and the P187S variant, respectively.

Individual time points of the labelling reaction were sampled by removing 7.5 μL after 10, 60, 360, and 2400 s and immediate quenching with 7.5 μL ice-cold buffer 200 mM ammonium formate (pH 2.6) in the presence of 2.7 M urea. After mixing the samples were immediately frozen in liquid nitrogen until further analysis by HPLC-MS. Samples were then thawed by rapid mixing with 45 μL ice-cold quench buffer and injected into a cooled HPLC setup as described in detail previously [17]. Briefly, samples were digested using an on-line pepsin column (Applied Biosystems) operated at 10 $^\circ\text{C}$ during a contact time of 1 min. Resulting peptides were desalted on a 2-cm C18 guard column (Discovery Bio C18, Supelco) and separated during a 5 min acetonitrile gradient (15 to 50%) in the presence of 0.6% formic acid on a reversed-phase column (XR ODS 75 mm \times 3 mm, 2.2 μm particle size; Shimadzu) prior to infusion into a maXis ESI-UHR-TOF mass spectrometer (Bruker). HDX-MS data were analysed using the software package Hexicon 2 [18].

Crystallization and crystal structure determination

NQO1 was co-crystallized with BPPSA using the vapor diffusion method employing different commercial crystallization screens (Index, PEG/Ion from Hampton Research and Morpheus Screen from Molecular Dimensions). Drops were prepared by mixing 0.5 μL of the protein solution (at a concentration of 17 mg/mL in 50 mM HEPES, pH 7.0) with an equal volume of mother liquor using an ORYX 8 pipetting robot (Douglas Instruments). The trays were incubated at 20 $^\circ\text{C}$. Yellow crystals were observed after approximately one month in various conditions. Diffracting crystals were obtained from the original condition A5 of the PEG/Ion screen consisting of 0.2 M magnesium chloride hexahydrate, 20% w/v polyethylene glycol 3350, pH 5.9.

Diffraction data were collected to a maximum resolution of 2.76 Å on beamline P11 ($\lambda=1.0089$ Å) at DESY Hamburg, Germany. The crystals were trigonal (space group $P3_112$) with unit-cell parameters $a=b=121.37$ Å and $c=158.25$ Å. The data were processed using iMOSFLM [19] and programs from the CCP4 suite [20]. The structure was solved by molecular replacement using the program PHASER [21] with the structure of the NQO1 variant P187S (PDB code: 4CET) as template. The structure was refined using the programs Coot [22] and PHENIX [23]. Clear residual electron density was observed for flavin adenine dinucleotide (FAD) bound to each of the four chains in the asymmetric unit. Only in one of the four independent active sites (associated with chain B) the difference electron density was clear enough to interpret it as a molecule of BPPSA in two alternate orientations. Detailed statistics pertaining to data processing and structure refinement are summarized in Table 1. Atomic coordinates and structure factors have been deposited in the Protein Data Bank under the accession number 6FY4.

Docking calculations

BPPSA was docked into the active site of NQO1 with the program ADFR[24] using 104 genetic-algorithm (GA) optimization runs with a maximum of 2.5 million energy evaluations per run. The receptor was kept rigid, while the ligand was flexible.

Cell Culture

Human colon cancer cell line HT29 (CLS, Eppelheim, Germany) and human breast cancer cell line MCF-7 (CLS) were cultured in Dulbecco's-modified Eagle's medium (DMEM-F12; Life Technology, Austria), containing 10% fetal bovine serum (FBS) (M&B Stricker, Bernried, Germany), 2mM L-glutamine (Life Technology), 100 units/ml Penicillin, 100 units/ml Streptomycin (Life Technology). Human colon carcinoma cell line Caco2 (DSMZ, Braunschweig, Germany) were cultured in MEM (Life Technology) containing 20% FBS and 2 mM L-glutamine. Human breast cancer cell line MCF-12a (ATCC, VA, US) was cultured in DMEM/Ham'sF12 (Life Technology), supplemented with 20 ng/ml human epidermal growth factor (Sigma-Aldrich), 100 ng/ml cholera toxin (Sigma-Aldrich), 0.01 mg/ml bovine insulin (Sigma-Aldrich), 500 ng/ml hydrocortisone and 5% horse serum. Human lung adenosquamous carcinoma NCI-H596 (ATCC) was cultured in RPMI 1640 (Life Technology), containing 10% FBS and 2 mM L-glutamine. All cell lines were verified by short tandem repeat analysis using PowerPlex 16 System Kit (Promega, Mannheim, Germany) and tested

for mycoplasma. Cells were kept at 37°C in a humidified atmosphere of 5% CO₂ and were passaged by trypsinization after reaching 80–90% confluence.

Cell Viability

To determine the IC₅₀ concentration of BPPSA, different cell amounts depending on the cell line were seeded in a 96 well plate and cultivated from 24-72 h (depending on the growth rate of the cell line) to achieve good attachment and 50-70% cell confluency. The cells were first treated with Mitomycin C in the range of 1 – 64 µM and with BPPSA in the range of 20-640 µM. The viability of cells was obtained using the CellTiter 96 AQueous Non-Radioactive Cell Proliferation Assay (Promega), by measuring the reduction of tetrazolium compound to formazan. For combination treatment the cells were treated with the concentrations closest to the range of IC₅₀ for both substances. After 48 h the cell proliferation assay was performed according to the manufacturer's protocol. Mitomycin C stock solution was prepared by diluting it with ddH₂O to concentration of 1497 µM and sterile filtered. The solution was discarded after 1 week. BPPSA stock solution was prepared by diluting it with DMSO to concentration of 98299.4 µM and sterile filtered.

Synergy Analysis

Synergy analysis was performed using Combenefit software [25], which assessed possible drug interactions using the Highest Single Agent (HSA) model [26]. We considered the combination of two agents Mitomycin C (a) and BPPSA (b). For the HSA model, the reference effect for the combination (a,b) is obtained by taking the greatest effect (lowest residual compared to control) between the two drugs as single agents:

$$R_{AB_HSA}(a, b) = \text{MIN}(E_A(a), E_B(b))$$

The matrix synergy plot showed the synergy/antagonism score ± the standard deviation for each combination and its statistical significance following a one sample t test (* p<5x10⁻²; **p<10⁻³, ***p<10⁻⁴). Synergy scores were also displayed as dose-response surface plots.

Acknowledgements

Thanks to Karin Koch, Shalinee Jha and Venogupal Gudapati for valuable discussions. This work was supported by the Austrian Fonds zur Förderung der wissenschaftlichen Forschung (FWF) through project P22361 to PM and KG and project P28854 to TM. Additional funding was received by the PhD programs “Molecular Enzymology” (W901) and “Molecular Basis of Cardiovascular Disease” (W1226) to KZ, KG, PM and to TM, respectively. We also thank the interuniversity program in natural sciences, NAWI Graz, for financial support. This work was supported by the Bavarian Ministry of Sciences, Research and the Arts (Bavarian Molecular Biosystems Research Network, to T.M.), the President’s International Fellowship Initiative of CAS (No.2015VBB045, to T.M.), the National Natural Science Foundation of China (No. 31450110423, to T.M.), the Austrian Science Fund (FWF: P28854 and I3792 to T.M.), the Austrian Research Promotion Agency (FFG: 864690), the Integrative Metabolism Research Center Graz, the Austrian infrastructure program 2016/2017, BioTechMed/Graz, the OMICS center Graz as well as the Deutsche Forschungsgemeinschaft (DFG) with the grant MA5703/1-1 (to T.M.).

References

- [1] M. Garate, R. P. Wong, E. I. Campos, Y. Wang, G. Li, NAD(P)H quinone oxidoreductase 1 inhibits the proteasomal degradation of the tumour suppressor p33(ING1b), *EMBO Rep.* 9 (2008) 576-581.
- [2] G. Asher, P. Tsvetkov, C. Kahana, Y. Shaul, A mechanism of ubiquitin-independent proteasomal degradation of the tumor suppressors p53 and p73, *Genes Dev.* 19 (2005) 316-321.
- [3] A. Begleiter, N. El-Gabalawy, L. Lange, M. K. Leith, L. J. Guziec, F. S. G. Jr, A Model for NAD(P)H:Quinoneoxidoreductase 1 (NQO1) Targeted Individualized Cancer Chemotherapy, *Drug Target Insights* 4 (2009) 1-8.
- [4] D. Siegel, C. Yan, D. Ross, NAD(P)H:quinone oxidoreductase 1 (NQO1) in the sensitivity and resistance to antitumor quinones, *Biochem. Pharmacol.* 83 (2012) 1033-1040.
- [5] Z. Dai, A. C. Papp, D. Wang, H. Hampel, W. Sadee, Genotyping panel for assessing response to cancer chemotherapy, *BMC Medical Genomics* 1 (2008) 24.
- [6] R. D. Traver, D. Siegel, H. D. Beall, R. M. Phillips, N. W. Gibson, W. A. Franklin, D. Ross, Characterization of a polymorphism in NAD(P)H: Quinone oxidoreductase (DT-diaphorase), *Br. J. Cancer* 75 (1997) 69-75.
- [7] K. T. Kelsey, D. Ross, R. D. Traver, D. C. Christiani, Z. F. Zuo, M. R. Spitz, M. Wang, X. Xu, B. K. Lee, B. S. Schwartz, J. K. Wiencke, Ethnic variation in the prevalence of a common NAD(P)H quinone oxidoreductase polymorphism and its implications for anti-cancer chemotherapy, *Br. J. Cancer* 76 (1997) 852-854.
- [8] D. W. Nebert, A. L. Roe, S. E. Vandale, E. Bingham, G. G. Oakley, NAD(P)H:quinone oxidoreductase (NQO1) polymorphism, exposure to benzene, and predisposition to disease: a HuGE review, *Genet. Med.* 4 (2002) 62-70.

- [9] R. Fagerholm, B. Hofstetter, J. Tommiska, K. Aaltonen, R. Vrtel, K. Syrjakoski, A. Kallioniemi, O. Kilpivaara, A. Mannermaa, V. M. Kosma, M. Uusitupa, M. Eskelinen, V. Kataja, K. Aittomaki, K. von Smitten, P. Heikkila, J. Lukas, K. Holli, J. Bartkova, C. Blomqvist, J. Bartek, H. Nevanlinna, NAD(P)H:quinone oxidoreductase 1 NQO1*2 genotype (P187S) is a strong prognostic and predictive factor in breast cancer, *Nat. Genet.* 40 (2008) 844-853.
- [10] W. D. Lienhart, V. Gudipati, M. K. Uhl, A. Binter, S. A. Pulido, R. Saf, K. Zangger, K. Gruber, P. Macheroux, Collapse of the native structure caused by a single amino acid exchange in human NAD(P)H:quinone oxidoreductase 1, *The FEBS Journal* 281 (2014) 4691-4704.
- [11] D. Siegel, C. Yan, D. Ross, NAD(P)H:quinone oxidoreductase 1 (NQO1) in the sensitivity and resistance to antitumor quinones, *Biochem. Pharmacol.* 83 (2012) 1033-1040.
- [12] J. J. Irwin, B. K. Shoichet, M. M. Mysinger, N. Huang, F. Colizzi, P. Wassam, Y. Cao, Automated docking screens: a feasibility study, *J. Med. Chem.* 52 (2009) 5712-5720.
- [13] F. Forneris, R. Orru, D. Bonivento, L. R. Chiarelli, A. Mattevi, ThermoFAD, a Thermofluor-adapted flavin ad hoc detection system for protein folding and ligand binding, *The FEBS Journal* 276 (2009) 2833-2840.
- [14] U. B. Ericsson, B. M. Hallberg, G. T. Detitta, N. Dekker, P. Nordlund, Thermofluor-based high-throughput stability optimization of proteins for structural studies, *Anal. Biochem.* 357 (2006) 289-298.
- [15] S. Chen, P. S. Deng, J. M. Bailey, K. M. Swiderek, A two-domain structure for the two subunits of NAD(P)H:quinone acceptor oxidoreductase, *Protein Sci.* 3 (1994) 51-57.
- [16] D. I. Svergun, Determination of the regularization parameter in indirect-transform methods using perceptual criteria, *Journal of Applied Crystallography* 25 (1992) 495-503.

- [17] A. Winkler, T. R. Barends, A. Udvarhelyi, D. Lenherr-Frey, L. Lomb, A. Menzel, I. Schlichting, Structural details of light activation of the LOV2-based photoswitch PA-Rac1, *ACS Chem. Biol.* 10 (2015) 502-509.
- [18] R. Lindner, X. Lou, J. Reinstein, R. L. Shoeman, F. A. Hamprecht, A. Winkler, Hexicon 2: automated processing of hydrogen-deuterium exchange mass spectrometry data with improved deuteration distribution estimation, *J. Am. Soc. Mass Spectrom.* 25 (2014) 1018-1028.
- [19] T. G. Battye, L. Kontogiannis, O. Johnson, H. R. Powell, A. G. Leslie, iMOSFLM: a new graphical interface for diffraction-image processing with MOSFLM, *Acta Crystallogr. D Biol. Crystallogr.* 67 (2011) 271-281.
- [20] M. D. Winn, C. C. Ballard, K. D. Cowtan, E. J. Dodson, P. Emsley, P. R. Evans, R. M. Keegan, E. B. Krissinel, A. G. Leslie, A. McCoy, S. J. McNicholas, G. N. Murshudov, N. S. Pannu, E. A. Potterton, H. R. Powell, R. J. Read, A. Vagin, K. S. Wilson, Overview of the CCP4 suite and current developments, *Acta Crystallogr. D Biol. Crystallogr.* 67 (2011) 235-242.
- [21] A. J. McCoy, R. W. Grosse-Kunstleve, P. D. Adams, M. D. Winn, L. C. Storoni, R. J. Read, Phaser crystallographic software, *Journal of Applied Crystallography*, 40 (2007) 658-674.
- [22] P. Emsley, B. Lohkamp, W. G. Scott, K. Cowtan, Features and development of Coot, *Acta Crystallogr. D Biol. Crystallogr.* 66 (2010) 486-501.
- [23] P. D. Adams, P. V. Afonine, G. Bunkoczi, V. B. Chen, I. W. Davis, N. Echols, J. J. Headd, L. W. Hung, G. J. Kapral, R. W. Grosse-Kunstleve, A. J. McCoy, N. W. Moriarty, R. Oeffner, R. J. Read, D. C. Richardson, J. S. Richardson, T. C. Terwilliger, P. H. Zwart, PHENIX: a comprehensive Python-based system for macromolecular structure solution, *Acta Crystallogr. D Biol. Crystallogr.* 66 (2010) 213-221.
- [24] P. A. Ravindranath, S. Forli, D. S. Goodsell, A. J. Olson, M. F. Sanner, AutoDockFR: Advances in Protein-Ligand Docking with Explicitly Specified Binding Site Flexibility, *PLoS Comput. Biol.* 11 (2015) e1004586.

- [25] G. Y. Di Veroli, C. Fornari, D. Wang, S. Mollard, J. L. Bramhall, F. M. Richards, D. I. Jodrell, Combenefit: an interactive platform for the analysis and visualization of drug combinations, *Bioinformatics* 32 (2016) 2866-2868.
- [26] L. A. Mathews Griner, R. Guha, P. Shinn, R. M. Young, J. M. Keller, D. Liu, I. S. Goldlust, A. Yasgar, C. McKnight, M. B. Boxer, D. Y. Dubeau, J. Jiang, S. Michael, T. Mierzwa, W. Huang, M. J. Walsh, B. T. Mott, P. Patel, W. Leister, D. J. Maloney, C. A. Leclair, G. Rai, A. Jadhav, B. D. Peyser, C. P. Austin, S. E. Martin, A. Simeonov, M. Ferrer, L. M. Staudt, C. J. Thomas, High-throughput combinatorial screening identifies drugs that cooperate with ibrutinib to kill activated B-cell-like diffuse large B-cell lymphoma cells, *Proc. Natl. Acad. Sci. U. S. A.* 111 (2014) 2349-2354.

Appendix

Additional publications

Flavoproteins from the yeast *Saccharomyces cerevisiae*

Structure, biochemical and kinetic properties of recombinant Pst2p from *Saccharomyces cerevisiae*, a FMN-dependent NAD(P)H:quinone oxidoreductase

Karin Koch¹, Altijana Hromic², Marija Sorokina¹, Emilia Strandback¹, Manuel Reisinger², Karl Gruber² and Peter Macheroux¹

¹Institute of Biochemistry, Graz University of Technology, Austria

²Institute of Molecular Biosciences, University of Graz, Austria

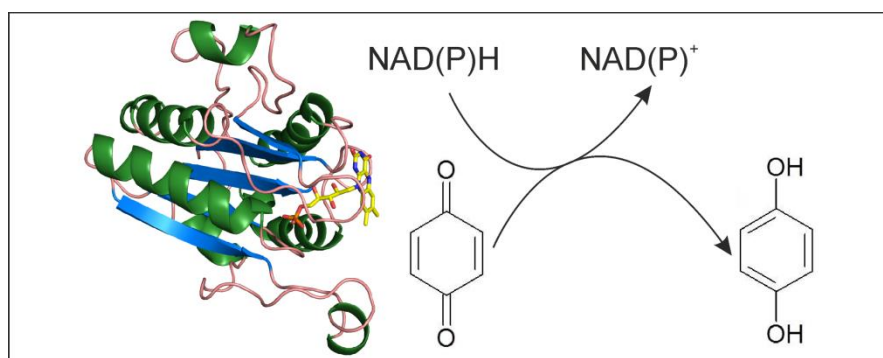
Author contributions

P.M. initiated the project; K.K., A.H., K.G. and P.M. designed the experiments and interpreted the data; K.K. and M.S. expressed *PST2*. K.K. purified Pst2p and performed analytical and biochemical experiments; K.K., M.S. and E.S. performed enzymatic experiments; K.K. performed the *in vivo* experiments; A.H., M.R. and K.G. crystallized Pst2p and determined the crystal structure; K.K., A.H., K.G. and P.M. wrote the manuscript.

Manuscript published in: *Biochimica et Biophysica Acta* 1865 (2017) 1046-1056.

Abstract

The genome of the yeast *Saccharomyces cerevisiae* encodes four flavodoxin-like proteins, namely Lot6p, Pst2p, Rfs1p and Ycp4p. Thus far only Lot6p was characterized in detail demonstrating that the enzyme possesses NAD(P)H:quinone oxidoreductase activity. In the present study, we heterologously expressed *PST2* in *Escherichia coli* and purified the produced protein to conduct a detailed biochemical and structural characterization. Determination of the three-dimensional structure by X-ray crystallography revealed that Pst2p adopts the flavodoxin-like fold and forms tetramers independent of cofactor binding. The lack of electron density for FMN indicated weak binding, which was confirmed by further biochemical analysis yielding a dissociation constant of $20 \pm 1 \mu\text{M}$. The redox potential of FMN bound to Pst2p was determined to $-89 \pm 3 \text{ mV}$ and is thus 119 mV more positive than that of free FMN indicating that reduced FMN binds ca. five orders of magnitude tighter to Pst2p than oxidized FMN. Due to this rather positive redox potential Pst2p is unable to reduce free FMN or azo dyes as reported for other members of the flavodoxin-like protein family. On the other hand, Pst2p efficiently catalyzes the NAD(P)H dependent two-electron reduction of natural and artificial quinones. The kinetic mechanism follows a ping-pong bi-bi reaction scheme. *In vivo* experiments with a *PST2* knock out and overexpressing strain demonstrated that Pst2p enables yeast cells to cope with quinone-induced damage suggesting a role of the enzyme in managing oxidative stress.



Highlights

Heterologous production of the flavoprotein Pst2p from *Saccharomyces cerevisiae*
The flavodoxin-like protein Pst2p forms tetramers independent of cofactor binding
Reduced FMN binds ca. five orders of magnitude tighter to Pst2p than oxidized FMN
Pst2p exhibits quinone reductase activity *in vitro* and *in vivo*

Keywords

enzyme kinetics; flavodoxin-like protein; redox potential; UV-visible absorption spectroscopy; x-ray crystallography;

Chemical compounds studied in this article

1,4-Benzoquinone (PubChem CID: 4650); Coenzyme Q1 (PubChem CID: 4462); Duroquinone (PubChem CID: 68238); Hydroquinone (PubChem CID: 785); Menadione (PubChem CID: 4055); NADH disodium salt (PubChem CID: 272471); NADPH tetra sodium salt (PubChem CID: 91654154);

Abbreviations

1,4-BQ, 1,4-benzoquinone; CoQ1, Coenzyme Q1; DQ, duroquinone; *S. cerevisiae*, *Saccharomyces cerevisiae*; *E. coli*, *Escherichia coli*; EtOH, ethanol; HQ, hydroquinone; Lot6, low temperature-responsive 6; MQ, menadione; Ni-NTA, nickel-nitrilotriacetic acid; NQO1 or 2; NAD(P)H:quinone oxidoreductase 1 or 2; ON, overnight; PDB, Protein Data Bank; Pst2, protoplasts-secreted 2; Rfs1, Rad55 suppressor 1; SD-ura, synthetic dextrose medium lacking uracil; SG-ura, synthetic galactose medium lacking uracil; Ycp4, yeast chromosomal protein 4; WrbA, tryptophan (W) repressor-binding protein;

Database

Atomic coordinates and structure factors have been deposited in the PDB database. Pst2p (PDB ID: 5MP4).

Introduction

The flavoproteome of the yeast *Saccharomyces cerevisiae* (*S. cerevisiae*) comprises 68 proteins with 47 distinct biological functions. Despite having served as a model organism for decades, many of the flavoproteins are poorly characterized with regard to their biochemical and enzymatic properties. Within the yeast flavoproteome, the group of flavodoxin-like proteins comprises four members, namely Lot6p (low temperature-responsive 6), Pst2p (protoplasts-secreted 2), Rfs1p (Rad55 suppressor 1) and Ycp4p (yeast chromosomal protein 4). However, only Lot6p was structurally, biochemically and enzymatically characterized [1]. In general, the flavodoxin-like protein superfamily comprises highly diverse members with regard to amino acid sequence, flavin cofactor, electron donor and acceptor as well as quaternary structure [2]. On the one hand, mammalian flavodoxin-like proteins, such as NQO1 and NQO2 (NAD(P)H:quinone oxidoreductase 1 and 2) are strictly homo-dimeric proteins, which possess a FAD-cofactor. The FAD cofactor can be reduced either by NAD(P)H or by dihydronicotinamide riboside and both enzymes catalyze the reduction of quinones, azo dyes and nitro compounds [3-6].

In the other kingdoms of life, quinone reductases more distantly related to NQO1 were found, for example WrbA (tryptophan (W) repressor-binding protein) from *Escherichia coli*, the founding member of a family of FMN-dependent proteins, which are present in archaea, bacteria, fungi and the *Viridiplantae* kingdom [7, 8 and references therein]. WrbA possesses FMN as cofactor and lacks the C-terminal subdomain present in NQO1 and is therefore able to form tetramers, assembled as a dimer of dimers [9]. Similar to NQO1, WrbA possesses NAD(P)H-dependent quinone reductase activity but no azo reductase activity [10,11].

The importance of quinone reductase activity *in vivo* is still under discussion. It was proposed that it protects the cell from oxidative stress provoked by exogenous toxic quinones and, on the other hand, may prevent cellular damage from lipid peroxidation by keeping endogenous quinones in their reduced form to maintain their anti-oxidative activity [12 and references therein]. In the past two decades, the redox activity of flavodoxin-like proteins was implicated also in other functions, such as the generation of reduced FMN for other enzymes [13], ubiquitin-independent proteasomal degradation [14 and references therein], superoxide scavenging [15] as

well as the pathogenicity of *Candida albicans* [16], *Botrytis cinerea* [17] and *Pseudomonas aeruginosa* [18]. In addition to this functional diversity of flavodoxin-like proteins, it was shown that many species possess more than one flavodoxin-like protein with distinct but overlapping functions [11 and references therein]. This complexity makes it difficult to define the cellular roles of flavodoxin-like proteins solely based on sequential or structural information.

In the present study we set out to express *PST2* from *S. cerevisiae* and purified the produced protein from *Escherichia coli* (*E. coli*) for a detailed biochemical and structural characterization. X-ray crystallography confirmed a flavodoxin-like topology and kinetic analysis revealed that the enzyme is an efficient NAD(P)H:quinone oxidoreductase. However, due to the unusual positive redox potential, Pst2p lacks FMN and azo reductase activity. *In vivo*, Pst2p appears to confer resistance to some exogenous quinones whereas in other cases it renders yeast cells more sensitive.

Results

3.1. Biochemical characterization of Pst2p

PST2 from *S. cerevisiae* was heterologously expressed in *E. coli* and the produced protein was purified from crude extracts using Ni-NTA affinity chromatography. From 1 L culture about ~70 mg of enzyme was obtained with a high purity as judged by visual inspection of the SDS-polyacrylamide gel (Figure 1, panel A).

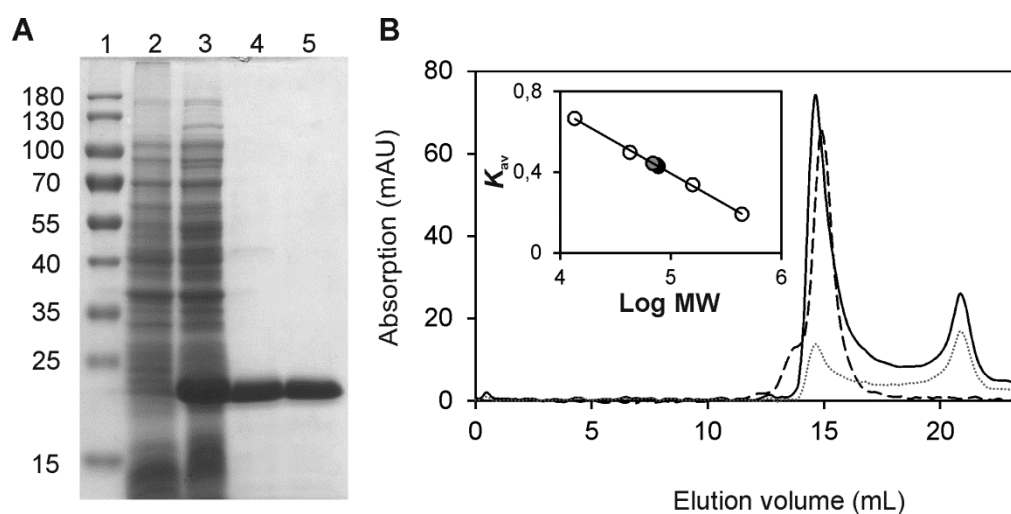


Figure 1. Determination of purity and molecular masses of Pst2p and apo-Pst2p using SDS-PAGE and analytical size exclusion chromatography. **(A)** Determination of purity and subunit molecular masses of Pst2p and apo-Pst2p by SDS-PAGE after purification by Ni-NTA-sepharose. Lane 1, PageRuler™ prestained protein ladder (10-180 kDa); lane 2, protein extract before induction; lane 3, protein extract after induction of Pst2p; lane 4, protein fraction after purification by Ni-NTA-sepharose; lane 5, protein fraction after apo-protein preparation. The subunit molecular mass of Pst2p was estimated to 22 kDa. **(B)** Determination of native molecular mass of Pst2p (black continuous line 280 nm and grey dotted line 450 nm) and apo-Pst2p (black dashed line) using analytical size exclusion chromatography. The elution profile of Pst2p indicates that the protein lost most of the FMN cofactor during chromatography. The insert shows a plot of the partition coefficient (K_{av}) against the logarithm of molecular mass of standard proteins (ferritin, 440 kDa; aldolase, 158 kDa; conalbumin, 75 kDa; ovalbumin, 43 kDa; ribonuclease A, 13.7 kDa). The calculated molecular masses of Pst2p (86 kDa, black circle) and apo-Pst2p (78 kDa, grey circle) indicate that Pst2p is present in a tetrameric form and that oligomerization is independent of cofactor binding.

The purified protein showed the characteristics of a flavoprotein with two distinct absorption peaks at 378 and 453 nm with a shoulder at ~469 nm. Denaturation of the protein resulted in a slight bathochromic shift of the absorption maxima (Figure 2). Using an extinction coefficient of $12.500 \text{ M}^{-1} \text{ cm}^{-1}$ at 450 nm for free FMN an extinction coefficient of $10.600 \text{ M}^{-1} \text{ cm}^{-1}$ at 453 nm was calculated for Pstp2. This extinction coefficient was used to determine the Pst2p concentration in further experiments.

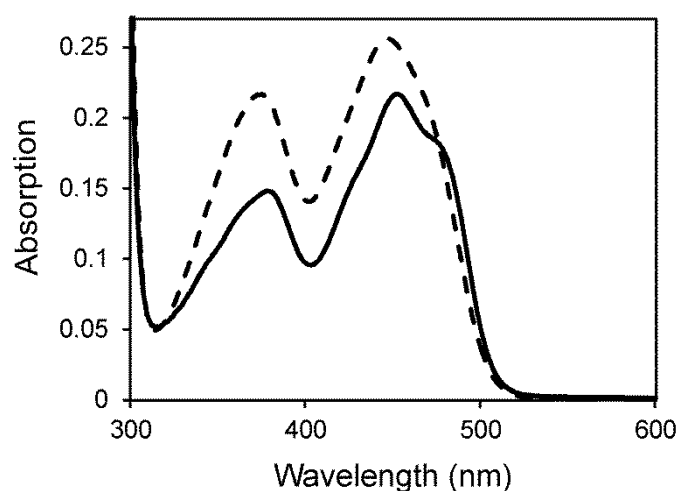


Figure 2. Spectra of native and denatured Pst2p. UV–visible absorption spectra of Pst2p before (solid line) and after denaturation (dashed line). Denaturation of purified Pst2p was carried out in buffer C (50 mM HEPES, 50 mM NaCl, pH 7.0) containing 0.2% SDS.

During purification we have noticed partial depletion of the cofactor, which is reflected by an increased absorption ratio at 280/450 nm (>9). However, reconstitution of apo-Pst2p was achieved by incubation with FMN and subsequent removal of free FMN by means of a PD10-column leading to an improved 280/453 ratio of 4.5, which is close to the theoretical value of 3. Similar observations were reported for several FMN-dependent enzymes, such as NAD(P)H:quinone oxidoreductases [7,11,39 and references therein]. Notably, the formation of tetramers found in solution as well as in the crystals (see below) is independent of FMN binding (Figure 1, panel B). On the other hand, we found that the thermal stability of holo-Pst2p is clearly higher than that of the apo-Pst2p as the melting temperature of holo- and apo-Pst2p was determined to 58 and 51 °C, respectively. In addition, apo-Pst2p is more susceptible

to limited proteolysis as shown in Figure 3. In comparison, ~54% of apo-Pst2p and ~26% of holo-Pst2p was digested within 80 min, respectively. Taken together, these results suggest that FMN binding leads to a structural stabilization of the protomer but is not relevant for the assembly of the quaternary structure.

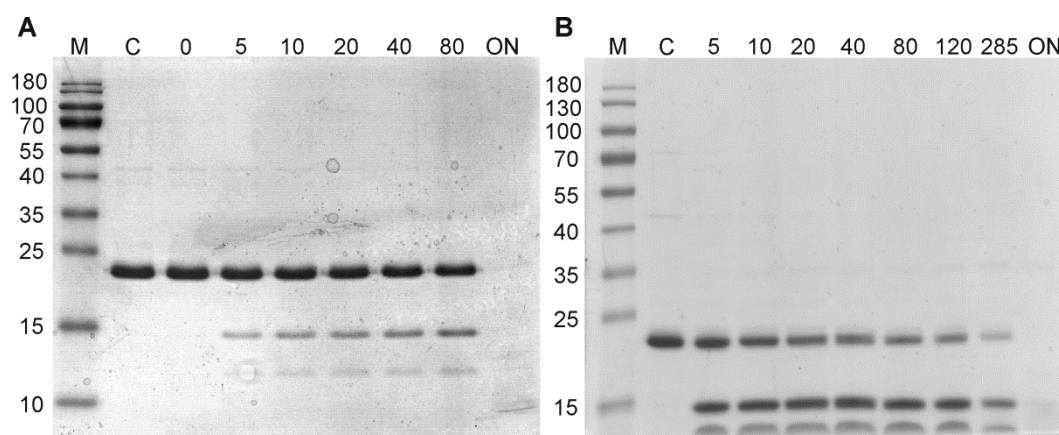


Figure 3. Limited trypsin proteolysis of Pst2p and apo-Pst2p. **(A)** SDS-PAGE showing a time course of trypsin digestion. The migration positions of the molecular weight marker (M) are indicated to the left of the gel. Lane 1, PageRuler™ prestained protein ladder (10-180 kDa); lane 2, protein without trypsin; lane 3-9 digestion times are given in minutes above the gel (ON, overnight). **(B)** SDS-PAGE showing trypsin digestion products of apo-Pst2p. The migration positions of the molecular weight marker (M) are indicated to the left of the gel. Lane 1, PageRuler™ prestained protein ladder (10-180 kDa); lane 2, protein without trypsin; lanes 3-10, digestion times are given in minutes above the gel (ON, overnight).

In order to determine the dissociation constant for the binding of FMN to apo-Pst2p, we followed the absorption changes occurring upon addition of FMN to the apo-protein. The obtained changes were fitted to a hyperbolic equation and indicated a binding ratio of one FMN molecule per subunit of apo-Pst2p with a dissociation constant of $20 \pm 1 \mu\text{M}$ (Figure 4, panel A). Similarly, we used difference titration experiments to determine the dissociation constants for MQ, DQ and CoQ1. A representative titration of DQ with Pst2p is shown in Figure 4, panel B. The dissociation constants obtained for quinones were in the range of 139 to 226 μM and are summarized in Table 1 (right column).

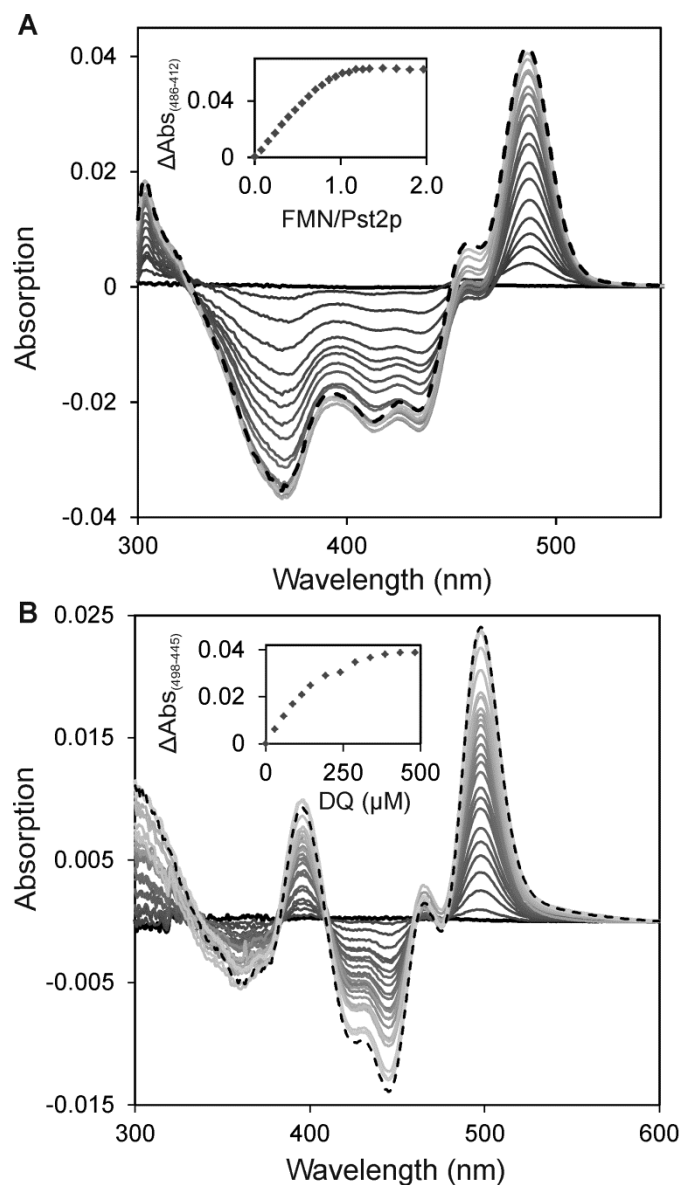


Figure 4. Binding of FMN and quinone substrates to Pst2p. **(A)** Difference titration of apo-Pst2p with FMN. 40 μM apo-Pst2p was titrated with FMN (0–90 μM) and absorption spectra were recorded from 300 to 550 nm. Representative and normalized spectra are depicted in different shades of grey. The final spectrum is shown as black dashed line. The inset shows a plot of the absorption change against the FMN/protein ratio. The data indicate a binding ratio of one FMN molecule per Pst2p subunit with a dissociation constant of $20 \pm 1 \mu\text{M}$. **(B)** Difference titration of Pst2p with DQ. 40 μM Pst2p was titrated with DQ (0–380 μM) and absorption spectra were recorded from 300 to 600 nm. Representative and normalized spectra are depicted in different shades of grey. The final spectrum is shown as black-dashed line. The inset shows a plot of the absorption change as a function of DQ concentration. A hyperbolic fit to the experimental data yielded a dissociation constant of $199 \pm 12 \mu\text{M}$.

Table 1. Enzymatic activities and dissociation constants with several substrates determined with purified Pst2p. (n.o., not observed; n.d., not determined;)

Substrate	K_M^a [μM]	k_{cat}^a [s^{-1}]	k_{cat}/K_M^a [$\text{M}^{-1}\cdot\text{s}^{-1}$]	$k_{red/ox}^b$ [$\text{M}^{-1}\cdot\text{s}^{-1}$]	K_d^c [μM]
NADH*	67 ± 6	280 ± 8	$4.2 \cdot 10^6$	$5.8 \cdot 10^6 \pm$ $4.5 \cdot 10^5$	n. o.
NADPH*	104 ± 7	279 ± 7	$2.7 \cdot 10^6$	$1.9 \cdot 10^6 \pm$ $1.1 \cdot 10^5$	n. o.
MQ**	41 ± 3	268 ± 7	$6.5 \cdot 10^6$	$2.7 \cdot 10^6 \pm$ $7.8 \cdot 10^5$	139 ± 14
1,4-BQ**	15 ± 2	1119 ± 46	$7.5 \cdot 10^7$	$>10^6$ ^d	n. o.
DQ**	72 ± 5	380 ± 10	$6.8 \cdot 10^6$	$7.0 \cdot 10^6 \pm 5.6$ 10^5	199 ± 12
CoQ1**	91 ± 8	33 ± 1	$3.6 \cdot 10^5$	n. d.	226 ± 21

^aSteady-state kinetic constants were determined by UV–visible absorption spectroscopy in the presence of a saturating second substrate (MQ* or NADH**) at pH 7.0 and 25 °C; ^bRapid reaction data ($k_{red/ox}$) were determined with a stopped flow device at pH 7.0 and 4 °C; ^cDissociation constants were determined by UV–visible absorption difference spectroscopy at pH 7.0 and 25 °C; ^dThe reduction of 1,4-BQ was complete within the dead time of the stopped-flow instrument (~5 ms).

Next, photoreduction of recombinant Pst2p was performed in the presence of EDTA by exposing the protein to light. Under the experimental conditions, FMN bound to Pst2p is continuously reduced to the hydroquinone (fully reduced flavin) (Figure 5).

Furthermore, the redox potential of the FMN cofactor was determined with the xanthine/xanthine oxidase system in the presence of suitable redox dyes, namely potassium indigotrisulfonate ($E_M = -81$ mV) and indigo carmine ($E_M = -125$ mV). As shown in Figure 6, a plot of $\log(\text{Pst2p}_{ox}/\text{Pst2p}_{red})$ versus $\log(\text{dye}_{ox}/\text{dye}_{red})$ was used to estimate the redox potential to -89 ± 3 mV [37]. In keeping with the reduction of the oxidized flavin directly to the hydroquinone observed in our photoreduction experiment, the slope of the logarithmic plot was close to unity indicating that both the reference dye and the flavin isoalloxazine ring are taking up two electrons. The

redox potentials of the FMN/FMNH₂ couple free and bound to Pst2p as well as the dissociation constant of the oxidized FMN (20 μM) can be used to calculate the K_d of the reduced flavin by using the thermodynamic relationship shown in Scheme 1 (section 2.17. in Materials & Methods). This yields a K_d of 2 nM for the reduced flavin and thus reduced FMN binds 10.000 times tighter to Pst2p than oxidized FMN.

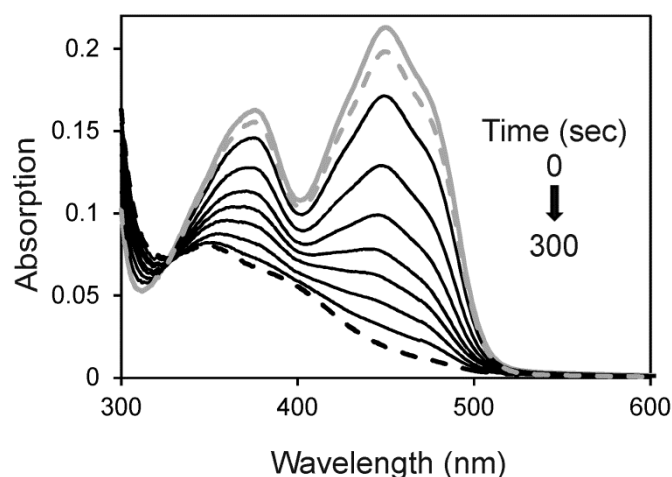


Figure 5. Absorption spectra observed during the anaerobic photoreduction of Pst2p in buffer C. The solid grey line represents the spectra before light illumination. For the time course of reduction selected spectra with decreasing absorption are shown in black, till complete reduction was achieved shown as dashed black line. After re-oxidation the initial spectra was restored (represented as dashed grey line).

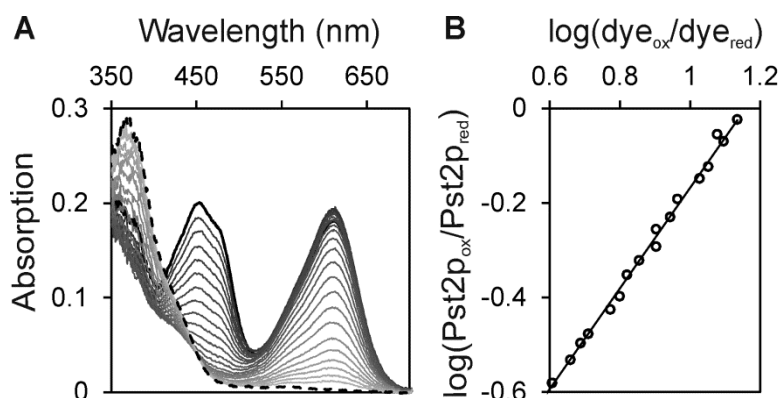


Figure 6. Redox potential determination of Pst2p in the presence of indigo carmine. **(A)** The fully oxidized spectrum is shown as black line and the fully reduced spectrum is shown as dashed black line. Selected spectra of the course of reduction are represented in different shades of grey. ~20 μM Pst2p was reduced by the

xanthine/xanthine oxidase system in the presence of indigo carmine over a time period of 50 min. Data points for evaluation were measured at 461 nm for the protein, where the dye shows no significant contribution to the absorbance. Data for the dye indigo carmine were extracted at 609 nm. Redox potential determinations with potassium indigotrisulfonate were done in a similar manner using values determined at 485 nm for the protein and 601 nm for the dye. Both dyes allowed estimating the redox potential to be -89 ± 3 mV. **(B)** Representation of the data evaluation.

3.2. Three dimensional structure of Pst2p

The X-ray crystal structure of Pst2p was determined at 2.8 Å resolution (Table 2). The orthorhombic crystal (space group $P2_12_12_1$) contained eight molecules in the asymmetric unit forming two tetramers. One of those tetramers is shown in Figure 7. The assignment of the oligomeric state was also verified using the PDBePISA server [40]. This analysis revealed that each tetramer could be viewed as a dimer of dimers with stronger interactions within the dimers (approximately 1200 Å² interaction surface) as compared to the interaction between dimers (800 Å² interaction surface).

The Pst2p protomer belongs to the flavodoxin-like fold family (CATH: 3.40.50.360) and exhibits the typical flavodoxin-fold consisting of five parallel β-strands forming a twisted β-sheet surrounded by α-helices with three additional loop regions. The chains in the asymmetric unit are very similar to each other with root-mean-square-deviations (rmsd) between 0.3 Å and 0.4 Å for all pairwise Cα-atom superpositions calculated using the program PyMOL [41].

Although the solution of Pst2p used for crystallization as well as the crystals themselves were yellow, no clear electron density for the bound FMN was observed in the present structure, indicating either a lower occupancy or high flexibility of the cofactor. Residual density in the predicted FMN binding site was interpreted as phosphate in all chains. These phosphate ions are bound in the same location as the phosphate group of FMN bound in WrbA from *E. coli* [29] which was used as the search structure for molecular replacement and shares 44% sequence identity with Pst2p. A structural superposition of protomers of Pst2p and WrbA yielded a Cα-rmsd of 0.9 Å underlining the close structural similarity of the two proteins (Figure 8, panel A).

Table 2. Data collection and refinement statistics. Values in parentheses are for the highest-resolution shell.

X-ray source	ID29, ESRF, Grenoble, France
Wavelength (Å)	0.972
Temperature	100 K
Space group	$P2_12_12_1$
Cell dimensions	
<i>a</i> , <i>b</i> , <i>c</i> (Å)	69.41, 110.56, 223.81
Resolution (Å)	46.17-2.79 (2.89-2.79)
Total no. reflections	208347 (19109)
No. unique reflections	43021 (4074)
Multiplicity	4.8 (4.7)
Completeness (%)	98.1 (94.5)
$\langle I/\sigma_I \rangle$	10.2 (1.8)
R_{merge} (%)	10.4 (83.4)
R_{meas} (%)	11.7 (93.5)
R_{pim} (%)	5.3 (40.9)
CC _{1/2}	0.998 (0.663)
CC*	0.999 (0.893)
Reflections used in refinement	43020 (4074)
$R_{\text{work}} / R_{\text{free}}$	0.2533 / 0.2855
No. atoms	11840
Protein	11800
Ligands	40
Mean B-factor (Å ²)	82.1
Wilson B-factor (Å ²)	66.9
R.m.s. deviations	
Bond lengths (Å)	0.003
Bond angles (°)	0.58
Ramachandran favored (%)	99.0
Ramachandran outliers (%)	0.0
Rotamer outliers (%)	1.02
Clashscore	7.73
PDB-entry	5MP4

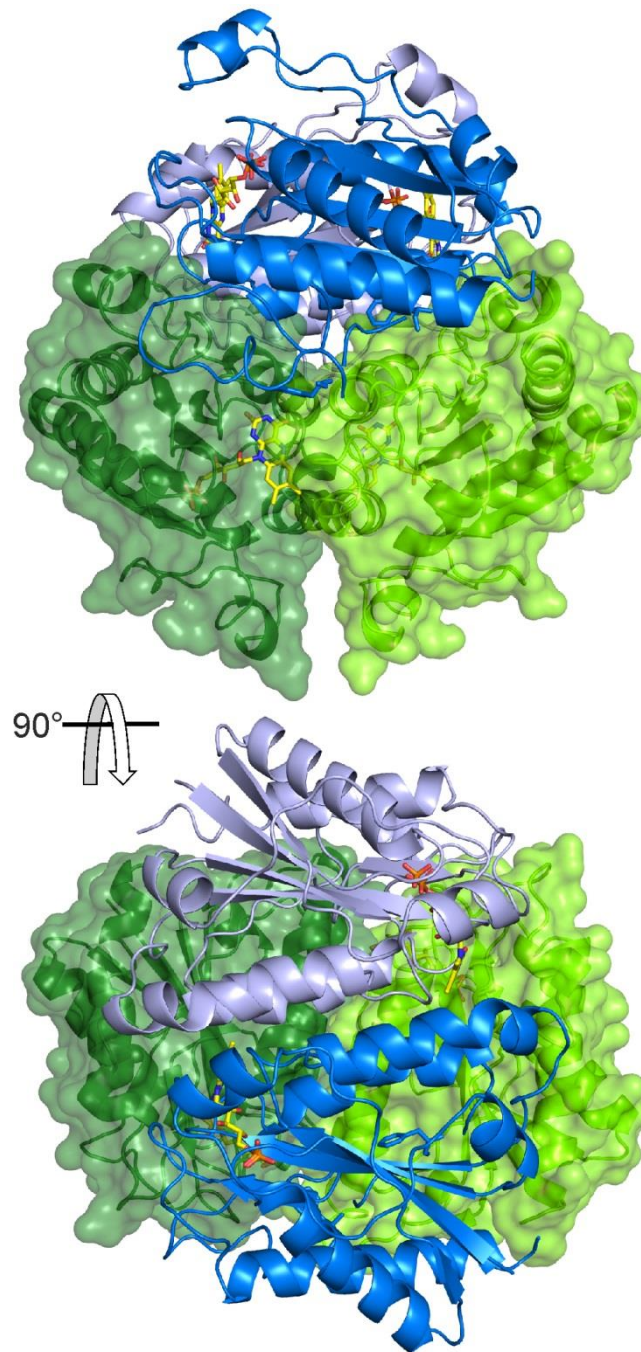


Figure 7. Tetrameric arrangement of Pst2p. The oligomeric state can be described as a dimer of dimers. One dimer is formed by the two green chains shown as surface model and the second by the two blue chains shown as cartoon model. Depicted FMN molecules were implemented according to a structural superposition with WrbA (PDB entry: 3B6l). Two views are presented, which are rotated by 90° around the x-axis. Figures were prepared with the software PyMOL [41].

The structure of the complex of Pst2p with FMN modelled based on the comparison with WrbA revealed that each of the four cofactor binding sites is composed of residues from three protomers of the tetramer (Figure 8, panel B). WrbA is a dimeric/tetrameric, FMN-dependent flavoprotein originally described as a tryptophan repressor-binding protein promoting complex formation between the repressor and DNA. Sequence comparisons, however, showed homology to certain NAD(P)H:quinone oxidoreductase [42]. The close structural similarity of Pst2p and WrbA as well as the conservation of amino acid residues in the active site (Figure 8, panel C) suggest that Pst2p may also catalyze the reduction of quinones as previously reported for WrbA [29].

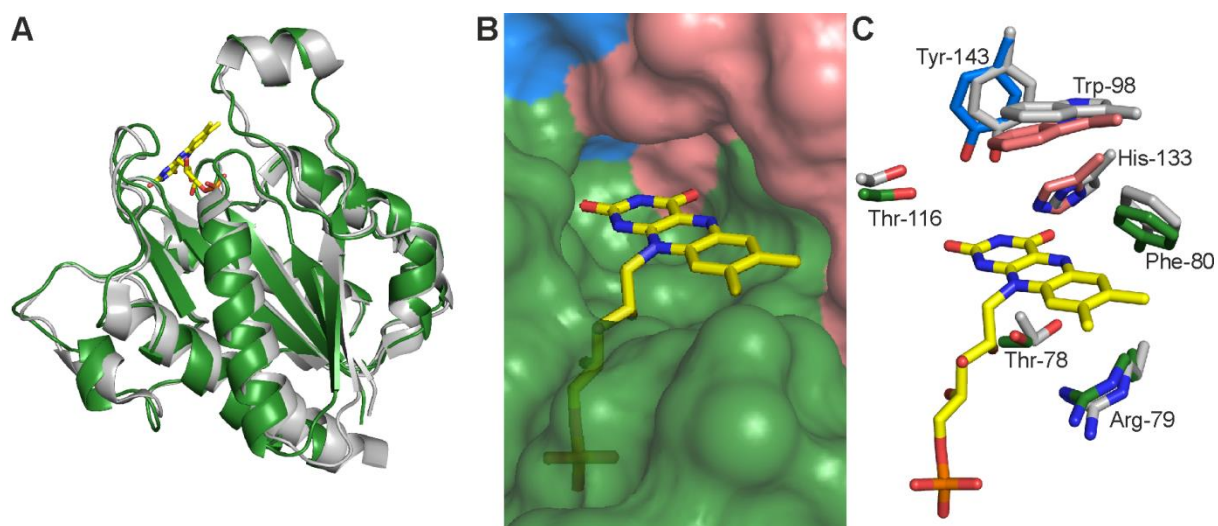


Figure 8. Overall structural similarity of WrbA with Pst2p. Because only the density of a phosphate group was observed in the electron density, the FMN molecule shown was introduced through structural superposition with WrbA (PDB entry: 3B6I). **(A)** Structural superposition of WrbA (grey, PDB code: 3B6I) and Pst2p (green). **(B)** Surface representation of Pst2p showing that residues from three protomers combine to create the active-site pocket. **(C)** Close-up view of the FMN binding site. Residues close to the FMN isoalloxazine ring are shown as grey sticks (WrbA) or in colors corresponding to the respective protomer (Pst2p). Figures were prepared with the software PyMOL (<http://www.pymol.org/>) [41].

3.3. Characterization of the catalytic properties of Pst2p

To evaluate the enzymatic activity of Pst2p, assays were performed with NADH or NADPH as electron donor and several quinones were tested as electron acceptors. In all cases saturation kinetics were observed that were fitted to a single-phase

hyperbolic equation (Figure 9). The extracted kinetic constants are given in Table 1.

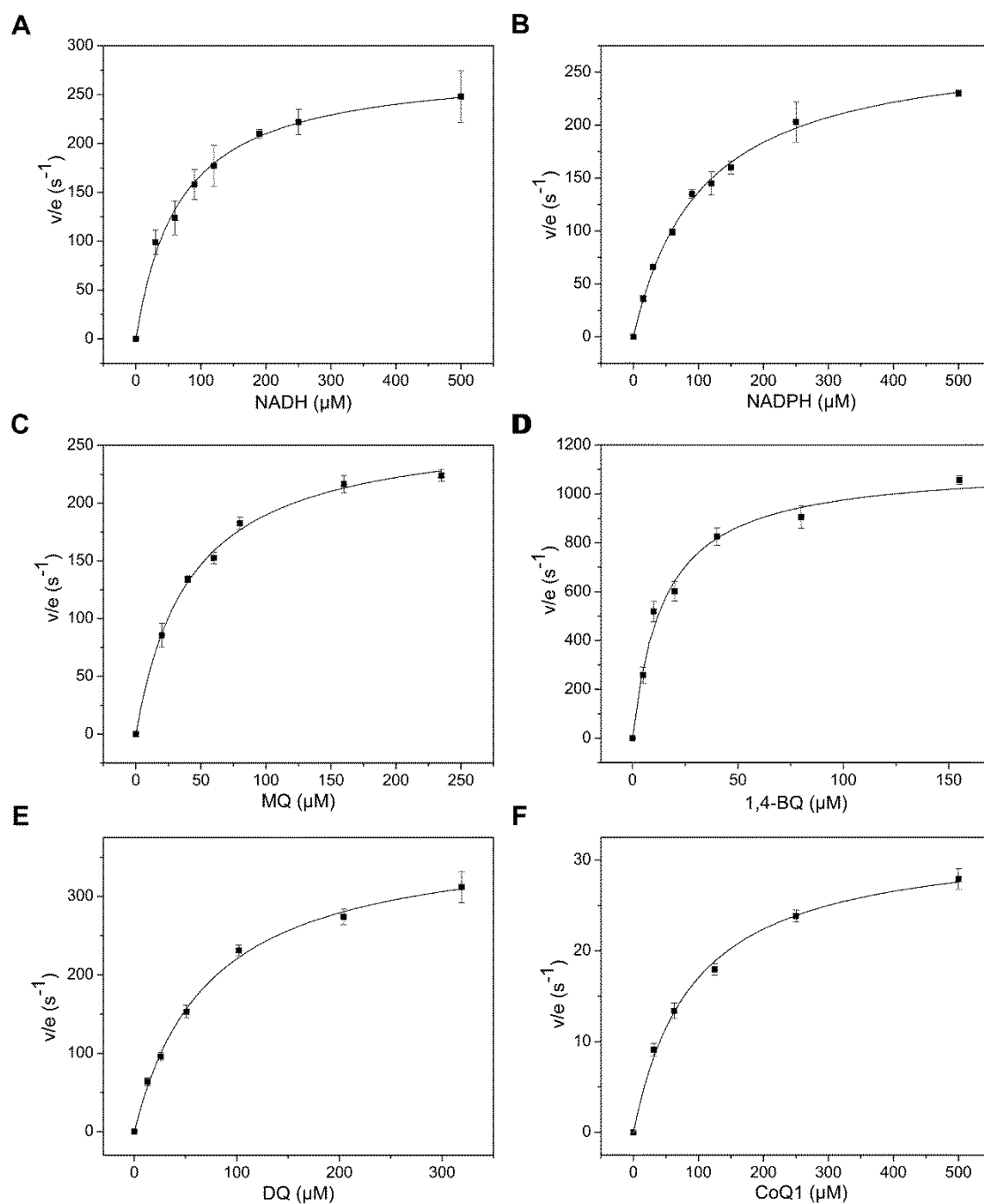


Figure 9. Steady state kinetics of Pst2p. Initial-velocity kinetic measurements were performed in triplicate with NAD(P)H, 1,4-BQ, MQ, DQ and CoQ1 by following the oxidation of NAD(P)H at 380 nm. Reaction mixtures were setup in 50 mM HEPES pH 7, 50 mM NaCl, 2% (v/v) EtOH. Substrates were varied as follows: **(A)** NADH (30-500 μM) and **(B)** NADPH (30-500 μM) at a saturating MQ concentration (200 μM); **(C)** 1,4-BQ (5-155 μM), **(D)** MQ (20-235 μM), **(E)** DQ (12-317 μM) or **(F)** CoQ1 (30-500 μM) at a saturating NADH concentration (350 μM).

The kinetic mechanism follows a ping-pong bi–bi reaction scheme (Figure 10, panel A) as it is the case for several other quinone reductases [2 and references therein]. The determined reaction mechanism is in good agreement with the crystal structures of WrbA in complex with NADH (PDB code: 3B6J) and 1,4-BQ (PDB code: 3B6K) obtained by Andrade *et al.* [29], which revealed that both substrates bind at similar positions close to the isoalloxazine ring of the FMN cofactor. Therefore, in the reaction pathway, NADH binds first to the active site, transfers two electrons to the FMN cofactor and NAD^+ dissociates from the active site. Afterwards 1,4-BQ binds to the active site and will be reduced to the HQ with concomitant oxidation of the FMN cofactor. Beside quinones, also FMN and different azo dyes, namely methyl orange, ethyl red and sudan black were tested as substrates, but no significant activity with Pst2p was observed.

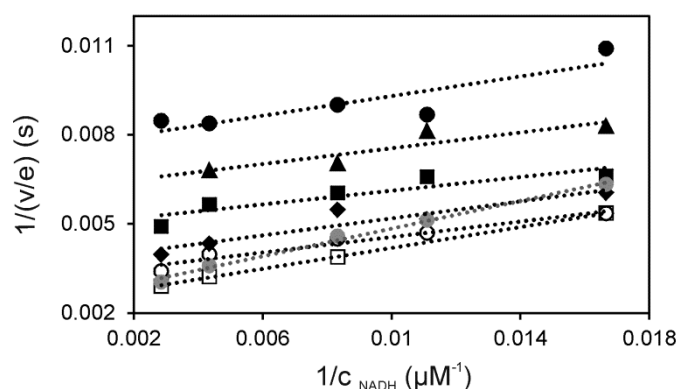


Figure 10. Determination of the kinetic mechanism of Pst2p. Rate of NADH oxidation as a function of MQ concentration. Double reciprocal plot of initial rates versus concentrations of NADH (30–350 μM) were NADH oxidation was determined at 380 nm at 25 °C in buffer C (50 mM HEPES, 50 mM NaCl, pH 7.0) at various concentrations of MQ (20 μM ●, 30 μM ▲, 40 μM ■, 60 μM ◆, 80 μM ○, 160 μM □, and 200 μM ●). The parallel lines in the double-reciprocal plot indicate a ping-pong bi–bi mechanism, with inhibitory effects at high MQ and low NADH levels.

To analyze the kinetic half reactions, Pst2p was mixed in a stopped-flow instrument at 4 °C with NAD(P)H, 1,4-BQ, DQ or MQ under anoxic conditions. For the reductive half reaction, concentrations of 25–250 μM of NADPH or NADH were used and FMN reduction was monitored at 453 nm. Bimolecular rate constants of $5.8 \times 10^6 \pm 4.5 \times 10^5 \text{ M}^{-1} \cdot \text{s}^{-1}$ for NADH and $1.9 \times 10^6 \pm 1.1 \times 10^5 \text{ M}^{-1} \cdot \text{s}^{-1}$ for NADPH were determined (Table 1). In accordance with the calculated catalytic efficiency ($k_{\text{cat}}/K_{\text{M}}$) obtained

from steady state experiments NADH appears to be a marginally better reductant compared to NADPH. In order to investigate the oxidative half reaction, Pst2p was first reduced by the addition of 0.9 equivalents of NADH and then mixed with 1,4-BQ (25 μ M), MQ (25-100 μ M) and DQ (34-910 μ M). The oxidation of the reduced FMN cofactor was monitored at 453 nm. Bimolecular rate constants of $2.7 \times 10^6 \pm 7.8 \times 10^5 \text{ M}^{-1} \cdot \text{s}^{-1}$ for MQ and $7.0 \times 10^6 \pm 5.6 \times 10^5 \text{ M}^{-1} \cdot \text{s}^{-1}$ for DQ were determined (Table 1). The reduction of 1,4-BQ was complete within the dead time of the stopped-flow instrument (~5 ms).

3.4. Examination of quinone sensitivity using *PST2* knock out and overexpressing strains

The efficient reduction of quinones by Pst2p prompted the question whether it plays a role in the detoxification of quinones *in vivo*. In order to investigate this potential function of Pst2p, yeast cells in the logarithmic growth phase were exposed to various concentrations of 1,4-BQ (50-250 μ M), DQ (25-150 μ M) and MQ (25-150 μ M) under aerobic conditions on solid cultures (for details see Experimental Procedures). In the case of 1,4-BQ, yeast cells lacking *PST2* showed higher sensitivity whereas *PST2* overexpressing strains showed increased resistance (Figure 11, rows 2 and 3). Interestingly, the opposite result was obtained for DQ. In this case the *PST2* knock out strain is more resistant while the *PST2* overexpression strain shows a higher sensitivity compared to the wild type strain (Figure 11, rows 7-9). As shown before by North *et al.* [43] the *PST2* knock out strain shows also a higher sensitivity against hydroquinone compared to the wild type strain (Figure 11, rows 4-6). In contrast to 1,4-BQ and DQ, no growth differences were observed when MQ was employed as a quinone (Figure 11, rows 10-12).

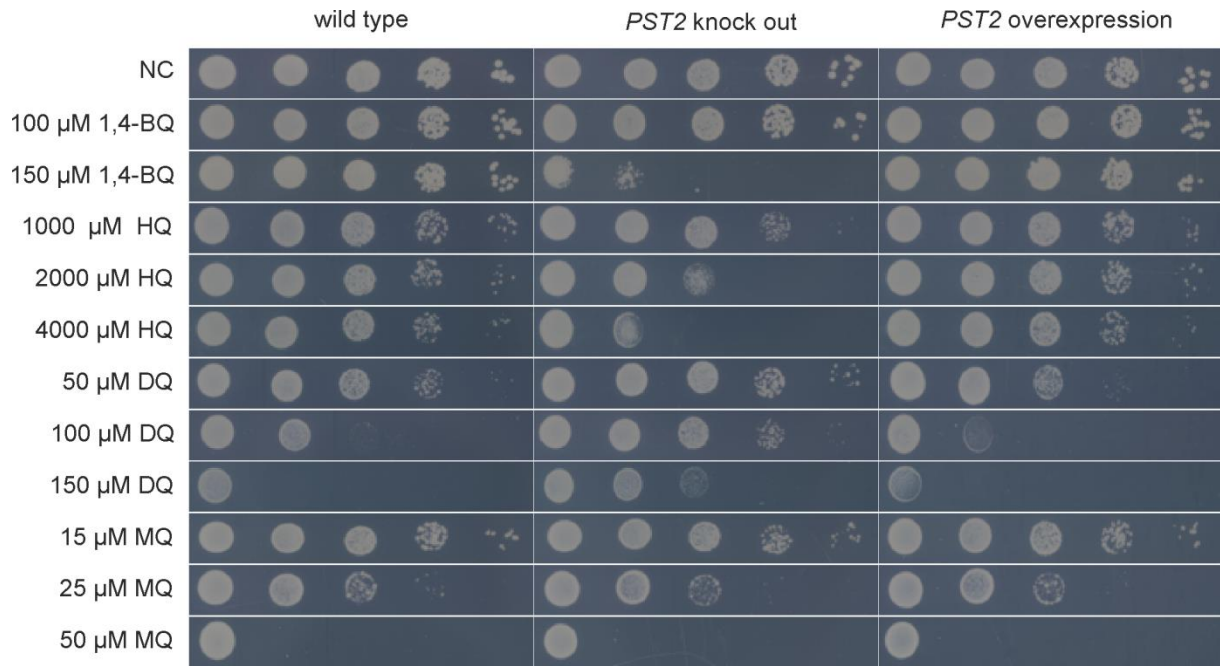


Figure 11. Spot assay on solid medium containing various quinones. Serial dilutions (10-fold) of yeast suspensions in logarithmic growth phase ($OD_{600} \sim 1$) were spotted on SG-ura containing various concentrations of 1,4-BQ, HQ, DQ or MQ solved in EtOH (2% end concentration). Negative controls (NC) including the solvent but no quinone were performed. Cells were grown for 2-3 days at 30 °C and photographs of the plates are shown.

Discussion

In this study we have demonstrated the expression of *PST2* from *S. cerevisiae* in *E. coli* and the purification and characterization of Pst2p, which turns out to be another member of the NAD(P)H-dependent quinone reductase family. Structure analysis revealed that Pst2p adopts the flavodoxin-like fold that is characteristic for the NAD(P)H-dependent FMN reductase family. Members of this family have an α/β subunit in addition to the α/β twisted open sheet fold that is characteristic for flavodoxins. Like other members of this family, namely YhdA from *Bacillus subtilis* [44], Azo1 from *Staphylococcus aureus* [45] and WrbA from *E. coli* [9], Pst2p is able to form stable tetramers in solution. However, in contrast to the mentioned proteins, tetramerization of Pst2p is independent of flavin binding since removal of the FMN cofactor does not affect the quaternary structure.

It is noteworthy that the redox potential of Pst2p is much more positive than that of free flavin (-89 ± 3 vs. -208 mV) and also significantly more positive than that for homologous enzymes like NQO1 (-159 mV) [46] or Lot6p (-172 mV) [39]. The redox potential of WrbA was not determined with accuracy because the dynamic equilibrium of the dimeric and tetrameric state of the protein appears to impede the measurements [7]. Clearly, the more positive redox potential indicates that reduced FMN binds much tighter than the oxidized cofactor. In fact, the dissociation constant of reduced FMN was calculated to 2 nM and is thus 10.000 fold more tightly bound than oxidized FMN (ca. 20 μ M) (Scheme 1). On the other hand, this also explains why reduced Pst2p lacks FMN reductase activity since this reaction is thermodynamically very unfavorable due to the redox potential difference to the free $\text{FMN}_{\text{ox}}/\text{FMN}_{\text{red}}$ couple. This activity is clearly present in other members of the flavodoxin-like family such as Lot6p [47]. Another enzymatic activity, which was found with Lot6p but not with Pst2p is the capability to couple oxidation of NAD(P)H to the reduction of azo dyes [47]. As discussed by Ryan *et al.* [18], differences in the redox potential of various substrates can be partly responsible for the activity variations within the flavodoxin-like superfamily. The quinones investigated in this study cover a range of $E^{\circ} = 286$ mV for 1,4-BQ [48] (best substrate) to $E^{\circ} = -13$ mV for MQ [49] for which the enzymatic efficiency is an order of magnitude lower. However, the poorest substrate for Pst2p was CoQ1 (CoQ10 $E^{\circ} = 100$ mV, [48]). In this case the low efficiency may be due to the bulky hydrophobic side chain that may

interfere with binding of the quinone to the active site. The redox potential of the azo dye methyl orange is also rather low (67 mV at pH 3 [50]), which may also contribute to the lack of activity. Recently, a study reporting the identification of novel azo reductases in *Pseudomonas aeruginosa* mentioned the importance of two structural differences between the classical azo reductase *PaAzoR1* and *PaWrbA*. *PaWrbA* lacks a β -hairpin that is important for substrate specificity in *PaAzoR1*. In addition, a tyrosine residue in the active site was replaced by arginine [11]. In the case of Pst2p, the structural features more closely resemble those in *PaWrbA* and are thus in agreement with the lack of an azo reductase activity. On the other hand, Lot6p features a similar active site as *PaAzoR1* (*i.e.* tyrosine rather than arginine) at the corresponding position. However, the β -hairpin structure is missing in Lot6p. Thus it appears that the active site composition is more relevant for azo reductase activity than the presence of the β -hairpin.

Several enzymes from *S. cerevisiae* have been shown to catalyze the two-electron reduction of quinones, such as the flavin-dependent enzymes Lot6p [39] and Ycp4p [43] and the flavin-independent enzyme Zta1 [51]. In the present study, we have shown that Pst2p is a very efficient NAD(P)H:quinone oxidoreductase rapidly reducing quinones such as 1,4-BQ, MQ, DQ and CoQ1. Not surprisingly, deletion of *PST2* or its overexpression revealed significant effects with regard to the sensitivity against quinones in comparison to the wild-type strain (Figure 11). In the case of 1,4-BQ and HQ the *PST2* knock-out strain was more susceptible whereas the *PST2* overexpressing strain showed increased resistance. Interestingly, the inverse behavior was seen with DQ (compare rows 2-6 and 7-9 in Figure 11). This finding can be rationalized by the higher rate of auto-oxidation of DQ due to additional methyl groups present in comparison to 1,4-BQ. The increased rate of auto-oxidation causes extensive redox cycling and leads to the generation of semiquinones and reactive oxygen species [52,53]. Thus, the expression of *PST2* enhances the toxicity of DQ. Similar observations were reported for naphthoquinones [54 and references therein]. It remains to be seen whether other electron acceptors exist and, if so, to define their biochemical roles in the yeast.

Materials & Methods

Materials

All chemicals, reagents and enzymes were of highest quality and were obtained from Sigma-Aldrich (St. Louis, USA), Roth (Karlsruhe, Germany) or Thermo Fisher Scientific (Waltham, USA), unless otherwise noted. Columns for affinity chromatography (Ni-NTA-sepharose), size exclusion chromatography (Superdex 200 10/300 GL) and buffer exchange (PD-10 desalting column) were from GE Healthcare (Little Chalfont, UK). *E. coli* strains Top10 and RosettaTM(DE3) were from Invitrogen (Carlsbad, USA) and Merck (Darmstadt, Germany), respectively. *S. cerevisiae* strains BY4741 (MATa, his3 Δ 1, leu2 Δ 0, met15 Δ 0, ura3 Δ 0) were from Euroscarf (Frankfurt, Germany) and correct depletion was ensured by colony PCR. The plasmids pET21a and pYES2 were from Merck (Darmstadt, Germany) and Invitrogen (Carlsbad, USA), respectively. The concentrations of holo- and apo-Pst2p and the following compounds were determined spectrophotometrically using molar extinction coefficients: Pst2p ($\epsilon_{453} = 10.600 \text{ M}^{-1} \text{ cm}^{-1}$, experimentally determined), apo-Pst2p ($\epsilon_{280} = 32.430 \text{ M}^{-1} \text{ cm}^{-1}$, based on amino acid sequence), NAD(P)H ($\epsilon_{340} = 6.220 \text{ M}^{-1} \text{ cm}^{-1}$), 1,4-benzoquinone (1,4-BQ) dissolved in ethanol (EtOH) ($\epsilon_{242} = 24.000 \text{ M}^{-1} \text{ cm}^{-1}$) [19], menadione (MQ) dissolved in EtOH ($\epsilon_{333} = 2.450 \text{ M}^{-1} \text{ cm}^{-1}$) [20], duroquinone (DQ) dissolved in EtOH ($\epsilon_{271\text{nm}} = 14.500 \text{ M}^{-1} \text{ cm}^{-1}$), and Coenzyme Q1 (CoQ1) dissolved in EtOH ($\epsilon_{278 \text{ nm}} = 14.500 \text{ M}^{-1} \text{ cm}^{-1}$) [21] and FMN ($\epsilon_{450} = 12.500 \text{ M}^{-1} \text{ cm}^{-1}$) [22].

Cloning of PST2 for large scale expression in E. coli and for yeast overexpression

All strains were generated using standard genetic techniques [23–25]. Briefly, genomic DNA from *S. cerevisiae* was extracted with yeast DNA extraction kit from VWR (Radnor, USA). According to the sequence for *PST2* from the *Saccharomyces* genome database [26] the following primers excluding the stop codon of the gene and including respective restriction sites for cloning were designed and synthesized from VBC (Vienna, Austria): fw-5'-GAGCCATATGCCAAGAGTAGCTATCATCATTTACACAC-3'; rev-5'-CCTGCTCGAGAACTTTGCAACGGTTTCGTAGAAAGTC-3'. To construct the heterologous expression vector pET1a(+)*PST2* introducing an additional C-terminal 6x-His tag the restriction enzymes NdeI/XhoI were used. Individual clones were sequenced before transforming the plasmid into *E. coli* RosettaTM(DE3) cells.

For overexpression of *PST2* in *S. cerevisiae* the construct was generated using PCR with pET1a(+)*PST2* as template to cover also the C-terminal 6xHis tag. The following primers including respective restriction sites were designed and synthesized from VBC (Vienna, Austria): (fw-5'-GAGCGGATCCCCAAGAGTAGCTATCATCATTTACACAC-3', rev-5'-GCTGCGGCCGCTCAGTGGTGGTGGTGGTG-3'). The restriction enzymes BamHI/NotI were used and the gene was ligated into the corresponding site of the vector pYES2, thus expressing C-terminal 6xHis tagged *PST2* under the control of the *GAL1* promoter. Individual clones were sequenced and *S. cerevisiae* BY4741Δ*PST2* cells were transformed from now on referred as *PST2* overexpression strain. Furthermore BY4717 and BY4741Δ*PST2* cells were transformed with empty pYES2 plasmid, from now on referred as wild-type and *PST2* knock out strain, respectively.

Heterologous expression of PST2 and purification of Pst2p

A single colony of *E. coli* Rosetta(DE3) comprising pET21a(+)*PST2* was used to inoculate a pre-culture that was aerobically incubated (37 °C, 16 h, 150 rpm) in lysogeny broth (bacto-tryptone 10 g/L, bacto-yeast extract 5 g/L, NaCl 5 g/L) supplemented with 100 µg/mL ampicillin and 20 µg/mL chloramphenicol. 1% pre-culture was used to inoculate the main-culture supplemented with 100 µg/mL ampicillin and 10 µg/mL chloramphenicol, which was incubated aerobically at 37 °C with agitation at 150 rpm until an OD_{600} of ~0,6 was reached. Expression of *PST2* was induced by addition of 0.5 mM isopropyl-thio-β-d-galactoside. The culture was further incubated for 16 h at 20 °C. Cells were harvested by centrifugation at 4.500 x *g* at 4 °C and washed once with 1% saline solution. Cell pellets were resuspended in 4 mL/1g pellet buffer A (50 mM HEPES, 150 mM NaCl, pH 7.0) supplemented with 20 mM imidazole, 1 mM phenylmethylsulfonyl fluoride solved in dimethylsulfoxide, 10 µM riboflavin 5'-monophosphate sodium salt and further 1 µL of protease inhibitor cocktail for use in the purification of histidine-tagged proteins from Sigma-Aldrich (St. Louis, USA) was added per g of cell pellet. Cell disruption was achieved by sonication with a Labsonic L instrument from Braun Biotech. International (Berlin, Germany) with 120 Watt for 3 x 3 min in an ice-water bath with 3 min pauses between each cycle. The cell lysate was centrifuged at 38.850 x *g* for 45 min at 4 °C, and the supernatant was loaded onto a 5-mL HisTrap HP column previously

equilibrated with buffer A supplemented with 20 mM imidazole. The column was washed with buffer A supplemented with 50 mM imidazole and subsequently proteins were eluted with buffer A supplemented with 300 mM imidazole. Fractions containing target protein were pooled and concentrated with centrifugal filter units (Amicon Ultra-15, 10 k; Millipore, Billerica, USA). Concentrated protein was re-buffered to buffer B (50 mM HEPES, pH 7.0) with a PD-10 desalting column. The protein solutions were shock frozen and stored at $-80\text{ }^{\circ}\text{C}$, if not used immediately.

Crystallization

Crystallization experiments were performed in microbatch plates using different commercial crystallization screens (i.e. the Index Screen from Hampton Research and the Morpheus Screen from Molecular Dimensions). Sitting drops were prepared by mixing 0.5 μL of the protein solution (at a concentration of 18 mg/mL) with an equal volume of mother liquor, which were pipetted using an ORYX 8 pipetting robot from Douglas Instruments. The trays were incubated at $20\text{ }^{\circ}\text{C}$. First crystal clusters were observed after one day, followed by further optimization using cross-seeding. Diffracting Pst2p crystals were obtained with 0.2 M ammonium acetate, 0.1 M HEPES pH 7.5, 25% w/v 3350 polyethylene glycol (Index screen; condition F8). Crystals were flash cooled in liquid nitrogen using 20% glycerol for cryoprotection.

Structure determination and refinement

X-ray diffraction data were collected to a maximum resolution of 2.8 \AA on beamline ID29 ($\lambda=0.972\text{ \AA}$) at the ESRF Grenoble, France. The crystals were orthorhombic (space group $P2_12_12_1$) with unit-cell dimensions $a=69.41\text{ \AA}$, $b=110.56\text{ \AA}$ and $c=223.81\text{ \AA}$. The data were processed using the XDS package [27] and programs from the CCP4 suite [28] and a randomly chosen set of 5% of the reflection was set aside for the calculation of R_{free} values. The structure was solved by molecular replacement using the structure of WrbA from *E. coli* in complex with 1,4-BQ (PDB code: 3B6K, 44% sequence identity) [29] as search template yielding eight chains in the asymmetric unit. Structure rebuilding and refinement were performed using the programs Coot [30] and PHENIX [31]. The electron density was improved by density modification and statistical phase improvement using the programs Parrot and Pirate from the CCP4 suite [28]. Non-crystallographic-symmetry (NCS) restraints were applied in the initial stages of the refinement but were removed for the final

refinement cycles. Sufficiently clear electron density was observed for all amino acids except of the first methionine in all chains. Detailed statistics pertaining to data processing and structure refinement are summarized in Table 2. Atomic coordinates and structure factors have been deposited in the Protein Data Bank under accession number 5MP4.

Determination of molecular masses of Pst2p

Subunit molecular mass of purified Pst2p was determined by SDS-PAGE under reducing conditions with a 12.5% separating gel and 5% stacking gel described by Laemmli [32]. The used protein molecular mass marker was the PageRuler™ prestained protein ladder (10-180 kDa) from Thermo Fisher Scientific (Waltham, USA).

To determine the native molecular mass of Pst2p size exclusion chromatography with buffer A using a Superdex 200 10/300 GL column attached to an Äktapurifier™ system from GE Healthcare (Little Chalfont, UK) was performed. Protein elution was monitored at 280 nm and 450 nm wavelength. The column was calibrated with molecular mass standards according to the instructions from GE healthcare.

Apo-protein preparation

Apo-Pst2p was prepared as described in [33]. In brief, purified Pst2p was loaded on a 5-mL HisTrap HP column previously equilibrated with buffer A. The column was washed with buffer A supplemented with 2 M urea, and 2 M KBr until no cofactor was noticed in the flow through and then re-equilibrated with 25 mL buffer A before eluting the protein. Fractions containing target protein were further processed as described for the holo-protein. Complete removal of the cofactor was verified spectrophotometrically.

Limited proteolysis

Limited proteolysis with 2 µg/mL trypsin from Promega (Madison, USA) of 30 µM holo-Pst2p or apo-Pst2p in buffer C was performed at 37 °C. The reaction was stopped at various time points by adding SDS sample buffer and boiling at 95 °C for 10 minutes. Samples were analysed by SDS-PAGE under reducing conditions with a

12.5% separating gel and 5% stacking gel. SDS-polyacrylamide gels were analysed with the program ImageJ (<http://imagej.nih.gov/ij/>) [34].

Thermal shift assay

Thermal shift assays were performed as described elsewhere [35,36]. 20 μ L of 0.5 mg/mL apo- or holo-Pst2p were pipetted into a white 96-well RT-PCR plate from Bio-Rad (California, USA). Five μ L of a 1:500 dilution of SYPRO[®] orange from Molecular Probes (Oregon, USA) was added to apo-Pst2p. The plates were sealed with an optical-quality sealing tape from Bio-Rad (California, USA) and heated in a CFX Connect™ Real-Time PCR detection system from Bio-Rad (California, USA) from 20 to 95 °C in increments of 0.5 °C. Fluorescence changes of the intrinsic FMN of Pst2p or the dye in the case of apo-Pst2p were detected at a wavelength between 470 and 500 nm. Melting temperatures (T_m) were determined using cfx manager 3.0 software from Bio-Rad (California, USA).

Methods using UV-visible absorption spectroscopy

Absorption spectra were recorded with a Specord 200 plus spectrophotometer from Analytik Jena (Jena, Germany) at 25 °C using 1-cm quartz cuvettes.

Extinction coefficient

The extinction coefficient of Pst2p was determined according to the protocol described in reference [22]. Briefly, Pst2p bound FMN was released by addition of 0.2% SDS. UV-visible absorption spectra were recorded before and after denaturation of the enzyme. The calculation led to an extinction coefficient of 10.600 $M^{-1} cm^{-1}$ at 453 nm for native Pst2p.

Difference titrations

Difference titrations were carried out in tandem quartz cuvettes as described in [33]. The cuvettes were filled with 800 μ L of a ~50 μ M protein solution (apo-Pst2p or Pst2p) in buffer C (50 mM HEPES, 50 mM NaCl, pH 7.0) in one chamber and 800 μ L of buffer C in the other chamber. The titration experiments were performed by stepwise addition of 2-8 μ M FMN (1 mM stock solution) to apo-Pst2p or by addition of 2-8 μ M quinone (1-4 mM stock solution dissolved in 50% EtOH) to Pst2p. After careful mixing and incubation for 3 min an absorption spectrum was recorded (250–

700 nm). The K_d values were determined by nonlinear hyperbolic fit in Origin 7.0 (OriginLab Corp., Northampton, USA).

Anaerobic Photoreduction

Photoreduction was carried out as described in [22]. Briefly, ~20 μM Pst2p in 1 mL buffer C supplemented with 1 mM EDTA was deoxygenated by incubation for 2 h in a glove box from Belle Technology (Weymouth, UK). A 10 W LED floodlight (Luminea) was used to reduce the cofactor by light irradiation. Spectra were recorded after each reduction step until no further spectral changes were observed. Thereafter the sample was exposed to air and a spectrum was recorded after complete reoxidation.

Steady state kinetics

Initial-velocity measurements were performed in triplicate with NAD(P)H, 1,4-BQ, MQ, DQ and CoQ1 by following the oxidation of NAD(P)H at 380 nm. Reaction mixtures were setup in 50 mM HEPES pH 7.0, 50 mM NaCl, 2% (v/v) EtOH. Substrate concentrations were as follows: NAD(P)H (30-500 μM) at a saturating concentration of 200 μM for MQ. Different quinone concentration, i.e. 1,4-BQ (5-155 μM), MQ (20-235 μM), DQ (12-317 μM) or CoQ1 (30-500 μM) were measured at a saturating NADH concentration of 350 μM . For the investigation of the kinetic mechanism of Pst2p various concentrations of NADH (30-350 μM) and MQ (20-200 μM) were used. All reactions were initiated by addition of 5 μL enzyme stock solution, supplemented with 400 μM FMN, to the reaction mixture – final enzyme concentrations were 2-10 nM (final FMN concentration: 2 μM). Controls were performed in the absence of enzyme. For each concentration, at least three measurements were performed. Initial velocities were determined by fitting the absorption change at 380 nm in the first minute using the appropriate extinction coefficients (NADH $\epsilon_{380} = 1.210 \text{ M}^{-1} \text{ cm}^{-1}$ or NADPH $\epsilon_{380} = 1.280 \text{ M}^{-1} \cdot \text{cm}^{-1}$). K_M and k_{cat} were determined by nonlinear hyperbolic fit in Origin 7.0 (OriginLab Corp., Northampton, USA).

Determination of reductive/oxidative rates

The protein was deoxygenated by incubation for 2 h in a glove box from Belle Technology (Weymouth, UK). The reductive half-reaction was investigated by mixing protein (~25 μM) in buffer B with 25-1.250 μM NAD(P)H. The oxidative half-reaction

was investigated by mixing reduced protein (~ 25 μM , reduced with 0.9 equivalents NADH) with 25-300 μM MQ, 25 μM 1,4-BQ and 25-100 μM DQ. These concentrations are final values after mixing in the flow cell. Experiments were performed with a SF-61SX2 stopped flow device from TgK Scientific Limited (Bradford-on-Avon, UK) positioned in an anaerobic glove box from Belle Technology (Weymouth, UK) at 4 °C. Changes in flavin absorption were followed with a PM-61s photomultiplier from TgK Scientific Limited (Bradford-on-Avon, UK) at 453 nm. Each concentration was measured in triplicates and the observed rate constants for different substrate concentrations (k_{obs}) were calculated using the exponential fitting function of the kinetic studio software (TgK Scientific Limited).

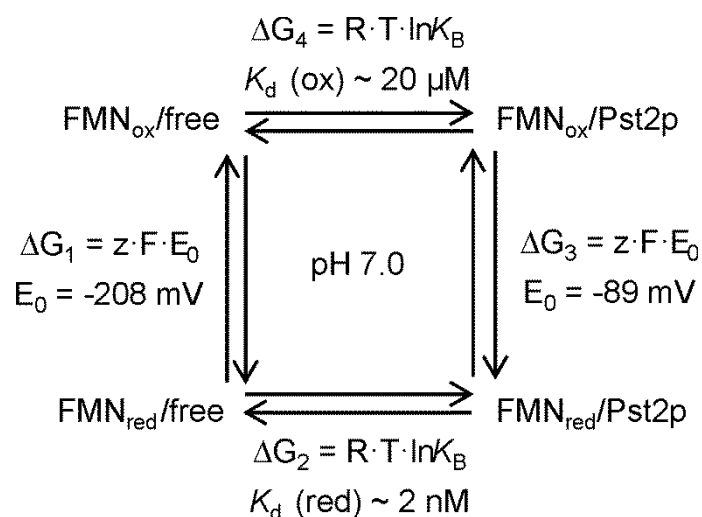
Redox potential

The redox potential was determined by the dye-equilibration method using the xanthine/xanthine oxidase electron delivering system as described by [37]. Reactions were carried out in buffer C supplemented with methyl viologen (2.5 μM) as mediator, 500 μM xanthine, and xanthine oxidase in catalytic amounts (~40 nM) and lasted 0.5 2 h. The protein concentration for a typical experiment was ~25 μM . These concentrations are final values after mixing in the flow cell. Experiments were performed with a SF-61SX2 stopped flow device from TgK Scientific Limited (Bradford-on-Avon, UK) equipped with an auto-shutter to reduce photochemical effects during the experiment. To maintain anaerobic conditions the device was positioned in a glove box from Belle Technology (Weymouth, UK). Spectra during the course of reduction were recorded with a KinetaScanT diode array detector from TgK Scientific Limited (Bradford-on-Avon, UK). Dyes used for analysis and their corresponding redox potentials were potassium indigo-trisulfonate (-81 mV) and indigo carmine (-125 mV). Due to spectral changes of the used dyes during the reduction process the amounts of oxidized and reduced Pst2p were quantified at the isosbestic points at 485 and 461 nm for potassium indigo-trisulfonate and for indigo carmine, respectively. The reduction oxidation potentials were calculated from plots of $\log([\text{ox}]/[\text{red}])$ of the protein versus $\log([\text{ox}]/[\text{red}])$ of the dye according to [38] using Excel 2010 (Microsoft, Redmond, USA).

Determination of the dissociation constants for reduced FMN bound to Pst2p

The redox potential of free FMN (-208 mV) and the determined value for the FMN/FMNH₂ couple in Pst2p was used to calculate the K_d of the reduced flavin by using the determined K_d for the oxidized flavin according to the thermodynamic relationship shown in Scheme 1. The Gibbs energy for the binding affinity between the reduced cofactor and the enzyme was calculated according to the relationship $\Delta G_1 + \Delta G_2 = \Delta G_3 + \Delta G_4$.

Scheme 1. Thermodynamic relationships between redox potentials and dissociation constants.



Strain sensitivity and growth assay

A single colony of the respective strains was grown for 24 h in synthetic dextrose medium [0.67% amino acid free yeast nitrogen base, 2% carbon source, 0.01% (adenine, arginine, cysteine, leucine, lysine, threonine, tryptophan, uracil) 0.005% (aspartic acid, histidine, isoleucine, methionine, phenylalanine, proline, serine, tyrosine, valine) lacking uracil (SD-ura)]. About 20 mL of fresh synthetic galactose medium lacking uracil (SG-ura) was inoculated with pre culture to an OD₆₀₀ of 0.1. The culture was then grown for several hours to a final OD₆₀₀ of 1.0. Samples were differentially diluted and plated on SG-ura plates supplemented with 1,4-BQ (50-250 μM), hydroquinone (HQ; 500-2000 μM), DQ (25-100 μM) and were grown for 2–3 days in an incubator at 30 °C. Quinones were added from stocks made in pure EtOH

to allow a homogenous distribution of the reagent in the agar medium. Final EtOH concentrations were 2% (v/v). To exclude growth differences, of the strains independent of the stressors, samples were also plated on SG-ura plates supplemented with the solvent and growth behavior in liquid media was monitored at OD₆₀₀.

Acknowledgements

The authors are grateful for the support by the interuniversity program in natural sciences (NAWI Graz) and the FWF-funded doctoral program *Molecular Enzymology* (W901). The authors thank the beamline staff of the European Synchrotron Radiation Facility (Grenoble, France) for their support during diffraction data collection.

References

- [1] V. Gudipati, K. Koch, W.-D. Lienhart, P. Macheroux, The flavoproteome of the yeast *Saccharomyces cerevisiae*, *Biochim. Biophys. Acta* 1844 (2014) 535–44.
- [2] S. Deller, P. Macheroux, S. Sollner, Flavin-dependent quinone reductases, *Cell. Mol. Life Sci.* 65 (2008) 141–160.
- [3] H.J. Prochaska, Purification and crystallization of rat liver NAD(P)H:(quinone-acceptor) oxidoreductase by cibacron blue affinity chromatography: Identification of a new and potent inhibitor, *Arch. Biochem. Biophys.* 267 (1988) 529–538.
- [4] R. Li, M.A. Bianchet, P. Talalay, L.M. Amzel, The three-dimensional structure of NAD(P)H:quinone reductase, a flavoprotein involved in cancer chemoprotection and chemotherapy: Mechanism of the two-electron reduction, *Proc. Natl. Acad. Sci. USA* 92 (1995) 8846–8850.
- [5] A.T. Dinkova-Kostova, P. Talalay, Persuasive evidence that quinone reductase type 1 (DT diaphorase) protects cells against the toxicity of electrophiles and reactive forms of oxygen, *Free Radical Biol. Med.* 29 (2000) 231–240.
- [6] R.J. Knox, S. Chen, Quinone reductase – mediated nitro-reduction: Clinical applications, *Methods Enzymol.* 382 (2004) 194–221.
- [7] R. Grandori, P. Khalifah, J.A. Boice, R. Fairman, K. Giovanielli, J. Carey, Biochemical characterization of WrbA, founding member of a new family of multimeric flavodoxin-like proteins, *J. Biol. Chem.* 273 (1998) 20960–20966.
- [8] E. V. Patridge, J.G. Ferry, WrbA from *Escherichia coli* and *Archaeoglobus fulgidus* is an NAD(P)H:quinone oxidoreductase, *J. Bacteriol.* 188 (2006) 3498–3506.
- [9] J. Wolfova, I. Kuta, J. Brynda, J.R. Mesters, M. Lapkouski, M. Kutý, A. Natalello, N. Chatterjee, S. Chern, E. Ebbel, A. Ricci, R. Grandori, R. Ettrich, J. Carey, Structural organization of WrbA in apo- and holoprotein crystals, *Biochim. Biophys. Acta* 1794 (2009) 1288–1298.

- [10] I. Kishko, B. Harish, V. Zayats, D. Reha, B. Tenner, J. Carey, Biphasic kinetic behavior of *E. coli* WrbA, an FMN- dependent NAD(P)H:quinone oxidoreductase, PLoS One 7 (2012) e43902.
- [11] V. Crescente, S.M. Holland, S. Kayhyap, E. Polycarpou, E. Sim, A. Ryan, Identification of novel members of the bacterial azoreductase family in *Pseudomonas aeruginosa*, Biochem. J. 473 (2016) 549–558.
- [12] A. Atia, N. Alrawaiq, A. Abdullah, A review of NAD(P)H:quinone oxidoreductase 1 (NQO1); a multifunctional antioxidant enzyme, J. Appl. Pharm. Sci. 4 (2014) 118–122.
- [13] A. Morokutti, A. Lyskowski, S. Sollner, E. Pointner, T.B. Fitzpatrick, C. Kratky, K. Gruber, P. Macheroux, Structure and function of YcnD from *Bacillus subtilis*, a flavin-containing oxidoreductase, Biochemistry 44 (2005) 13724–13733.
- [14] S. Sollner, P. Macheroux, New roles of flavoproteins in molecular cell biology: An unexpected role for quinone reductases as regulators of proteasomal degradation, FEBS J. 276 (2009) 4313–4324.
- [15] D. Siegel, D.L. Gustafson, D.L. Dehn, J.Y. Han, P. Boonchoong, L.J. Berliner, D. Ross, NAD(P)H:quinone oxidoreductase 1: Role as a superoxide scavenger, Mol. Pharmacol. 65 (2004) 1238–1247.
- [16] L. Li, S. Naseem, S. Sharma, J.B. Konopka, Flavodoxin-like proteins protect *Candida albicans* from oxidative stress and promote virulence, PLoS Pathog. 11 (2015) e1005147.
- [17] E. Heyno, N. Alkan, R. Fluhr, A dual role for plant quinone reductases in host-fungus interaction, Physiol. Plant. 149 (2013) 340–353.
- [18] A. Ryan, E. Kaplan, J.-C. Nebel, E. Polycarpou, V. Crescente, E. Lowe, G.M. Preston, E. Sim, Identification of NAD(P)H quinone oxidoreductase activity in azoreductases from *P. aeruginosa*: azoreductases and NAD(P)H quinone oxidoreductases belong to the same FMN-dependent superfamily of enzymes, PLoS One. 9 (2014) e98551.
- [19] H. Du, R.A. Fuh, J. Li, L.A. Corkan, J.S. Lindsey, Technical and software note

- photochemCAD: A computer-aided design and research tool in photochemistry, *Photochem. Photobiol.* 68 (1998) 141–142.
- [20] J.C. Overeem, G.J.M. Kerk, Mollisin, a naturally occurring chlorine-containing quinone: Part III. The synthesis of dechloromollisin methyl ether and of related compounds, *Recl. Des Trav. Chim. Des Pays-Bas.* 83 (1964) 1005–1022.
- [21] M.A. Moxley, J.J. Tanner, D.F. Becker, Steady-state kinetic mechanism of the proline:ubiquinone oxidoreductase activity of proline utilization A (PutA) from *Escherichia coli*, *Arch Biochem. Biophys.* 516 (2011) 113–120.
- [22] P. Macheroux, UV-visible spectroscopy as a tool to study flavoproteins, *Methods Mol. Biol.* 131 (1999) 1–7.
- [23] C. Pashley, S. Kendall, Cloning in plasmid vectors, *Methods Mol. Biol.* 235 (2003) 121–135.
- [24] W.E. Swords, Chemical transformation of *E. coli*, *Methods Mol. Biol.* 235 (2003) 49–53.
- [25] R. Gietz, Yeast transformation by the LiAc/SS carrier DNA/PEG method, *Methods Mol. Biol.* 1205 (2014) 1–12.
- [26] J.M. Cherry, E.L. Hong, C. Amundsen, R. Balakrishnan, G. Binkley, E.T. Chan, K.R. Christie, M.C. Costanzo, S.S. Dwight, S.R. Engel, D.G. Fisk, J.E. Hirschman, B.C. Hitz, K. Karra, C.J. Krieger, S.R. Miyasato, R.S. Nash, J. Park, M.S. Skrzypek, M. Simison, S. Weng, E.D. Wong, *Saccharomyces* genome database: The genomics resource of budding yeast, *Nucleic Acids Res.* 40 (2012) 700–705.
- [27] W. Kabsch, Xds, *Acta Crystallogr.* 66 (2010) 125–132.
- [28] M.D. Winn, C. Charles, K.D. Cowtan, E.J. Dodson, A.G.W. Leslie, A. McCoy, J. Stuart, N. Garib, H.R. Powell, J. Randy, Overview of the CCP4 suite and current developments, *Acta Crystallogr.* 67 (2011) 235–242.
- [29] S.L.A. Andrade, E.V. Patridge, J.G. Ferry, O. Einsle, Crystal structure of the NADH:quinone oxidoreductase WrbA from *Escherichia coli*, *J. Bacteriol.* 189 (2007) 9101–9107.

- [30] P. Emsley, B. Lohkamp, Features and development of Coot, *Acta Crystallogr.* 66 (2010) 486–501.
- [31] P.D. Adams, V. Pavel, V.B. Chen, W. Ian, N. Echols, N.W. Moriarty, R.J. Read, D.C. Richardson, S. Jane, C. Thomas, PHENIX: a comprehensive Python-based system for macromolecular structure solution, *Acta Crystallogr.* 66 (2010) 213–221.
- [32] K. Laemmli, Cleavage of structural proteins during the assembly of the head of bacteriophage T4, *Nature.* 227 (1970) 680–685.
- [33] W.-D. Lienhart, V. Gudipati, M.K. Uhl, A. Binter, S.A. Pullido, R. Saf, K. Zangger, K. Gruber, P. Macheroux, Collapse of the native structure caused by a single amino acid exchange in human NAD(P)H:quinone oxidoreductase 1, *FEBS J.* 281 (2014) 4691–4704.
- [34] W.S. Rasband, ImageJ, U. S. National Institutes of Health, Bethesda, Maryland, USA, <http://imagej.nih.gov/ij/>, 1997-2016.
- [35] F. Forneris, R. Orru, D. Bonivento, L.R. Chiarelli, A. Mattevi, ThermoFAD, a Thermofluor-adapted flavin ad hoc detection system for protein folding and ligand binding, *FEBS J.* 276 (2009) 2833–2840.
- [36] U.B. Ericsson, B.M. Hallberg, G.T. DeTitta, N. Dekker, P. Nordlund, Thermofluor-based high-throughput stability optimization of proteins for structural studies, *Anal. Biochem.* 357 (2006) 289–298.
- [37] V. Massey, A simple method for the determination of redox potentials, in B. Curti, G. Zanetti, S. Ronchi (Eds.), *Flavin and Flavoproteins*, Walter de Gruyter & Co, Berlin, 1990, pp. 59-66.
- [38] K. Minnaert, Measurement of the equilibrium constant of the reaction between cytochrome c and cytochrome a, *Biochim. Biophys. Acta* 110 (1965) 42–56.
- [39] S. Sollner, R. Nebauer, H. Ehammer, A. Prem, S. Deller, B. a Palfey, G. Daum, P. Macheroux, Lot6p from *Saccharomyces cerevisiae* is a FMN-dependent reductase with a potential role in quinone detoxification, *FEBS J.* 274 (2007) 1328–39.

- [40] E. Krissinel, K. Henrick, Inference of macromolecular assemblies from crystalline state, *J. Mol. Biol.* 372 (2007) 774–797.
- [41] DeLano Warren Lyford, The PyMOL Molecular Graphics System Version 1.5.0.4, 2002.
- [42] J. Carey, J. Brynda, J. Wolfova, R. Grandori, T. Gustavsson, R. Ettrich, I.K. Smatanova, WrbA bridges bacterial flavodoxins and eukaryotic NAD(P)H:quinone oxidoreductases, *Protein Sci.* 16 (2007) 2301–2305.
- [43] M. North, V.J. Tandon, R. Thomas, A. Loguinov, I. Gerlovina, A.E. Hubbard, L. Zhang, M.T. Smith, C.D. Vulpe, Genome-wide functional profiling reveals genes required for tolerance to benzene metabolites in yeast., *PLoS One* 6 (2011) e24205.#
- [44] S. Deller, S. Sollner, R. Trenker-el-Toukhy, I. Jelesarov, G.M. Gübitz, P. Macheroux, Characterization of a thermostable NADPH:FMN oxidoreductase from the mesophilic bacterium *Bacillus subtilis*, *Biochemistry* 45 (2006) 7083–7091.
- [45] H. Chen, S.L. Hopper, C.E. Cerniglia, Biochemical and molecular characterization of an azoreductase from *Staphylococcus aureus*, a tetrameric NADPH-dependent flavoprotein, *Microbiology* 151 (2016) 1433–1441.
- [46] G. Tedeschi, S. Chen, V. Massey, DT-Diaphorase: redox potential, steady-state, and rapid reaction studies, *J. Biol. Chem.* 270 (1995) 1198–1204.
- [47] D. Liger, M. Graille, C. Zhou, N. Leulliot, S. Quevillon-cheruel, K. Blondeau, H. Van Tilbeurgh, Crystal structure and functional characterization of yeast YLR011wp, an enzyme with NAD(P)H-FMN and ferric iron reductase activities, *J. Biol. Chem.* 279 (2004) 34890–34897.
- [48] P.A. Loach, Oxidation-reduction potentials, absorbance bands and molar absorbance of compounds used in biochemical studies., in: G.D. Fasman (Ed.), *Handb. Biochem. Mol. Biol. Phys. Chem. Data*, 3rd ed., CRC Press, Cleveland, 1976, pp. 122–130.
- [49] E. Denke, T. Merbitz-Zahradnik, O.M. Hatzfeld, C.H. Snyder, T.A. Link, B.L.

- Trumpower, Alteration of the midpoint potential and catalytic activity of the Rieske iron-sulfur protein by changes of amino acids forming hydrogen bonds to the iron-sulfur cluster, *J. Biol. Chem.* 273 (1998) 9085–9093.
- [50] J. Peral, M. Trillas, X. Doménech, Heterogeneous photochemistry - an easy experiment, *J. Chem. Educ.* 72 (1995) 565–566.
- [51] S. Porté, E. Crosas, E. Yakovtseva, J.A. Biosca, J. Farrés, M.R. Fernández, X. Parés, Chemico-biological interactions MDR quinone oxidoreductases: The human and yeast ζ -crystallins, *Chem. Biol. Interact.* 178 (2009) 288–294.
- [52] T.H. James, A. Weissberger, Oxidation processes. XI. The autoxidation of durohydroquinone, *J. Am. Chem. Soc.* 60 (1934) 98–104.
- [53] T.H. James, J.M. Snell, A. Weisberger, Oxidation processes. XII. The autoxidation of hydroquinone and of the mono-, di- and trimethylhydroquinones, *J. Am. Chem. Soc.* 60 (1938) 2084–2093.
- [54] B.R. Munday, Activation and detoxification of naphthoquinones by NAD(P)H:quinone oxidoreductase, *Methods Enzymol.* 382 (2004) 364–380.

Oxidative stress induced structural changes in the microtubule-associated flavoenzyme Irc15p from *Saccharomyces cerevisiae*

Karin Koch^{1‡}, Emilia Strandback^{1‡}, Shalinee Jha¹, Gesa Richter², Benjamin Bourgeois², Tobias Madl² and Peter Macheroux^{1,*}

¹Institute of Biochemistry, Graz University of Technology, Austria

²Institute of Molecular Biology and Biochemistry, Medical University of Graz, Austria

Author contributions

P.M. initiated the project; K.K., E.S., G.R., S.J., B.B., T.M. and P.M. designed the experiments and interpreted the data. K.K. and E.S. produced and purified Irc15p. K.K, E.S. and S.J. performed analytical, biochemical and enzymatic experiments. G.R. and B.B. performed SAXS measurements. K.K., E.S., S.J. G.R., B.B. and P.M. wrote the manuscript.

Manuscript published in: Protein Science (2018) doi: 10.1002/pro.3517.

Abstract

The genome of the yeast *Saccharomyces cerevisiae* encodes a canonical lipoamide dehydrogenase (Lpd1p) as part of the pyruvate dehydrogenase complex and a highly similar protein termed Irc15p (increased recombination centers 15). In contrast to Lpd1p, Irc15p lacks a pair of redox active cysteine residues required for the reduction of lipoamide and thus it is very unlikely that Irc15p performs a similar dithiol-disulfide exchange reaction as reported for lipoamide dehydrogenases. We expressed *IRC15* in *Escherichia coli* and purified the produced protein to conduct a detailed biochemical characterization. Here, we show that Irc15p is a dimeric protein with one FAD per protomer. Photoreduction of the protein generates the fully reduced hydroquinone without the occurrence of a flavin semiquinone radical. Similarly, reduction with NADH or NADPH yields the flavin hydroquinone without the occurrence of intermediates as observed for lipoamide dehydrogenase. The redox potential of Irc15p was -313 ± 1 mV and is thus similar to lipoamide dehydrogenase. Reduced Irc15p is oxidized by several artificial electron acceptors, such as potassium ferricyanide, 2,6-dichlorophenol-indophenol, 3-(4,5-dimethyl-2-thiazolyl)-2,5-diphenyl-2*H*-tetrazolium bromide and menadione. However, disulfides, such as cystine, glutathione and lipoamide were unable to react with reduced Irc15p. Limited proteolysis and SAXS-measurements revealed that the NADH-dependent formation of hydrogen peroxide caused a substantial structural change in the dimeric protein. Therefore, we hypothesize that Irc15p undergoes a conformational change in the presence of elevated levels of hydrogen peroxide, which is a putative biomarker of oxidative stress. This conformational change may in turn modulate the interaction of Irc15p with other key players involved in regulating microtubule dynamics.

Abbreviations

A. vinelandii, *Azotobacter vinelandii*; DCPIP, 2,6-dichlorophenol-indophenol; DTT, dithiothreitol; *E. coli*, *Escherichia coli*; Irc15, increased recombination centers 15; LPD, lipoamide dehydrogenase; MQ, menadione; MTT, 3-(4,5-Dimethyl-2-thiazolyl)-2,5-diphenyl-2H-tetrazolium bromide; ROS, reactive oxygen species; *S. cerevisiae*, *Saccharomyces cerevisiae*; *S. seoulensis*, *Streptomyces seoulensis*; STH, soluble pyridine nucleotide-transhydrogenases;

Keywords

oxidative stress; thiol modification; flavin adenine dinucleotide; lipoamide dehydrogenase; microtubule-binding protein;

Introduction

Reactive oxygen species (ROS), such as hydrogen peroxide (H_2O_2), superoxide anions ($\cdot\text{O}_2^-$), and hydroxyl radicals ($\cdot\text{OH}$) are constantly generated during aerobic respiration. Organisms employ various strategies to preserve an intrinsic balance in the overall redox environment within the cell by simultaneously producing low levels of ROS essential for physiological signaling processes. An imbalance between the production of ROS and the antioxidant defenses to eliminate these toxic intermediates can lead to oxidative damage to DNA, lipids, and proteins, generating cellular stress. [1] In the recent past, an increasing number of proteins have been identified that use reversible ROS-mediated thiol modifications to regulate their function. Similar to other post-translational modifications, oxidative thiol modifications are fully reversible, the extent of which depend on the reactivity and accessibility of cysteine thiols and the concentration of ROS present. Under oxidative stress conditions in the cell, these thiol modifications can become irreversible, leading to deleterious effects on protein structure and function. [2-4]

In this study we report an uncharacterized flavoprotein from the yeast *Saccharomyces cerevisiae*, which was found to be structurally sensitive to oxidative damage. The genome of *S. cerevisiae* features 68 genes that were identified to encode a flavoprotein. Despite being a widely utilized model organism biochemical information on the flavoproteome is rather limited. For example, Irc15p (increased recombination centers 15) has a sequence similarity of 59% to the FAD-containing yeast lipoamide dehydrogenase 1 (Lpd1p) [5]. Although it was demonstrated that Irc15p is associated with microtubules and regulates their dynamics [6], it is currently unclear whether the protein carries a flavin cofactor not to mention the potential properties and function of the putative enzymatic activity. This lack of information prompted us to recombinantly produce Irc15p and study its properties.

Lipoamide dehydrogenases (LPDs) orchestrate the reversible transfer of electrons between dihydrolipoamide to the enzyme-bound FAD cofactor and NAD^+ . Generally, LPDs possess a second redox active group that is composed of two cysteine residues capable of forming an internal disulfide. This internal dithiol-disulfide exchange communicates the electrons between the lipoamide and the FAD cofactor

and is thus an essential asset of LPDs [7, 8]. LPDs also constitute a component of oxoacid dehydrogenases that are large multienzyme complexes. In these complexes, LPDs reoxidize the covalently bound lipoamide cofactor of the transacylase component. [9] Interestingly, Irc15p lacks the two essential cysteines required for the formation of a disulfide and therefore it is most unlikely that Irc15 is a redundant LPD or even exhibits similar enzymatic properties. Apparently, *IRC15* evolved after the whole genome duplication of *S. cerevisiae* and the duplicated *LPD1* sequence subsequently evolved to attain a new function (“neofunctionalization”) [10, 11]. This new function appears to be connected to the regulation of microtubule dynamics and chromosome segregation. [6] However, it is not known what exactly this function is let alone whether this function is compatible with the properties of a putative LPD homolog.

LPDs are members of the family of flavoprotein disulfide reductases that catalyze the NAD(P)H-dependent reduction of disulfide containing substrates. To perform this reaction the enzymes are equipped with a flavin cofactor and another non-flavin redox center. Initially only three members, namely LPD, glutathione reductase and thioredoxin reductase composed the enzyme family, which has expanded significantly in recent years. [7] In 2012, the family was classified according to the nature and position of the non-flavin redox center into five sub groups. [8] Group one comprises the flavoprotein disulfide reductases with the classical sequence motif CXXXXC, such as LPD. Members of group two are structurally related but contain a second cysteine based redox center. Enzymes from group three contain only one cysteine, which either forms a cysteine sulfenic acid or a cysteine-coenzyme A mixed disulfide during the reaction. Members of group four contain the classical sequence motif but catalyze a non-disulfide reductase reaction. Finally, members of group five feature two cysteines that are widely separated in the primary sequence.

In addition to these five sub-groups, several proteins described in the literature exhibit high sequence similarity with flavoprotein disulfide reductases, but lack some significant features. For example, pyridine nucleotide transhydrogenases (STH) catalyzes the reversible transfer of electrons between NADH and NADP⁺ and lack at least one of the redox active cysteines and a histidine residue essential for catalytic activity. [7, 12] These enzymes are also closely related to LPD, for example, STH

from *Escherichia coli* exhibits 27% identity and 45% similarity to several LPDs. [13] However, also LPDs themselves are able to catalyze transhydrogenase reactions. [14] Another example is LpdA from *Mycobacterium tuberculosis*, which lacks one cysteine as well as the catalytic histidine and glutamate. Like STH the protein is not able to catalyze the reduction of disulfides but instead features quinone reductase activity. The physiological relevance of this protein is unknown. [15] In the present work, we recombinantly produced Irc15p in *E. coli*. The purified Irc15p shows the typical characteristics of a flavoenzyme. We have demonstrated that Irc15p is efficiently reduced by NADH but lacks disulfide reductase activity. However, reduced Irc15p reduces a range of artificial electron acceptors, such as potassium ferricyanide, 2,6-dichlorophenol-indophenol (DCPIP) and quinones. The potential role of Irc15p as a microtubule-associated protein is discussed in light of our findings concerning the enzymatic properties and structural changes that occur upon exposure to hydrogen peroxide.

Results

Biochemical characterization of Irc15p

Initially, Irc15p was produced with a C-terminal hexa-histidine tag as described by Keyes and Burke. [6] However, the protein could not be purified successfully due to weak binding to the Ni-NTA sepharose resin. Therefore, we employed a C-terminal nona-histidine tag enabling the successful purification of ~13 mg of protein from 1 L culture with a purity of >95% as judged by visual inspection of SDS-PAGE and by using the program ImageJ (<http://imagej.nih.gov/ij/>) [16] (Figure 1, panel A). The presence of DTT in the buffer was critical to prevent the precipitation of Irc15p.

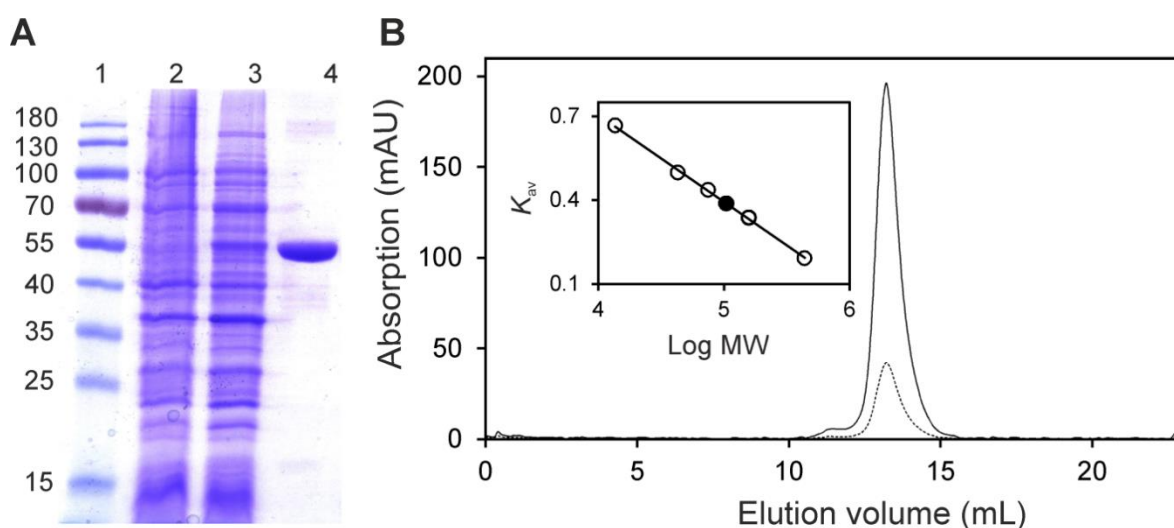


Figure 1. Determination of the purity and molecular mass of Irc15p using SDS-PAGE and analytical size exclusion chromatography. (A) Determination of purity and subunit molecular mass of Irc15p by SDS-PAGE after purification by affinity chromatography. Lane 1, PageRuler™ prestained protein ladder (10-180 kDa); lane 2, protein extract before induction; lane 3, protein extract after induction of IRC15; lane 4, protein fraction after purification by Ni-NTA-sepharose. The subunit molecular mass of Irc15p was estimated to ~55 kDa. (B) Determination of native molecular mass of Irc15p (solid and dotted line display the absorption at 280 nm and 450 nm, respectively) using analytical size exclusion chromatography. The insert shows a plot of the partition coefficient (K_{av}) against the logarithm of molecular mass of standard proteins (ferritin, 440 kDa; aldolase, 158 kDa; conalbumin, 75 kDa; ovalbumin, 43 kDa; ribonuclease A, 13.7 kDa). The calculated molecular mass of Irc15p (~ 113 kDa, black circle) indicates that Irc15p is present as a dimer.

Analytical size exclusion chromatography yielded a molecular mass of ~115 kDa confirming that Irc15p forms a homodimer as previously reported by Keyes and

Burke. [6] The protein peak was associated with a yellow color indicating the presence of a flavin cofactor in agreement with the high sequence similarity to the FAD-dependent LPD (Figure 1, panel B).

To assess the chemical identity of the flavin cofactor, Irc15p was denatured and the released flavin was analyzed by HPLC. A peak was obtained at a retention time of 9.1 min closely corresponding to the retention time of authentic FAD (9.05 min). Furthermore, the purified protein exhibited the absorption characteristics of a flavoprotein and also looks very similar to lipoamide dehydrogenases, with two distinct peaks at 377 and 453 nm with a shoulder at ~470 nm.[17] Denaturation of the protein resulted in a slight bathochromic shift of the absorption maxima at 453 nm (Figure 2, panel A). Using an extinction coefficient of $11.300 \text{ M}^{-1} \text{ cm}^{-1}$ at 450 nm for free FAD [18] an extinction coefficient of $11.900 \text{ M}^{-1} \text{ cm}^{-1}$ at 453 nm was calculated for Irc15p. This extinction coefficient was used to determine the concentration of Irc15p in further experiments. The A_{280}/A_{450} ratios of purified Irc15p were usually between 4.3 and 4.5.

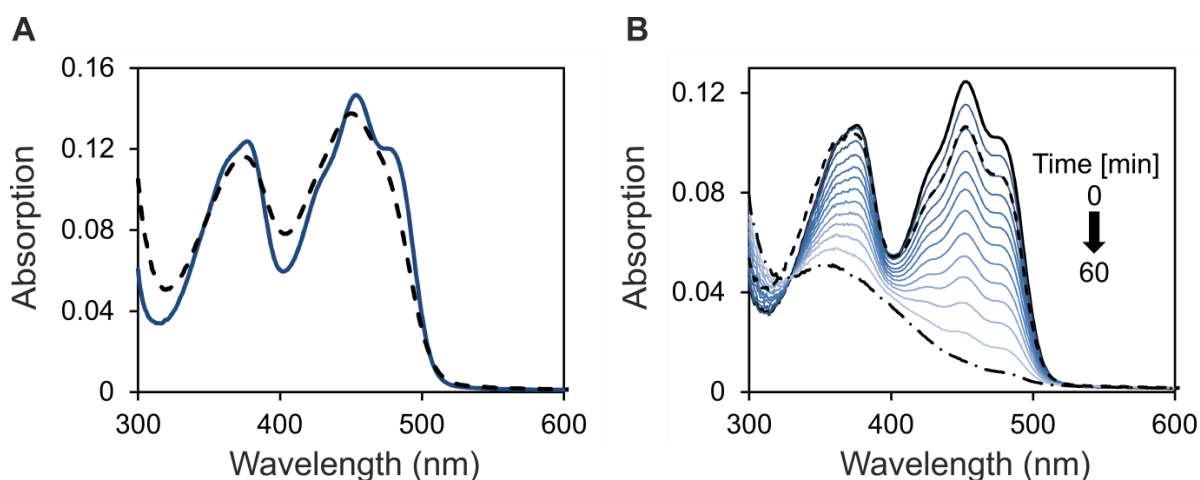


Figure 2. UV/Vis absorption spectroscopy. (A) UV-visible absorption spectrum of Irc15p before (solid line) and after denaturation (dashed line). Denaturation of purified Irc15p was carried out in buffer B (50 mM HEPES, 50 mM NaCl, 1 mM DTT, pH 7.0) containing 0.2% SDS. (B) Absorption spectra observed during the anaerobic photoreduction of Irc15p in 50 mM HEPES, 50 mM NaCl, 1 mM DTT, 1 mM EDTA, pH 7.0. The solid black line represents the spectrum before irradiation. The reduction proceeds as indicated by the arrow with the dashed dotted line representing the final spectrum. After reoxidation by dioxygen the protein was partially denatured. The solution was cleared by centrifugation and the spectrum recorded (dashed line).

Photoreduction of Irc15p in the presence of EDTA led to the formation of the fully reduced flavin (hydroquinone) without the formation of a semiquinone radical (Figure 2, panel B). After reoxidation and removal of precipitated protein the obtained UV-vis absorption spectrum was similar to the initial spectrum indicating that reduction is fully reversible and does not give rise to chemical alterations of the flavin (Figure 2, panel B).

The redox potential of the FAD cofactor was determined with the xanthine/xanthine oxidase system in the presence of safranin T ($E_M = -289$ mV). According to the method of Minnaert [19] a plot of $\log(Irc15p_{ox}/Irc15p_{red})$ versus $\log(dye_{ox}/dye_{red})$ was used to estimate the redox potential to -313 ± 1 mV (six independent measurements). In agreement with the photoreduction, reduction of Irc15p occurred without formation of a semiquinone and accordingly the slope of the logarithmic plot was close to unity indicating that the reference dye as well as the isoalloxazine moiety of the flavin took up two electrons (Figure 3).

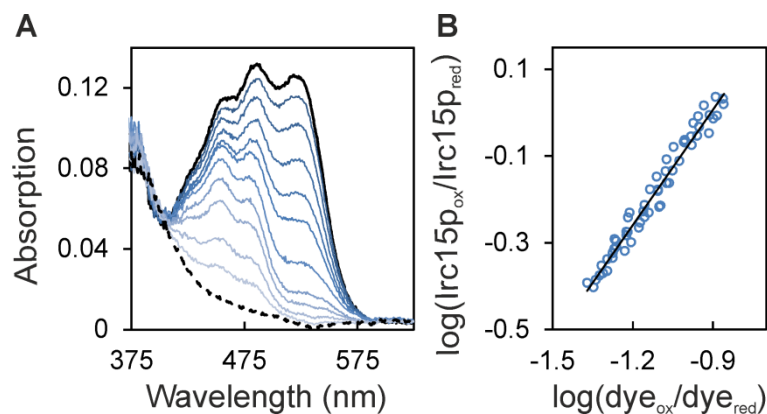


Figure 3. Redox potential determination of Irc15p in the presence of safranin T. (A) The absorption spectrum of the fully oxidized and fully reduced species are represented by a solid and dashed black line, respectively. Selected spectra of the course of reduction are represented in different shades of blue. Ten μ M Irc15p was reduced by the xanthine/xanthine oxidase electron delivering system in the presence of safranin T over a time period of ~ 100 min. Data points for evaluation were extracted at 430 nm and 530 nm for Irc15p and for the dye safranin T, respectively. (B) Double logarithmic plot of the concentration of oxidized/reduced Irc15p vs. the concentration of oxidized/reduced safranin T (Nernst plot).

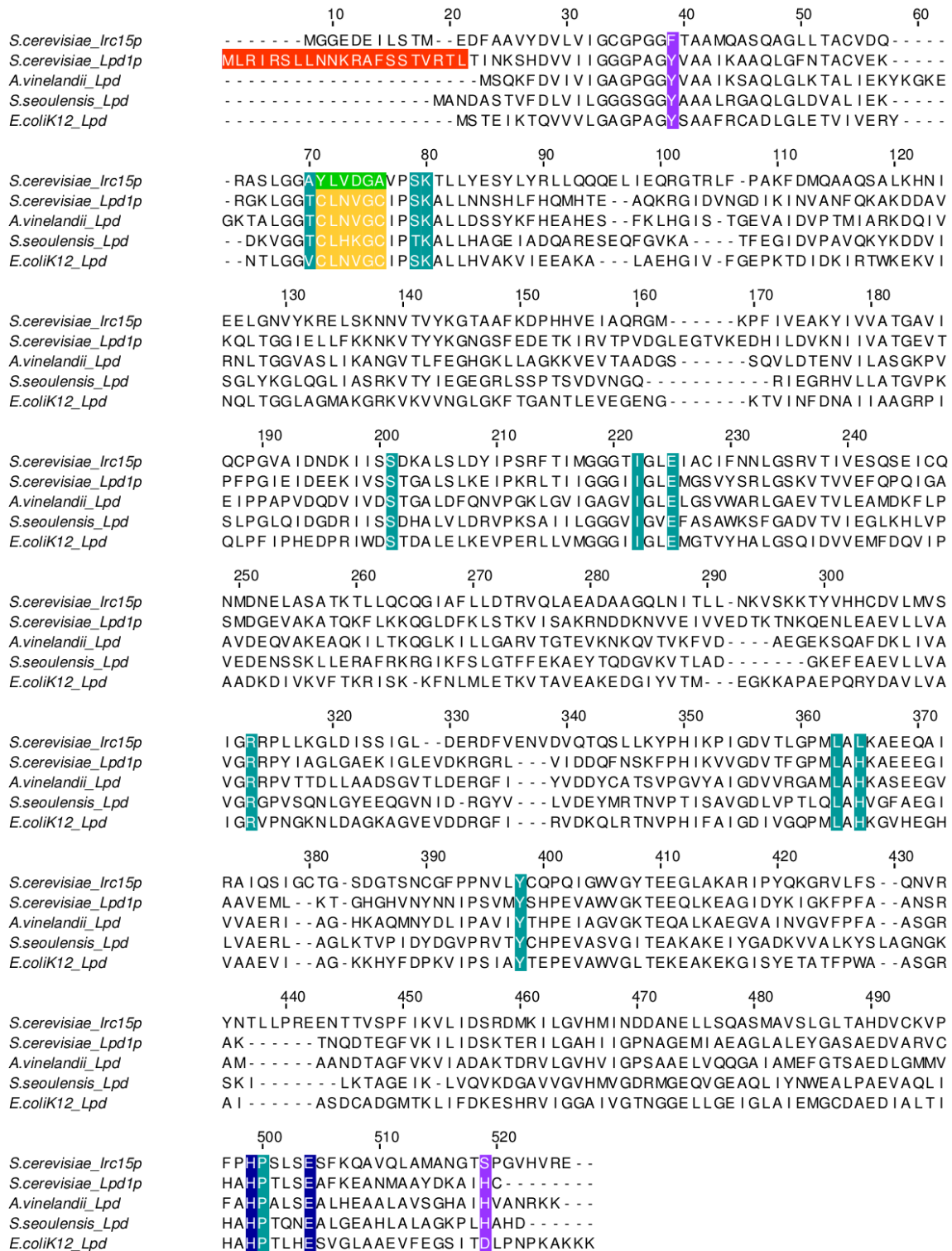


Figure 4. Alignment of the Irc15p protein sequence with sequences of LPD from *S. cerevisiae*, *E. coli*, *S. seoulensis* and *A. vinelandii*. The mitochondrial targeting sequence of Lpd1p is highlighted in red. The amino acid signature near the redox-active disulfide is highlighted in yellow. The respective sequence in Irc15p is highlighted in green. The catalytic His-Glu diad is highlighted in blue. Other residues in the active site are highlighted in petrol. Residues involved in structural stabilization are highlighted in purple.

Sequence alignment and homology modeling

A multiple sequence alignment using the amino acid sequence of Irc15p and the sequences of LPD from *S. cerevisiae*, *E. coli*, *Streptomyces seoulensis* and *Azotobacter vinelandii* was generated (Figure 4). The sequence identities of Irc15p and various LPDs are presented in Table 1. [20, 21]

Table 1. Sequence identity of Irc15p in comparison to other LPDs from *S. cerevisiae*, *E. coli*, *Streptomyces seoulensis* and *Azotobacter vinelandii*.

Percent identity to Irc15p	
<i>S. cerevisiae</i> _Lpd1p	40
<i>A. vinelandii</i> _Lpd	30
<i>S. seoulensis</i> _Lpd	28
<i>E. coli</i> K12_Lpd	27

A structural model of Irc15p was computationally generated using Lpd1p from *S. cerevisiae* (PDB entry: 1V59) as template (Figure 5, panel A and B). [22, 23] A comparison of the close environment of the FAD cofactor from Irc15p (Figure 5, panel C) and Lpd1p (Figure 5, panel D) reflects a high sequence conservation: out of 16 residues that are within 4 Å of the flavin isoalloxazine ring only four are different. Notably, among these are the two cysteines, C44 and C49, which make up the dithiol/disulphide redox centre of Lpd1p. These are replaced by tyrosine and alanine, respectively. The two amino acid residues that compose the catalytic diad, *i.e.* H457 and E462 are conserved in both proteins. [17]

Enzymatic properties and thermal stability of Irc15p

To gain information on the specificity of the electron donor, the reductive half-reaction was studied using stopped-flow spectrophotometry. Reduction of Irc15p with NADH was fast and monophasic. The rate of reduction was analysed as a function of substrate concentration and fitted to a hyperbolic equation yielding a limiting reductive rate of $250 \pm 3 \text{ s}^{-1}$ and a dissociation constant of $100 \pm 5 \text{ }\mu\text{M}$ (Figure 6,

panel A). As noted above, no semiquinone radical was observed (Figure 6, panel A, inset). In contrast to reduction by NADH, the reduction with NADPH exhibited two phases (Figure 6, compare panel B and C) and the bimolecular rate constant determined at 100 μM NAD(P)H is an order of magnitude lower (NADH = $1.2 \cdot 10^6 \text{ M}^{-1} \cdot \text{s}^{-1}$, NADPH = $3.4 \cdot 10^5 \text{ M}^{-1} \cdot \text{s}^{-1}$).

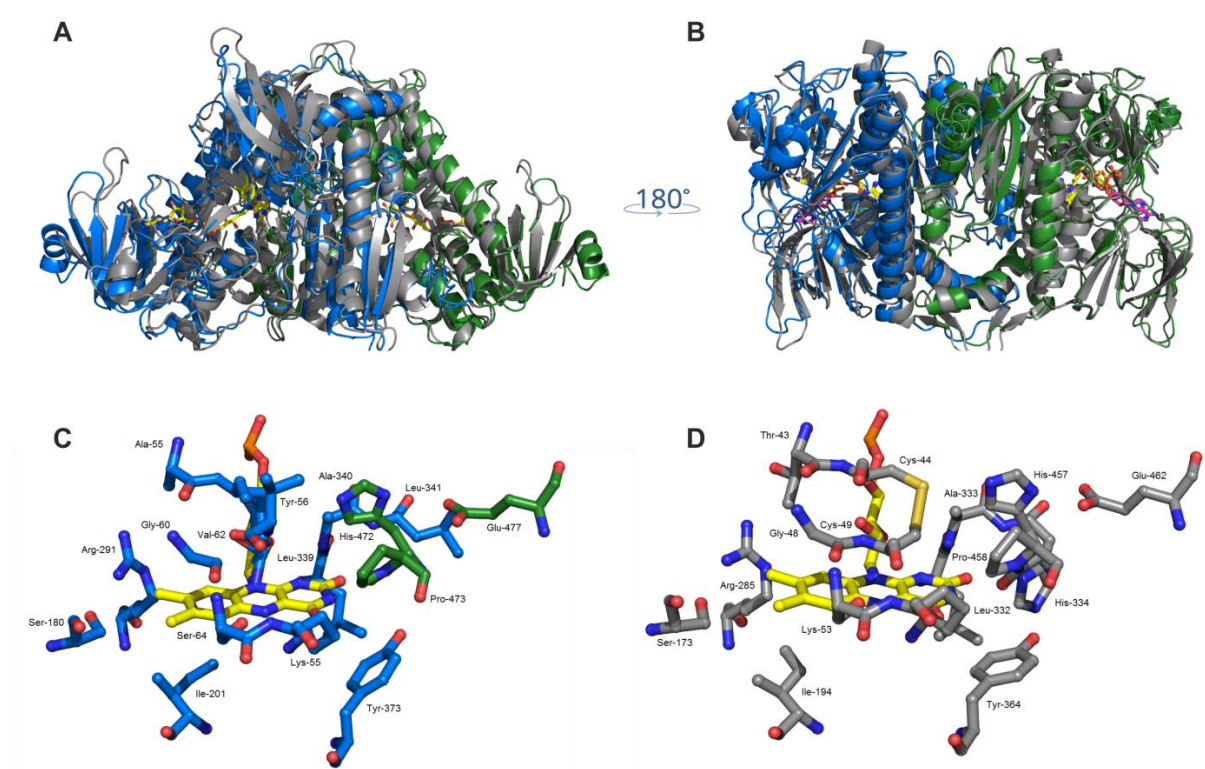


Figure 5. Overall structural similarity of Irc15p and Lpd1p. (A) and (B): Structural superposition of Lpd1p (grey, PDB code: 1V59) and Irc15p (blue/green). The FAD cofactor is displayed in yellow and NADH is shown in magenta. Close-up view of the active sites of Irc15p (C) and Lpd1p (D). Residues close to the FAD isoalloxazine ring are illustrated as grey sticks for both protomers (Lpd1p) or in colors corresponding to the respective protomer (Irc15p). Figures were prepared with the software PyMOL [24].

To evaluate the enzymatic activity of Irc15p, assays with NAD(P)H and several potential electron acceptors were performed (Table 2). No activity was observed with disulfides such as lipoic acid, glutathione or cystine. On the other hand, the enzyme showed diaphorase activity with the non-specific electron acceptors potassium ferricyanide, 3-(4,5-dimethyl-2-thiazolyl)-2,5-diphenyl-2*H*-tetrazolium bromide (MTT), and 2,6-dichlorophenol-indophenol (DCPIP) and quinone reductase activity with menadione (MQ). Furthermore the reduced cofactor was reoxidized by molecular

oxygen, however at a comparatively sluggish rate. A clear preference for NADH as electron donor is only observed in steady-state assays employing potassium ferricyanide as electron acceptor.

Table 2. Specific activities with standard deviations of Irc15p with NAD(P)H [$\mu\text{mol}/\text{min}^{-1}/\text{mg}^{-1}$] as electron donor in comparison with the specific activity of LPD from *S. seoulensis* [25] and LPD from *S. cerevisiae* (in brackets) [26] with NADH. Reduction of ferricyanide, DCPIP and MTT was determined at 420, 600 and 578 nm, respectively. All other reactions were monitored at 380 nm.

Substrate	Specific Activity with NADH [$\mu\text{mol}/\text{min}^{-1}/\text{mg}^{-1}$] ^a	Specific Activity with NADPH [$\mu\text{mol}/\text{min}^{-1}/\text{mg}^{-1}$] ^a	Specific Activity of LPD with NADH [$\mu\text{mol}/\text{min}^{-1}/\text{mg}^{-1}$] ^c
Ferricyanide	179.5 ± 3.41	17.9 ± 1.14	7.87 (1670.0 ^d)
DCPIP ^b	3.88 ± 0.14	4.72 ± 0.22	61.4 (2.0 ^d)
MQ ^{*,b}	19.7 ± 0.82	19.3 ± 2.12	7.18
MTT [*]	1.62 ± 0.08	1.28 ± 0.02	-
Lipoic acid [*]	0	0	15.6
Cystine [*]	0	0	0.80
Glutathione [*]	0	0	0.18
Oxygen [*]	1.0 ± 0.02	1.0 ± 0.02	0

^aThe reaction mixture for the measurements of Irc15p contained 50 mM HEPES, pH 7.0, 50 mM NaCl, 10 nM DTT, 500 μM NAD(P)H, 500 μM electron acceptors (except MQ and DCPIP). ^bThe concentration of DCPIP and MQ were 50 and 200 μM , respectively. ^cThe reaction mixture for the measurements of LPD from *S. seoulensis* contained 50 mM sodium phosphate buffer, pH 7.4, 0.3 mM substrates and 0.2 mM NADH. ^dThe reaction mixture for the potassium ferricyanide assay of LPD1 from *S. cerevisiae* contained 165 mM sodium acetate, pH 4.8, 0.7 mg/mL bovine serum albumin, 1 mM EDTA, 600 μM NADH, 670 μM potassium ferricyanide. The DCPIP assay contained phosphate buffer, pH 7.2, 0.7 mg/mL bovine serum albumin, 1 mM EDTA; 600 μM NADH and 40 μM DCPIP.

The potassium ferricyanide assay was further used to determine the influence of various pH values and salt concentrations on the enzymatic activity of Irc15p. The

highest activity was observed at pH 7.0 without salt in the assay buffer. Below and above pH 7.0 the activity is reduced by about 14-49%, and the presence of 150 mM NaCl decreased the activity at pH 7.0 by 40%.

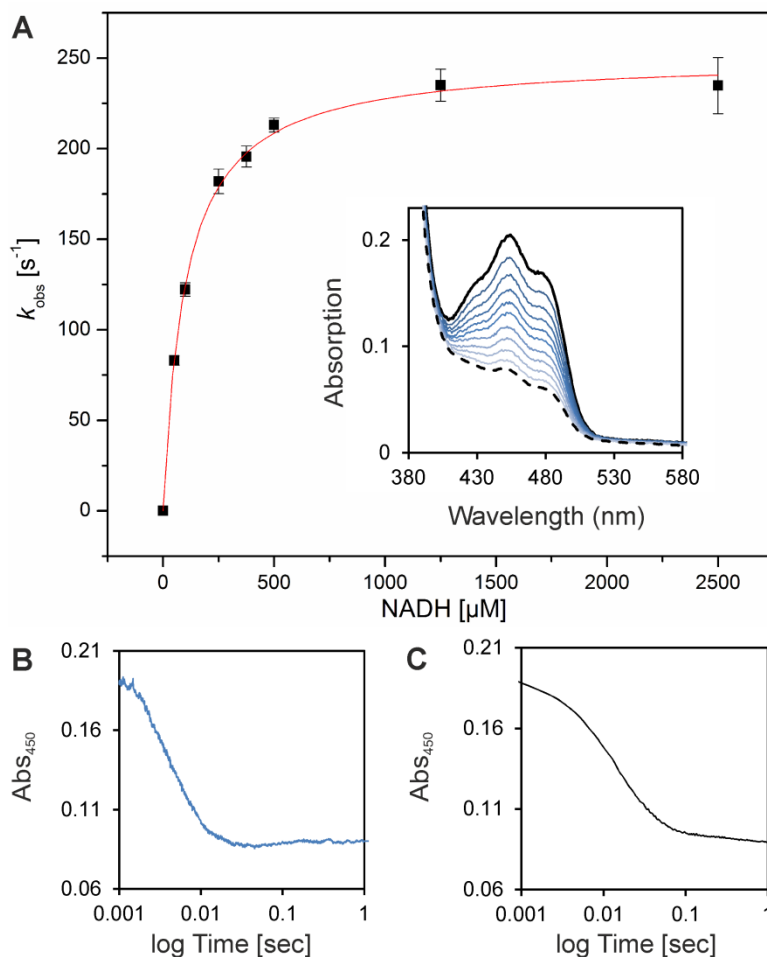


Figure 6. Pre-steady-state kinetics of Irc15p to determine reductive rates for NADH. (A) The rate of reduction was determined under anoxic conditions with the stopped flow device equipped with a diode array detector. At least three independent measurements were performed (error bars are shown as standard deviations). The inset displays selected absorption spectra of the reduction of $\sim 20 \mu\text{M}$ Irc15p with $375 \mu\text{M}$ NADH. (B) Absorption change at 450 nm of the reduction of $\sim 20 \mu\text{M}$ Irc15p with $1250 \mu\text{M}$ NADH. (C) Absorption change at 450 nm of the reduction of $\sim 20 \mu\text{M}$ Irc15p with $1000 \mu\text{M}$ NADPH.

The thermal stability of Irc15p was monitored using a thermal shift assay, performed with the fluorescent dye SYPRO[®] Orange. [27] Under optimal conditions, Irc15p displays a rather high thermal stability of about $70 \text{ }^\circ\text{C}$ (Table 3).

Table 3. Activity and thermal stability of Irc15p at various pH and in the absence and presence of NaCl. Melting points are given as the average of two independent measurements.

Buffer composition	Activity [%]	T _m [°C]
50 mM HEPES, pH 6.0	51	70
50 mM HEPES, pH 7.0	100	69
50 mM HEPES, pH 8.0	86	62
50 mM Tris/HCl, pH 9.0	46	56
50 mM HEPES, pH 7.0, 150 mM NaCl	61	69

The reaction mixture for the activity assay contained also 10 nM DTT, 500 μM NADH and 500 μM ferricyanide.

Additionally, measurements were performed in the presence and absence of NADH, NAD⁺, NADPH and NADP⁺, as summarized in Table 4. Interestingly a significant decrease in melting temperature could be observed after addition of an excess of NADH or NADPH.

Limited proteolysis

To further study the effect of NAD(P)H on the protein stability, limited proteolysis using tryptic digestion was performed under oxic and anoxic conditions in the presence and absence of NADH. As displayed in Figure 7A, Irc15p is more sensitive to proteolysis in the presence of NADH and molecular oxygen showing degradation already after 1 hour whereas the control sample is stable overnight. Interestingly, when the same experiment was performed under anoxic conditions, no degradation was detectable after six hours and became apparent only after 16 hours.

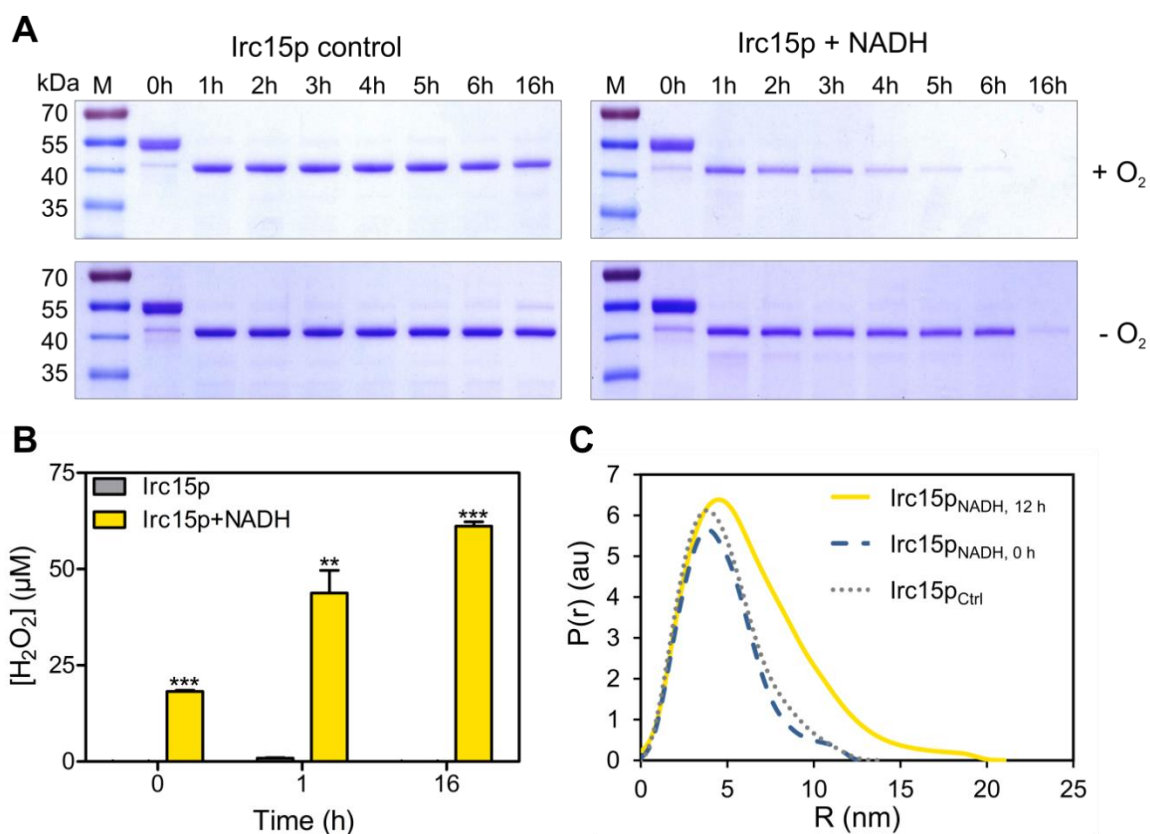


Figure 7. Limited proteolysis, hydrogen peroxide formation and SAXS data for Irc15p in the presence and absence of NADH. (A) SDS-PAGE from the limited proteolysis experiment illustrating the effect of NADH and oxygen on the stability of the protein. Each gel has the marker PageRuler™ prestained protein ladder in lane 1, the remaining lanes display the samples incubated for 0-16 hours. (B) Hydrogen peroxide formation in Irc15p over time (0, 1 and 16 hours) and in the presence and absence of NADH. (C) SAXS data comparing the experimental radial density distribution ($P(r)$) of Irc15p incubated with NADH measured after 0 and 12 hours compared to a control sample without NADH.

Hydrogen peroxide production

Since our limited proteolysis experiments demonstrated that NADH and molecular oxygen play a synergistic role, we hypothesized that the reduction of Irc15p by NADH and subsequent reoxidation by dioxygen led to the generation of hydrogen peroxide, which in turn may oxidize cysteine residues accessible on the surface of the protein. To assess this, we determined the production of hydrogen peroxide over a period of time by Irc15p in the presence of NADH under aerobic conditions. As expected, there was a marked increase in the level of hydrogen peroxide in the presence of NADH. In contrast, Irc15p without NADH showed no significant peroxide production (see Figure 7B).

Table 4. Thermal stability of Irc15p in 50 mM HEPES, 50 mM NaCl, 1 mM DTT, pH 7.0 in the presence and absence of 50 mM NADH, 50 mM NAD⁺, 50 mM NADPH, 50 mM NADP⁺ and 50 mM sodium dithionite. Melting points are determined as the average of two independent measurements.

Condition	T _m [°C]
Control	68
NADH	47
NAD ⁺	64
NADPH	45
NADP ⁺	68
Sodium dithionite	65

SAXS measurements of Irc15p

In order to further investigate the potential impact of thiol oxidation on the overall structure of the protein, SAXS measurements were employed. Irc15p formed a dimer in solution with a radius of gyration (R_g) of 3.64 ± 0.02 and with a maximum distance (D_{max}) of 14 nm. However, incubation of Irc15p with NADH in the presence of molecular oxygen resulted in a substantial change of the radius of gyration (R_g) and of the maximal diameter (D_{max}) indicating that the dimer adopts a more extended conformation (Irc15p with NADH measured directly: $R_g = 3.56 \pm 0.01$, $D_{max} = 13$ nm, Irc15p with NADH measured after 12 hours: $R_g = 5.44 \pm 0.03$, $D_{max} = 21$ nm, Figure 7, panel B). The SAXS data implicate that the presence of NADH is extending the conformation of Irc15p by 60%.

Discussion

In this study, we have demonstrated that Irc15p is a flavoprotein with FAD as the cofactor. Recombinant Irc15p features characteristic spectral properties that are similar to those reported for LPDs (Figure 2, panel A). In contrast to LPDs, reduction of Irc15p does not give rise to the typical red charge transfer absorption at longer wavelength (~530 nm) owing to the lack of a pair of redox active cysteines near the FAD cofactor. [25, 28] Instead, reduction by light as well as with NAD(P)H yielded the fully reduced FAD hydroquinone without the occurrence of a semiquinone radical (Figures 2, panel B and Figure 6).

The redox potential determined for Irc15p is shifted by 93 mV to -313 ± 1 mV compared to free flavin (= -220 mV). The redox potentials determined for LPD from *E. coli* were $E_{ox}/EH_2 = -264$ mV and $EH_2/EH_4 = -314$ mV and were assigned to the redox potentials of the disulfide/dithiol and the FAD/FADH₂ couple, respectively [28]. In order to confirm this assignment, Hopkins *et al.* [29] created two variants lacking either one of the two participating thiol groups, *i.e.* the variants C44S and C49S. The redox potentials of these variants were -379 and -345 mV, respectively, suggesting that the more negative redox potential determined for wild-type LPD belongs to the FAD/FADH₂ couple. Thus the redox potential of the FAD/FADH₂ couple of Irc15p is very similar to that of LPD suggesting that the environment of the FAD cofactors in these proteins is comparable.

Furthermore, we have demonstrated that the thermal stability of the protein is rather high ($T_m = 70$ °C). This is not unusual as the reported melting temperature for LPD from *A. vinelandii* is even higher ($T_m = 80$ °C). [30] Interestingly, it was shown that an exchange of Y16 to phenylalanine leads to a decrease of the melting temperature to 72 °C, since Y16 stabilizes the interaction of the subunits via hydrogen bond formation to H470. [31] In Irc15p phenylalanine is found in position 16 and H470 is replaced by serine. Therefore, the lower melting temperature of Irc15p may be accounted for, at least in part, by the amino acid changes in these positions.

To determine the substrate specificity of Irc15p the reductive half reaction was investigated using either NADH or NADPH. These measurements established a clear preference for NADH as electron donor proceeding with a limiting rate of $k_{red} = 250$ s⁻¹ (Figure 6). Thus, the limiting rate of Irc15p is an order of magnitude lower than that

of lipoamide dehydrogenase (250 s^{-1} vs. $>3000 \text{ s}^{-1}$). [32, 33] Since Irc15p is associated with microtubules and was shown to regulate their dynamics, the rapid reduction by NADH and the obvious conformational change occurring in the presence of NADH sheds new light on its potential role in processes such as mitosis. In recent years, several studies concluded that the NAD^+/NADH ratio and the overall redox status are regulatory elements of the cell cycle and the dynamics of the cytoskeleton. [34-36] It was shown that the NAD^+/NADH ratio is high during the G0 phase, decreases during the S phase before it increases again in the G2 phase. However, no information is available of the NAD^+/NADH ratio during mitosis. [35] Furthermore, it has been demonstrated that NAD^+ has an influence on the stability and curvature of microtubules. Since it is not interacting directly with the polymer it has been proposed, that NAD^+ affects microtubule binding proteins on the plus-end of the polymer. [36] How exactly the redox state influences the cell cycle and the cytoskeletal dynamics is not known, but several proteins regulating the cell cycle as well as tubulin contain redox sensitive elements like cysteines or cofactors where modifications may occur. [37, 38] Therefore, it is conceivable that reduced Irc15p interacts with these proteins and reduces oxidized groups, e.g. disulfides, to enable for example the polymerization of tubulins. This reactivity would clearly fit to the mode of action found in LPDs, where an internal disulfide in proximity to the isoalloxazine moiety of FAD is reduced to the dithiol via reduction of the flavin by NAD(P)H. In search for such an activity we tested a variety of disulfides, such as cystine, glutathione and lipoamide but we were unable to detect any reduction of these compounds (Table 2). However, we discovered that artificial electron acceptors such as potassium ferricyanide, DCPIP, MTT and MQ were good to excellent electron acceptors (Table 2).

A similar observation was reported for LpdA from *Mycobacterium tuberculosis*, which contains five homologs of flavoprotein disulfide reductases [7]. Apparently, LpdA does not reduce disulfide containing compounds but similar to Irc15p reduces quinones. [7] Interestingly, LpdA lacks one of the two cysteines near the FAD and the catalytic His-Glu diad, in other words it shares the absence of the dithiol-disulfide redox center with Irc15p but on the other hand also lacks the catalytic diad, which is present in Irc15p. Since the catalytic diad is important in the oxidative half reaction of disulfide reductases, *i.e.* the formation of the internal disulfide by oxidation through

the external disulfide (the “dithiol-disulfide exchange reaction”), its presence in Irc15p suggests that it has retained the ability to catalyze a similar reaction.

Limited proteolysis experiments performed in the presence and absence of NADH under oxic and anoxic conditions showed that Irc15p became more susceptible to degradation in the presence of NADH and oxygen. Furthermore, we showed that the formation of hydrogen peroxide was responsible for the increased sensitivity toward tryptic digestion. In keeping with this, SAXS measurements for Irc15p indicated time-dependent conformational change in Irc15p that resulted in a more extended and possibly more flexible structure. This structural change can be attributed to the presence of 11 cysteine residues per subunit of Irc15p, many of which are present on the surface. Cysteine is the most reactive and oxygen-sensitive amino acid due to the presence of the side chain thiol group. ROS-mediated oxidation of these thiols involves formation of sulfenic, sulfinic and sulfonic acids. While the sulfenic intermediates can be re-converted to their reduced form, thereby modulating protein activity, the sulfinic and sulfonic acid states are irreversible in nature and can cause decreased protein stability. This phenomenon is called hyperoxidation and can be induced during oxidative stress. [39] NADH-mediated generation of H₂O₂ shown here mimics oxidative stress conditions in the yeast cell, where the excessive ROS accumulation may result from a plethora of sources such as electron leakage originating in the mitochondrial transport chain, hyperoxia, upregulation of certain enzymes such as D-amino acid oxidases and peroxisomal acyl-coenzyme A oxidases, xenobiotics and environmental factors such as heat stress. [1] The study presented here showed that the yeast flavoprotein Irc15p is susceptible to redox-regulated conformational change, which can potentially impair its interaction with tubulin leading to a negative regulation of the microtubule dynamics. [6]

Materials & Methods

Materials

All chemicals, reagents and enzymes were of highest quality and from Sigma-Aldrich (St. Louis, USA), Roth (Karlsruhe, Germany) or Thermo Fisher Scientific (Waltham, USA), unless otherwise noted. Columns for affinity chromatography (Ni-NTA-sepharose), size exclusion chromatography (Superdex 200 10/300 GL) and buffer exchange (PD-10 desalting column) were from GE Healthcare (Little Chalfont, UK). The *E. coli* strains Top10 and RosettaTM(DE3) were from Invitrogen (Carlsbad, USA) and Merck (Darmstadt, Germany), respectively. The plasmid pET21d was from Merck (Darmstadt, Germany).

Cloning of IRC15 for large scale expression in E. coli

All strains were generated using standard genetic techniques [40, 41]. Briefly, genomic DNA from *S. cerevisiae* was extracted with the yeast DNA extraction kit from VWR (Radnor, USA). According to the sequence for *IRC15* from the *Saccharomyces* genome database [42] the following primers were designed and synthesized from VBC (Vienna, Austria): fw_5'-GAACCATGGCAATGGGAGGTGAAGACGAAATATTAAGCAC-3'; rev_5'-GAGCCTCGAGTTAATGGTGATGATGGTGATGATGATGATGTTCCCGGACATGTACGCCAG-3'. To construct the heterologous expression vector pET21d(+)/*IRC15* introducing an additional C-terminal 9x-histidine tag the restriction enzymes NcoI/XhoI were used. Individual clones were sequenced before transforming the plasmid into *E. coli* RosettaTM(DE3) cells.

Heterologous production and purification of Irc15p

A single colony of *E. coli* Rosetta(DE3) comprising pET21d(+)/*IRC15* was used to inoculate a pre-culture that was aerobically incubated (37 °C, 16 h, 150 rpm) in terrific broth media (bacto-tryptone 12 g/L, bacto-yeast extract 24 g/L, glycerol 4g/L, KH₂PO₄ 2.31 g/L and K₂HPO₄ 12.54 g/L) supplemented with 100 µg·mL⁻¹ ampicillin and 20 µg·mL⁻¹ chloramphenicol. 1% pre-culture was used to inoculate the main-culture supplemented with 100 µg·mL⁻¹ ampicillin and 10 µg·mL⁻¹ chloramphenicol, which was incubated aerobically at 37 °C with agitation at 150 rpm until an OD₆₀₀ of

~0.6 was reached. Production of the recombinant protein was induced by addition of 0.5 mM isopropyl- β -D-thiogalactoside and the culture was further incubated for 16 h at 20 °C. Cells were harvested by centrifugation at 4.500 g at 4 °C and washed once with 1% saline solution. Cell pellets were resuspended in 4 mL/g pellet buffer A (50 mM HEPES, 150 mM NaCl, 1 mM dithiothreitol, pH 7.0) supplemented with 30 mM imidazole, 1 mM phenylmethylsulfonyl fluoride dissolved in dimethylsulfoxide, 10 μ M flavin adenine dinucleotide disodium salt hydrate. Furthermore, 1 μ L of protease inhibitor cocktail for the purification of histidine-tagged proteins from Sigma-Aldrich (St. Louis, USA) was added per 1 g of cell pellet. Cell disruption was achieved by sonication with a Labsonic L instrument from Braun Biotech International (Berlin, Germany) with 120 Watt for 3 x 3 min in an ice-water bath with 3 min pauses between each cycle. The cell lysate was centrifuged at 38.850 g for 45 min at 4 °C, and the supernatant was loaded onto a 5-mL HisTrap HP column previously equilibrated with buffer A supplemented with 30 mM imidazole. The column was washed with five column volumes with buffer containing 50 mM HEPES, pH 7.0, 150 mM NaCl, 1 mM DTT and 100 mM imidazole. Then the column was washed with buffer A supplemented with 100 mM imidazole and subsequently proteins were eluted with buffer A supplemented with 350 mM imidazole. Fractions containing target protein were pooled and concentrated with centrifugal filter units (Amicon Ultra-15, 50 kDa; Millipore, Massachusetts, USA). Concentrated protein was re-buffered to buffer B (50 mM HEPES, 50 mM NaCl, 1 mM DTT, pH 7.0) with a PD-10 desalting column. The protein solutions were shock frozen and stored at -80 °C if not used immediately.

Determination of molecular mass of Irc15p

The subunit molecular mass of purified Irc15p was determined by SDS-PAGE with a 12.5% separating gel and 5% stacking gel under reducing conditions described by Laemmli [43]. The molecular mass marker PageRuler™ (prestained protein ladder 10-180 kDa) from Thermo Fisher Scientific (Waltham, USA) was used.

To determine the native molecular mass of Irc15p size exclusion chromatography with Buffer A using a Superdex 200 10/300 GL column attached to an Äktapurifier™ system from GE Healthcare (Little Chalfont, UK) was performed. Protein elution was monitored at 280 nm and 450 nm. The column was calibrated with molecular mass standards according to the instructions from GE healthcare.

Determination of the flavin cofactor bound to Irc15p

To determine the nature of the flavin cofactor concentrated protein samples were treated with 8 M guanidine hydrochloride (pH 2 adjusted with concentrated HCl). Denatured protein was removed by centrifugation (13.000 g, 5 min) and the solution was neutralized with concentrated NaOH. To remove residual protein centrifugal filter units (Amicon Ultra-0.5 mL 10 kDa; Millipore, Massachusetts, USA) were used. The flow-through was concentrated at 50 °C under reduced pressure and subsequently analysed by HPLC (UltiMate® 3000 HPLC system from Dionex, California, USA) using an Atlantis® dC18 5 µM (4.6 x 250 mm) column. As liquid phase a 0.1% TFA solution and acetonitrile containing 0.1% TFA were used. The concentration of the organic solvent was increased within 20 min from 0% to 95% in a linear gradient (T = 25 °C; flow rate = 1 mL/min). The samples were analysed using a diode array detector at 280, 370 and 450 nm. The retention times of authentic FAD, FMN and riboflavin were 9.05, 9.75 and 10.4 min, respectively.

Determination of the redox potential

The redox potential was determined by the dye-equilibration method using the xanthine/xanthine oxidase electron delivering system as described by Massey [44]. Reactions were carried out in buffer C (50 mM HEPES, 50 mM NaCl, pH 7) supplemented with methyl viologen (2.5 µM) as mediator, 500 µM xanthine, and xanthine oxidase in catalytic amounts (~40 nM) and lasted 0.5-2 h at 25 °C. The protein concentration for a typical experiment was ~10 µM. The concentrations given are final values after mixing in the flow cell. Experiments were performed with a SF-61SX2 stopped flow device from TgK Scientific Limited (Bradford-on-Avon, UK) equipped with an auto-shutter to reduce photochemical effects during the experiment. To maintain anoxic conditions the device was positioned in a glove box from Belle Technology (Weymouth, UK). Absorption spectra during the course of reduction were recorded with a KinetaScanT diode array detector from TgK Scientific Limited (Bradford-on-Avon, UK). Safranin T was used as a reference dye for the analysis (-289 mV). The amounts of oxidized and reduced Irc15p and safranin T were quantitated at 430 nm and 530 nm, respectively. The reduction-oxidation potentials were calculated from plots of $\log(Irc15p_{ox}/Irc15p_{red})$ versus $\log(dye_{ox}/dye_{red})$ according to Minnaert [19] using Excel 2010 (Microsoft, Redmond, WA, USA).

Sequence alignment and homology modeling

A multiple sequence alignment was generated with the program Clustal Omega [21] with sequences taken from the *Saccharomyces* genome database⁴⁰ and from the UniProt database²⁰. A computational prediction approach was employed to construct the model structure of Irc15p. Tertiary structure of the protein was generated using protein homology-based molecular modeling software Swiss-Model [22] and *ab initio* threading based software I-TASSER [23]. Both the programs used Lpd1p from *S. cerevisiae* (PDB entry: 1V59) as the top threading template for automated model building.

Methods using UV-visible absorption spectroscopy

Absorption spectra were recorded with a Specord 200 plus spectrophotometer from Analytik Jena (Jena, Germany) at 25 °C using 1-cm quartz cuvettes.

Extinction coefficient: The extinction coefficient of Irc15p was determined according to Macheroux [18]. Briefly, Irc15p bound FAD was released by addition of 0.2% SDS. Absorption spectra were recorded before and after denaturation of the enzyme. The calculation yielded an extinction coefficient of 11.900 M⁻¹ cm⁻¹ at 453 nm for Irc15p.

Anoxic photoreduction: Photoreduction was carried out as described by Macheroux [18]. Briefly, ~10 µM Irc15p in 1 mL buffer B (50 mM HEPES, 50 mM NaCl, 1 mM DTT, pH 7.0) supplemented with 1 mM EDTA was deoxygenated by incubation for 2 h in a glove box from Belle Technology (Weymouth, UK). A 10 W LED floodlight (Luminea) was used to reduce the cofactor by light irradiation. Absorption spectra were recorded after each reduction step until no further spectral changes were observed. Thereafter the sample was exposed to air and a spectrum was recorded after complete reoxidation.

Steady state kinetics: Initial-velocity kinetic measurements were performed in triplicates with NAD(P)H as electron donor and the disulfide containing electron acceptors lipoic acid, glutathione and cystine and the artificial electron acceptors potassium ferricyanide, MQ, MTT and DCPIP. Reaction mixtures were setup in buffer C (50 mM HEPES, 50 mM NaCl, pH 7). All reactions were initiated by addition of 5 µL enzyme stock solution supplemented with 200 nM DTT to the reaction mixture –

final enzyme concentrations were 10 nM. Controls were performed in the absence of enzyme. Rates of reduction with MQ, oxygen and disulfide containing substrates were determined by fitting the observed absorption change at 380 nm in the first minute using adapted extinction coefficients (NADH $\epsilon_{380 \text{ nm}} = 1.210 \text{ M}^{-1}\cdot\text{cm}^{-1}$ or NADPH $\epsilon_{380 \text{ nm}} = 1.280 \text{ M}^{-1}\cdot\text{cm}^{-1}$). For the other electron acceptors pertinent wavelengths and extinction coefficients were used (ferricyanide $\epsilon_{420 \text{ nm}} = 1.040 \text{ M}^{-1}\cdot\text{cm}^{-1}$; MTT $\epsilon_{578 \text{ nm}} = 13.000 \text{ M}^{-1}\cdot\text{cm}^{-1}$; DCPIP $\epsilon_{600 \text{ nm}} = 21.000 \text{ M}^{-1}\cdot\text{cm}^{-1}$) [39].

Thermal shift assay

Thermal shift assays were performed as described by Ericsson *et al.* [27]. 20 μL of $\sim 13 \mu\text{M}$ Irc15p protein solution was pipetted into a white 96-well RT-PCR plate from Bio-Rad (California, USA) both at different pH, in the absence and presence of 150 mM NaCl and in buffer B in the presence and absence of a final concentration of 50 mM NADH, 50 mM NAD^+ , 50 mM NADPH, 50 mM NADP^+ or 50 mM sodium dithionite. Two μL of a 1:500 dilution of SYPRO[®] orange from Molecular Probes (Oregon, USA) was added. The plates were sealed with an Optical-Quality Sealing Tape from Bio-Rad (California, USA) and heated in a CFX Connect[™] Real-Time PCR detection system from Bio-Rad (California, USA) from 20 to 95 °C in increments of 0.5 °C/5 sec. Fluorescence changes of the dye were detected at a wavelength between 470 and 500 nm. Melting temperatures (T_m) were determined using CFX Manager 3.0 software from Bio-Rad (California, USA).

Determination of kinetic rates

The protein was deoxygenated by incubation for 2 h in a glove box from Belle Technology (Weymouth, UK) kept in nitrogen atmosphere. The reductive half-reaction was investigated by mixing protein ($\sim 20 \mu\text{M}$) in buffer B with 25-2.500 μM NADH or 25-1.000 μM NAD(P)H. The concentrations given are final values after mixing in the flow cell. Experiments were performed with a SF-61SX2 stopped flow device from TgK Scientific Limited (Bradford-on-Avon, UK) positioned in an anoxic glove box from Belle Technology (Weymouth, UK) at 4 °C. Changes in flavin absorption were followed with a PM-61s photomultiplier from TgK Scientific Limited (Bradford-on-Avon, UK) at 453 nm.

Limited proteolysis

12 μM Irc15p in buffer D (50 mM HEPES, 50 mM NaCl, 5 mM EDTA and 1 mM DTT, pH 7.0) in the presence and absence of 50 mM NADH and under oxic or anoxic conditions was digested using 5 $\mu\text{g}/\text{mL}$ trypsin from Promega (Madison, WI, USA). The reactions were also supplemented with 8 mM DTT. The reactions were performed at 37 °C. Reactions in the absence of dioxygen were conducted in a glove box from Belle Technology (Weymouth, UK) filled with nitrogen gas. After preincubation of trypsin at 37 °C for 15 minutes, the digestion was started and samples were taken out after different time points (0, 1, 2, 3, 4, 5, 6 and 16 hours). The reactions were stopped by adding SDS sample buffer and the samples were boiled at 95 °C for 10 minutes. The samples were then analysed by SDS-PAGE with a 12.5% separating and 5% stacking gel. [45, 46]

Hydrogen peroxide assay

A time-dependent generation of H_2O_2 by Irc15p in the presence and absence of NADH was monitored using the Pierce™ Quantitative Peroxide Assay Kit (ThermoFischer Scientific). For the assay, 20 μM Irc15p in buffer C (50mM HEPES, 50 mM NaCl, pH 7.0) was incubated with 50 mM NADH at room temperature. A sample without NADH, also incubated at room temperature, was used as a control. The reactions were terminated at 0, 1 and 16 h by addition of 10% TCA solution. Samples of this reaction mixture (10 μl) were added to 100 μl of the working reagent in a 96-well plate and incubated for 20 min at room temperature. Working reagent was prepared according to the protocol specified in the kit (1 vol of reagent A in 100 vol of reagent B). Absorbance was recorded at 595 nm on a plate reader (FLUOStar Omega plate reader, BMG Labtech). The values were normalized to account for the intrinsic absorption of the working reagent. A standard curve containing 0 to 100 μM of H_2O_2 was prepared to determine the amount of H_2O_2 present in each sample.

Small-angle X-ray scattering

For successful SAXS measurements, an additional purification step of Irc15p was needed. Therefore, Irc15p in buffer D (50 mM HEPES, 50 mM NaCl, 5 mM EDTA and 1 mM DTT, pH 7.0) was purified by size exclusion chromatography on a Superdex 200 Increase 10/300 GL column from GE Healthcare (Little Chalfont, UK) connected to an ÄKTApurifier™ system (GE Healthcare, Little Chalfont, UK). The protein

containing fractions were then collected, centrifuged and used for further sample preparation.

For the SAXS measurements, three separate reaction mixtures were prepared, including one control with a concentration of 119 μM Irc15p and two samples with a concentration of 61 μM Irc15p, measured after 0 and 12 hours incubation with 50 mM NADH at 4 °C. Buffers for background corrections were also prepared from buffer D with either 119 μM or 61 μM FAD in the absence or presence of 50 mM NADH. All samples contained 8.3 mM DTT to prevent precipitation of Irc15p.

SAXS data for Irc15p were recorded with an in-house SAXS instrument (SAXSspace, Anton Paar, Graz, Austria) equipped with a Kratky camera, a sealed X-ray tube source and a Mythen2 R 1K Detector (Dectris). Thereby Irc15p and the buffers for background subtraction were loaded via an ASX autosampler and measured in a flow cell. The scattering patterns were measured with a 180-min exposure time (180 frames, each 1 min). Radiation damage was excluded on the basis of a comparison of individual frames of the 180-min exposures, wherein no changes were detected. A range of momentum transfer of $0.010 < s < 0.63 \text{ \AA}^{-1}$ was covered ($s = 4\pi \sin(\theta)/\lambda$, where 2θ is the scattering angle, and λ is the X-ray wavelength, in this case 1.5 \AA). Obtained SAXS data were processed using the SAXSanalysis package (Anton Paar, version 3.0). and analyzed using the ATSAS package (version 2.8.2, Hamburg, Germany). The data were desmeared using GIFT (PCG-Software). The forward scattering ($I(0)$), the radius of gyration, (R_g), the maximum dimension (D_{max}) and the interatomic distance distribution function ($P(r)$) were computed with GNOM [47]. The masses of the solutes were evaluated based on their Porod volume.

Acknowledgements

The authors are grateful for the support by the interuniversity program in natural sciences (NAWI Graz) and appreciate the help of Chaitanya R. Tabib for his support with the HPLC analysis and Eva-Maria Frießer for the help with routine work, as protein expression and purification. This work was supported by the Bavarian Ministry of Sciences, Research and the Arts (Bavarian Molecular Biosystems Research Network, to T.M.), the President's International Fellowship Initiative of CAS (No.2015VBB045, to T.M.), the National Natural Science Foundation of China (No. 31450110423, to T.M.), the Austrian Science Fund (FWF: P28854 and I3792 to

T.M.), the Austrian Research Promotion Agency (FFG: 864690), the Integrative Metabolism Research Center Graz, the Austrian infrastructure program 2016/2017, BioTechMed/Graz, the OMICS center Graz as well as the Deutsche Forschungsgemeinschaft (DFG) with the grant MA5703/1-1 (to T.M.).

References

- [1] G. Farrugia, R. Balzan, Oxidative stress and programmed cell death in yeast, *Front.Oncol.* 2 (2012).
- [2] A. Zeida, R. Babbush, M. C. G. Lebrero, M. Trujillo, R. Radi, D. A. Estrin, Molecular basis of the mechanism of thiol oxidation by hydrogen peroxide in aqueous solution: challenging the SN2 paradigm, *Chem. Res. Toxicol.* 25 (2012) 741-746.
- [3] B. Groitl, U. Jakob, Thiol-based redox switches, *Biochim. Biophys. Acta.* 1844 (2014) 1335-1343.
- [4] S. Lindhoud, W. A. van den Berg, R. H. van den Heuvel, A. J. Heck, C. P. van Mierlo, W. J. van Berkel, Cofactor binding protects flavodoxin against oxidative stress, *PLoS ONE* 7 (2012) e41363.
- [5] V. Gudipati, K. Koch, W. D. Lienhart, P. Macheroux, The flavoproteome of the yeast *Saccharomyces cerevisiae*, *Biochim. Biophys. Acta.* 1844 (2014) 535-544.
- [6] B. E. Keyes, D. J. Burke, Irc15 Is a Microtubule-Associated Protein that Regulates Microtubule Dynamics in *Saccharomyces cerevisiae*, *Curr. Biol.* 19 (2009) 472-478.
- [7] A. Argyrou, J. S. Blanchard, Flavoprotein disulfide reductases: advances in chemistry and function, *Prog. Nucleic Acid Res. Mol. Biol.* 78 (2004) 89-142.
- [8] S. M. Miller, Flavoprotein disulfide reductases and structurally related flavoprotein thiol/disulfide-linked oxidoreductases, in: H. Russ, S. Miller, B. Palfey (Eds.), *Handb. Flavoproteins Vol. 2 Complex Flavoproteins, Dehydrogenases Phys. Methods*, Walter de Gruyter & Co, Berlin, 2012, pp. 165–201.
- [9] A. Mattevi, G. Obmolova, K. H. Kalk, W. J. van Berkel, W. G. Hol, Three-dimensional structure of lipoamide dehydrogenase from *Pseudomonas*

- fluorescens* at 2.8 Å resolution. Analysis of redox and thermostability properties, *J. Mol. Biol.* 230 (1993) 1200-1215.
- [10] M. Kellis, B. W. Birren, E. S. Lander, Proof and evolutionary analysis of ancient genome duplication in the yeast *Saccharomyces cerevisiae*, *Nature* 428 (2004) 617-624.
- [11] K. P. Byrne, K. H. Wolfe, The yeast gene order browser: combining curated homology and syntenic context reveals gene fate in polyploid species, *Genome Res.* 15 (2005) 1456-1461.
- [12] C. E. French, B. Boonstra, K. A. Bufton, N. C. Bruce, Cloning, sequence, and properties of the soluble pyridine nucleotide transhydrogenase of *Pseudomonas fluorescens*, *J. Bacteriol.* 179 (1997) 2761-2765.
- [13] B. Boonstra, C. E. French, I. Wainwright, N. C. Bruce, The *udhA* gene of *Escherichia coli* encodes a soluble pyridine nucleotide transhydrogenase, *J. Bacteriol.* 181 (1999) 1030-1034.
- [14] R. Komuniecki, H. J. Saz, Purification of lipoamide dehydrogenase from *Ascaris* muscle mitochondria and its relationship to NADH:NAD⁺ transhydrogenase activity, *Arch. Biochem. Biophys.* 196 (1979) 239-247.
- [15] A. Argyrou, J. S. Blanchard, *Mycobacterium tuberculosis* lipoamide dehydrogenase is encoded by Rv0462 and not by the *lpdA* or *lpdB* genes, *Biochemistry* 40 (2001) 11353-11363.
- [16] C. A. Schneider, W. S. Rasband, K. W. Eliceiri, NIH Image to ImageJ: 25 years of image analysis, *Nat. Methods* 9 (2012) 671-675.
- [17] J. Benen, W. van Berkel, Z. Zak, T. Visser, C. Veeger, A. de Kok, Lipoamide dehydrogenase from *Azotobacter vinelandii*: site-directed mutagenesis of the His450-Glu455 diad. Spectral properties of wild type and mutated enzymes, *Eur. J. Biochem.* 202 (1991) 863-872.
- [18] P. Macheroux, UV-visible spectroscopy as a tool to study flavoproteins, *Methods Mol. Biol.* 131 (1999) 1-7.

- [19] K. Minnaert, Measurement of the equilibrium constant of the reaction between cytochrome c and cytochrome a, *Biochim. Biophys. Acta.* 110 (1965) 42-56.
- [20] UniProt Consortium, UniProt: a hub for protein information, *Nucleic Acids Res.* 43 (2015) 204-212.
- [21] F. Sievers, A. Wilm, D. Dineen, T. J. Gibson, K. Karplus, W. Li, R. Lopez, H. McWilliam, M. Remmert, J. Soding, J. D. Thompson, D. G. Higgins, Fast, scalable generation of high-quality protein multiple sequence alignments using Clustal Omega, *Mol. Syst. Biol.* 7 (2011) 539.
- [22] K. Arnold, L. Bordoli, J. Kopp, T. Schwede, The SWISS-MODEL workspace: a web-based environment for protein structure homology modelling, *Bioinformatics* 22 (2006) 195-201.
- [23] Y. Zhang, I-TASSER server for protein 3D structure prediction, *BMC Bioinformatics* 9 (2008) 40.
- [24] Schrödinger LLC, The PyMOL Molecular Graphics System Version 1.5.0.4.
- [25] H. Youn, J. Kwak, H. D. Youn, Y. C. Hah, S. O. Kang, Lipoamide dehydrogenase from *Streptomyces seoulensis*: biochemical and genetic properties, *Biochim. Biophys. Acta.* 1388 (1998) 405-418.
- [26] P. Heinrich, H. Ronft, W. Schartau, G. B. Kresze, Lipoamide dehydrogenase from baker's yeast. Improved purification and some molecular, kinetic, and immunochemical properties, *Hoppe Seylers Z. Physiol. Chem.* 364 (1983) 41-50.
- [27] U. B. Ericsson, B. M. Hallberg, G. T. Detitta, N. Dekker, P. Nordlund, Thermofluor-based high-throughput stability optimization of proteins for structural studies, *Anal. Biochem.* 357 (2006) 289-298.
- [28] K. D. Wilkinson, C. H. Williams Jr, Evidence for multiple electronic forms of two-electron-reduced lipoamide dehydrogenase from *Escherichia coli*, *J. Biol. Chem.* 254 (1979) 852-862.

- [29] N. Hopkins, C. H. Williams, Lipoamide dehydrogenase from *Escherichia coli* lacking the redox active disulfide: C44S and C49S. Redox properties of the FAD and interactions with pyridine nucleotides, *Biochemistry* 34 (1995) 11766-11776.
- [30] W. J. van Berkel, A. G. Regelink, J. J. Beintema, A. de Kok, The conformational stability of the redox states of lipoamide dehydrogenase from *Azotobacter vinelandii*, *Eur. J. Biochem.* 202 (1991) 1049-1055.
- [31] J. Benen, W. van Berkel, C. Veeger, A. de Kok, Lipoamide dehydrogenase from *Azotobacter vinelandii*. The role of the C-terminus in catalysis and dimer stabilization, *Eur. J. Biochem.* 207 (1992) 499-505.
- [32] R. G. Matthews, D. P. Ballou, C. H. Williams, Reactions of pig heart lipoamide dehydrogenase with pyridine nucleotides. Evidence for an effector role for bound oxidized pyridine nucleotide, *J. Biol. Chem.* 254 (1979) 4974-4981.
- [33] J. Benen, W. van Berkel, N. Dieteren, D. Arscott, C. Williams Jr, C. Veeger, A. de Kok, Lipoamide dehydrogenase from *Azotobacter vinelandii*: site-directed mutagenesis of the His450-Glu455 diad. Kinetics of wild-type and mutated enzymes, *Eur. J. Biochem.* 207 (1992) 487-497.
- [34] F. Yu, R. Dai, S. Goh, L. Zheng, Y. Luo, Logic of a mammalian metabolic cycle: An oscillated NAD⁺/NADH redox signaling regulates coordinated histone expression and S-phase progression, *Cell Cycle* 8 (2009) 773-779.
- [35] J. da Veiga Moreira, S. Peres, J. M. Steyaert, E. Bigan, L. Pauleve, M. L. Nogueira, L. Schwartz, Cell cycle progression is regulated by intertwined redox oscillators, *Theor. Biol. Med. Model.* 12 (2015) 10.
- [36] W. T. Harkcom, A. K. Ghosh, M. S. Sung, A. Matov, K. D. Brown, P. Giannakakou, S. R. Jaffrey, NAD⁺ and SIRT3 control microtubule dynamics and reduce susceptibility to antimicrotubule agents, *Proc. Natl. Acad. Sci. USA* 111 (2014) 2443-2452.

- [37] S. G. Menon, P. C. Goswami, A redox cycle within the cell cycle: ring in the old with the new, *Oncogene* 26 (2007) 1101-1109.
- [38] C. Wilson, C. González-Billault, Regulation of cytoskeletal dynamics by redox signaling and oxidative stress: implications for neuronal development and trafficking, *Front. Cell. Neurosci.* 9: 381 (2015) 1-10.
- [39] J. C. Lim, H.-I. Choi, Y. S. Park, H. W. Nam, H. A. Woo, K.-S. Kwon, Y. S. Kim, S. G. Rhee, K. Kim, H. Z. Chae, Irreversible Oxidation of the Active-site Cysteine of Peroxiredoxin to Cysteine Sulfonic Acid for Enhanced Molecular Chaperone Activity, *J. Biol. Chem.* 283 (2008) 28873-28880.
- [40] C. Pashley, S. Kendall, Cloning in plasmid vectors, *Methods in Molecular Biology* (Clifton, N.J.), 235 (2003) 121-125.
- [41] W. E. Swords, Chemical transformation of *E. coli*, *Methods Mol. Biol.* (Clifton, N.J.), 235 (2003) 49-53.
- [42] J. M. Cherry, E. L. Hong, C. Amundsen, R. Balakrishnan, G. Binkley, E. T. Chan, K. R. Christie, M. C. Costanzo, S. S. Dwight, S. R. Engel, D. G. Fisk, J. E. Hirschman, B. C. Hitz, K. Karra, C. J. Krieger, S. R. Miyasato, R. S. Nash, J. Park, M. S. Skrzypek, M. Simison, S. Weng, E. D. Wong, *Saccharomyces Genome Database: the genomics resource of budding yeast*, *Nucleic Acids Res.* 40 (2012) 700-705.
- [43] U. K. Laemmli, Cleavage of structural proteins during the assembly of the head of bacteriophage T4, *Nature* 227 (1970) 680-685.
- [44] V. Massey, A simple method for the determination of redox potentials, in *Flavins and Flavoproteins*, B. Curti, S Ronchi, G Zanetti (eds), Ed. 1990, pp. 59-60.
- [45] W. D. Lienhart, V. Gudipati, M. K. Uhl, A. Binter, S. A. Pulido, R. Saf, K. Zangger, K. Gruber, P. Macheroux, Collapse of the native structure caused by a single amino acid exchange in human NAD(P)H:quinone oxidoreductase 1, *The FEBS Journal* 281 (2014) 4691-4704.

- [46] S. Chen, P. S. Deng, J. M. Bailey, K. M. Swiderek, A two-domain structure for the two subunits of NAD(P)H:quinone acceptor oxidoreductase, *Protein Science* 3 (1994) 51-57.
- [47] D. I. Svergun, Determination of the regularization parameter in indirect-transform methods using perceptual criteria, *J. Appl. Crystallogr.* 25 (1992) 495-503.

Curriculum vitae

Emilia Strandback

Date of birth: 08.04.1988

Citizenship: Finland

Address: Schießstattgasse 8a/6, 8010 Graz, Austria

Email: emilia.strandback@tugraz.at

Mobile phone: +4368864758918



Education and Research Experience

2013 - present	Institute of Biochemistry, Graz University of Technology, Graz, Austria <i>PhD student</i> ; PhD Program DK Molecular Enzymology
June 2012 – July 2013	Department of Medical Biochemistry and Biophysics, Karolinska Institutet, Stockholm, Sweden <i>Research assistant</i>
June-August 2011	Department of Chemistry and The Molecular Design Institute, New York University, New York, USA <i>Summer Research Participant</i>
2010 – 2012	Royal Institute of Technology, Stockholm, Sweden <i>Master of Science</i> within the master's program Molecular Science and Engineering with a major in Biotechnology
2007 – 2010	Royal Institute of Technology, Stockholm, Sweden <i>Bachelor of Science</i> with a major in Chemistry and Technology

Publications

October 2018	Koch K., Strandback E. , Jha S., Richter G., Bourgeois B., Madl T., Macheroux P., <i>Oxidative stress induced structural changes in the microtubule-associated flavoenzyme Irc15p from Saccharomyces cerevisiae</i> . Protein Sci. 2018, doi: 10.1002/pro.3517.
August 2017	Koch K., Hromic A., Sorokina M., Strandback E. , Reisinger M., Gruber K., Macheroux P., <i>Structure, biochemical and kinetic properties of recombinant Pst2p from Saccharomyces cerevisiae, a FMN-dependent NAD(P)H:quinone oxidoreductase</i> . Biochim Biophys Acta. 2017 Aug, 1865(8):1046-1056.
April 2017	Lienhart W.-D., Strandback E. , Gudipati V., Koch K., Binter A, Uhl M. K., Rantasa D. M., Bourgeois B., Madl T., Zangger K., Gruber K., Macheroux P., <i>Catalytic competence, structure and stability of the cancer associated R139W variant of the human NAD(P)H:quinone oxidoreductase 1 (NQO1)</i> . FEBS J. 2017, 284(8):1233-1245.
January 2016	Brock J. S., Hamberg M., Balagunaseelan N., Goodman M., Morgenstern R., Strandback E. , Samuelsson B., Rinaldo-Matthis A., Haeggström J. Z., <i>A dynamic Asp-Arg interaction is essential for catalysis in microsomal prostaglandin E2 synthase</i> . Proc Natl Acad Sci U S A. 2016, 113(4), 972-977.

Experimental Skills

Molecular biology	DNA isolation, PCR, primer design, cloning, mutagenesis, yeast and <i>E. coli</i> transformation, gel electrophoresis
Biochemistry	Recombinant protein expression and purification in yeast and <i>E. coli</i> , Flavin dependent protein chemistry, enzyme kinetics, Western blot, FPLC, SDS-PAGE
Biophysical methods	UV-Vis spectroscopy, stopped flow spectroscopy, spectrofluorometry, Isothermal titration calorimetry, Thermofluor

Distinctions

June 2017	Scholarship from the Parliament of Åland, the Åland Islands
July 2015	Best Poster Award at the 14th Doc Day NAWI Graz Doctoral School of Molecular Biosciences and Biotechnology, Graz, Austria
July 2014	Travel fellowship for the 18th International Symposium on Flavins and Flavoproteins, Cha-Am, Thailand
April 2012	Scholarship from Lemlands kommun, the Åland Islands
November 2011	Scholarship from "Gunvor Plantings Stiftelse för Studier", Finland

Scientific Presentations and Conferences

Discussion leader:

July 2017	Gordon Research Seminar on Enzymes, Coenzymes & Metabolic Pathways, New Hampshire, USA
-----------	--

Selected presentations:

July 2015 and July 2017	Gordon Research Seminar and Conference on Enzymes, Coenzymes & Metabolic Pathways, New Hampshire, USA (poster presentations)
July 2017	19th International Symposium on Flavins and Flavoproteins, Groningen, The Netherlands (poster presentation)
February 2017	17th Doc Day NAWI Graz Doctoral School of Molecular Biosciences and Biotechnology, Graz, Austria (oral presentation)
September 2016	Retreat at Semmering 2016, Joint retreat with DK Biomolecular Technology of Proteins, Vienna, Semmering, Austria (oral presentation)

Other Qualifications and Interests

Languages	Swedish as mother tongue Intermediate level (B2-C1) in English and German Elementary level (A1-A2) in Finnish and French
Computer knowledge	Operative system: Windows, Mac OS X Applications: Microsoft Office, ChemBioDraw, Swiss-PdbViewer, PyMOL, Kaleidagraph, GraphPad Prism, Origin
Teaching experience	Teaching assistant in the lab course "Biochemistry I", Graz University of Technology, Austria
Additional training	<i>Effective scientific writing in English</i> (2 days course, Graz University of Technology, Dr. Katherine Tiede) <i>The art of scientific storytelling</i> (seminar, Graz University of Technology, Dr. Rafael Luna)
Driving license	B
Interests	Travelling, art, culture

Publication list

E. Strandback[‡], W.-D. Lienhart[‡], A. Hromic-Jahjefendic, L. Brvar, B. Bourgeois, A. Högler, D. Waltenstorfer, A. Winkler, K. Zangger, E. Heitzer, B. Rinner, T. Madl, K. Gruber, P. Macheroux, Rescuing the stability and activity of a cancer associated variant of human NAD(P)H:quinone oxidoreductase 1 (NQO1) by small-molecular chaperones, (2018) Manuscript in preparation

‡ The first two authors have contributed equally to this work.

K. Koch, **E. Strandback**, S. Jha, G. Richter, B. Bourgeois, T. Madl, P. Macheroux, Oxidative stress induced structural changes in the microtubule-associated flavoenzyme Irc15p from *Saccharomyces cerevisiae*. Protein Sci. (2018) doi: 10.1002/pro.3517.

K. Koch, A. Hromic, M. Sorokina, **E. Strandback**, M. Reisinger, K. Gruber, P. Macheroux, Structure, biochemical and kinetic properties of recombinant Pst2p from *Saccharomyces cerevisiae*, a FMN-dependent NAD(P)H:quinone oxidoreductase. Biochim Biophys Acta. 1865 (2017) 1046-1056.

W.-D. Lienhart[‡], **E. Strandback**[‡], V. Gudipati, K. Koch, A. Binter, M. K. Uhl, D. M. Rantasa, B. Bourgeois, T. Madl, K. Zangger, K. Gruber, P. Macheroux, Catalytic competence, structure and stability of the cancer associated R139W variant of the human NAD(P)H:quinone oxidoreductase 1 (NQO1). FEBS J. 2017, 284(8):1233-1245.

‡ The first two authors have contributed equally to this work.

J. S. Brock, M. Hamberg, N. Balagunaseelan, M. Goodman, R. Morgenstern, **E. Strandback**, B. Samuelsson, A. Rinaldo-Matthis, J. Z. Haeggström, A dynamic Asp-Arg interaction is essential for catalysis in microsomal prostaglandin E2 synthase. Proc Natl Acad Sci U S A. 2016, 113(4), 972-977.

Presentations at international conferences

E. Strandback, W.-D. Lienhart, A. Hromic, A. Högler, A. Winkler, K. Zangger, N. Dandachi, E. Heitzer, B. Bourgeois, T. Madl, R. Breinbauer, K. Gruber, P. Macheroux, Rescuing the stability and activity of a cancer associated variant of human NQO1 by small molecular chaperones, Gordon Research Seminar and Conference on Enzymes, Coenzymes & Metabolic Pathways, New Hampshire, USA, 2017, poster presentation

E. Strandback, W.-D. Lienhart, A. Hromic, A. Högler, D. Waltenstorfer, A. Winkler, K. Zangger, N. Dandachi, E. Heitzer, B. Bourgeois, T. Madl, R. Breinbauer, K. Gruber, P. Macheroux, Stabilization of a cancer associated variant of human NQO1 by the use of small-molecular chaperones, 19th International Symposium on Flavins and Flavoproteins, Groningen, The Netherlands, 2017, poster presentation

E. Strandback, W.-D. Lienhart, A. Hromic, J. Pletz, C. Köberl, V. Gudipati, K. Gruber, R. Breinbauer, P. Macheroux, Novel insights into structural destabilization of a cancer associated variant of human NQO1, OxiZymes Meeting, Wageningen, The Netherlands, 2016, poster presentation

E. Strandback, W.-D. Lienhart, V. Gudipati, P. Macheroux, Structural and Biochemical Investigation of New NAD(P)H:quinone oxidoreductase 1 (NQO1) P187X Variants, Gordon Research Seminar and Conference on Enzymes, Coenzymes & Metabolic Pathways, New Hampshire, USA, 2015, poster presentation

E. Strandback, W.-D. Lienhart, V. Gudipati, M. K. Uhl, A. Binter, S. Pulido, K. Zangger, K. Gruber, P. Macheroux, Insight into the structural behaviour of a natural variant of NAD(P)H:quinone oxidoreductase 1 (NQO1), 18th International Symposium on Flavins and Flavoproteins, Cha-Am, Thailand, 2014, poster presentation

E. Strandback, W.-D. Lienhart, V. Gudipati, M. K. Uhl, A. Binter, S. Pulido, K. Zangger, K. Gruber, P. Macheroux, Insight into the structural behaviour of a natural variant of NAD(P)H:quinone oxidoreductase 1 (NQO1), Enzyme Mechanisms by Biological Systems, Manchester, UK, 2014, poster presentation

Other presentations

E. Strandback, W.-D. Lienhart, J. Pletz, V. Gudipati, A. Winkler, K. Zangger, K. Gruber, R. Breinbauer, P. Macheroux, Rescuing the stability of a cancer associated variant of human NQO1 by small molecular chaperones, 17th Doc Day NAWI Graz Doctoral School of Molecular Biosciences and Biotechnology, Graz, Austria, 2017, oral presentation

E. Strandback, W.-D. Lienhart, C. Köberl, A. Hromic, J. Pletz, V. Gudipati, K. Zangger, K. Gruber, R. Breinbauer, P. Macheroux, On the way to rescue the stability and activity of a cancer associated variant of human NQO1, Retreat at Semmering, Joint retreat with DK Biomolecular Technology of Proteins, Vienna, Semmering, Austria, 2016, oral presentation

E. Strandback, W.-D. Lienhart, C. Köberl, A. Hromic, J. Pletz, V. Gudipati, K. Gruber, R. Breinbauer, P. Macheroux, Towards understanding the structural destabilization of a cancer associated variant of human NQO1, 8th ÖGMBT Annual Meeting, Graz, Austria, 2016, poster presentation

E. Strandback, W.-D. Lienhart, V. Gudipati, P. Macheroux, Investigation of the Reasons for the Destabilization of a Natural Variant of NAD(P)H:quinone oxidoreductase 1, 15th Doc Day NAWI Graz Doctoral School of Molecular Biosciences and Biotechnology, Graz, Austria, 2016, poster presentation

E. Strandback, W.-D. Lienhart, V. Gudipati, P. Macheroux, Structural and biochemical investigation of new NAD(P)H:quinone oxidoreductase 1 (NQO1) P187X variants, 14th Doc Day NAWI Graz Doctoral School of Molecular Biosciences and Biotechnology, Graz, Austria, 2015, poster presentation